Exploration of Parameters for the Continuous Blending of Pharmaceutical Powders

by

Ben Chien Pang Lin

University of Rochester, 2006

Submitted to the Department of Chemical Engineering
in partial fulfillment of the requirements for the degree of
Doctor of Philosophy in Chemical Engineering Practice

at the

MASSACHUSETTS INSTITUTE OF TECHNOLOGY

May 2011

[June 2011]

Author .....

Ben Chien Pang Lin

Department of Chemical Engineering

May 23, 2011

Certified by ....

Charles L. Cooney

Robert T. Haslam (1911) Professor of Chemical Engineering

Thesis Supervisor

Accepted by .....

William M. Deen

Carbon P. Dubbs Professor of Chemical Engineering

Chairman, Department Committee for Graduate Students

Abstract

The transition from traditional batch blending to continuous blending is an opportunity for the pharmaceutical industry to reduce costs and improve quality control. This operational shift necessitates a deeper understanding of the mixing process informed by particle dynamics and variable interdependencies. The thesis aims to establish a framework for characterizing and improving continuous pharmaceutical blending using a tiered experimental methodology and multivariate analysis. This parameter space exploration attempts to reconcile previous research within the context of cohesive pharmaceutical powders and develop general design principles for maximizing blender performance.

A design of experiments was conducted to determine mixing performance with respect to three factors – physical design, operating parameters, and material properties. Multivariate analysis using projections to latent structures was employed to quantify the effect of raw and intermediate variables on the variance reduction ratio. Significant parameters identified included the choice of API, fill fraction, the number of blade passes, the mean residence time, the Bodenstein number, and the period of input feed fluctuations. The results highlight the importance of shear and radial mixing for cohesive powders, which suggest that one-dimensional axial models common in blending literature may not be a sufficient theoretical framework for pharmaceutical applications.

The research yielded several insights into design principles for optimizing blending performance. Increasing mean residence time and radial mixing create more robust processing by reducing the impact of material properties and fluctuations in feed consistency. The variance reduction ratio can be improved in a cost-effective manner by determining the fill fraction which maximizes intermediate metrics such as space time, mean residence time, and the number of blade passes. Multivariate analysis was demonstrated to be a practical tool for parameter space optimization and a promising technique for characterizing the effect of material properties on processing.

Thesis Supervisor: Charles L. Cooney
Title: Robert T. Haslam (1911) Professor of Chemical Engineering

Acknowledgements

I would like to thank my advisor, Professor Charles Cooney, for all his kind support during my research, and my thesis committee members, Professors Alan Hatton and Bernhardt Trout, for their guidance and input throughout the process. I would also like to acknowledge my funding from Novartis and the Center for Continuous Manufacturing.

I owe a debt of gratitude to my colleagues in the Cooney Lab – Lakshman Pernenkil, Matthew Abel, Kangyi Mao, and Erin Bell – for their help and encouragement through the years. My work also would not be possible without the handy assistance of my undergraduate researchers – Diana Wu, Sunshine Zhou, Danielle Smith, and Kavita Chandra.

Lastly, I want to thank my friends and classmates, for all the fun along the way, and my parents, who were there with me for the entire ride.

Table of Contents

1 Introduction 13
1.1 What Is Pharmaceutical Blending? 14
1.2 What Is Continuous Manufacturing? 15
1.3 Current Challenges 16
1.4 Thesis Outline 16
2 Literature Review 19
2.1 Models of Continuous Mixing 19
2.1.1 Axial Dispersion Equation 19
2.1.2 Markov Chain Theory 22
2.2 Mechanics of Mixing 22
2.3 Experimental Mixing 24
2.3.1 Powder Characterization 24
2.3.2 Analytical Setup 25
2.3.3 Experimental Characterization 26
3 Thesis Objectives 29
4 Theoretical Work 31
4.1 Implementation of Markov Model 31
4.2 Markov Model Results 35
5 Experimental Methodology 39
5.1 Materials 39
5.1.1 Active Ingredients 40
5.1.2 Excipients 40
5.2 Equipment 41
5.2.1 Blender 41
5.2.2 Feeder 44
5.2.3 Near-Infrared Spectroscopy 45
5.3 Multivariate Data Analysis 45
5.3.1 Principal Component Analysis 46
5.3.2 Projections to Latent Structures 47

5.4 Experimental Procedure 48
5.4.1 Fill Weights 49
5.4.2 NIR Calibration 49
5.4.3 Residence Time Distribution 51
5.4.4 Blending 53
6 Double Helical Ribbon Blending Results 55
6.1 Fill Weight Experiments 55
6.2 Residence Time Distribution Experiments 64
6.3 Blending Experiments 72
7 Paddle Blending Results 75
7.1 Fill Weight Experiments 75
7.2 Residence Time Distribution Experiments 80
7.3 Blending Experiments 84
8 Implications for Process Design 87
8.1 Multivariate Analysis 87
8.2 Design Principles for Continuous Blending 92
8.2.1 Physical Design 92
8.2.2 Operating Parameters 94
8.2.3 Material Properties 95
8.3 Research Expansion Strategies 97
9 Multivariate Analysis of Pharmaceutical R&D 101
9.1 Background 101
9.2 Scope 102
9.3 Methodology 103
9.4 Results 104
9.5 Discussion 107
9.6 Summary 109
10 Conclusion 111
11 Works Cited 113

Table of Figures

Figure 1-1: Branded Drugs Facing the Patent Cliff 13
Figure 1-2: Process Schematic of Pharmaceutical Manufacturing 14
Figure 2-1: Residence Time Distributions for Varying Axial Dispersions 21
Figure 3-1: Design Framework for Continuous Blending 29
Figure 4-1: Fitting Markov Model to Axial Dispersion Equation 33
Figure 4-2: Markov Simulation, Normalized Residence Time = 1 34
Figure 4-3: Markov Simulation, Normalized Residence Time = 2 34
Figure 4-4: Variance Reduction Ratio during Markov Simulations 35
Figure 4-5: Output Relative Standard Deviation during Markov Simulations 36
Figure 4-6: Projected Tablet Failure Rate during Markov Simulations 37
Figure 5-1: Physical Configuration of Blender 42
Figure 5-2: Blender Outer Assembly 42
Figure 5-3: Blender Shafts 43
Figure 5-4: Original Scale Ribbon Blender 44
Figure 5-5: Double Length Ribbon Blender 44
Figure 5-6: Half Scale Ribbon Blender 44
Figure 5-7: Original Scale Paddle Blender 44
Figure 5-8: Schenck AccuRate Feeder 45
Figure 5-9: Chain of Experiments 48
Figure 5-10: Intermediate NIR Data Processing 50
Figure 5-11: PLS NIR Calibration 51
Figure 5-12: Fitting of RTD Data to Axial Dispersion Model 52
Figure 5-13: Sample of Full Blending Data 54
Figure 6-1: Sample Set of Fill Weight Results over Mass Flow Rates 56
Figure 6-2: Fill Weight Results Converted to Estimated Fill Fraction 56
Figure 6-3: Space Time vs. Fill Fraction in Ribbon Blender 57
Figure 6-4: Fill Fraction vs. Mass Flow Rate for Different Rotation Rates 58
Figure 6-5: Space Time vs. Fill Fraction for Different Rotation Rates 58

Figure 6-6: 3D Plot of Fill Fraction vs. Operating Parameters in Ribbon Blender 59
Figure 6-7: 3D Plot of Space Time vs. Operating Parameters in Ribbon Blender 59
Figure 6-8: Fill Fractions for Different Excipients, Adjusted by Bulk Density 60
Figure 6-9: Space Times for Different Excipients 61
Figure 6-10: Fill Fraction vs. Volumetric Flow Rate for Different Blender Lengths 62
Figure 6-11: Comparison of Fill Fraction across Different Blender Lengths 62
Figure 6-12: Space Time vs. Fill Fraction for Original Blender 63
Figure 6-13: Comparison of Space Time across Different Blender Lengths 63
Figure 6-14: Mean Residence Time vs. Fill Fraction in Ribbon Blender 64
Figure 6-15: Blade Passes vs. Fill Fraction in Ribbon Blender 65
Figure 6-16: Mean Residence Time vs. Fill Fraction for Different Excipients 66
Figure 6-17: Mean Residence Time vs. Fill Fraction for Original Blender 66
Figure 6-18: Comparison of Mean Residence Time across Different Blender Lengths 67
Figure 6-19: Comparison of Bodenstein number across Different Blender Lengths 67
Figure 6-20: Comparison of Mean Residence Time across Different API 68
Figure 6-21: Comparison of Bodenstein number across Different API 68
Figure 6-22: Comparison of Mean Residence Time to Space Time 69
Figure 6-23: Relative Mixing vs. Fill Fraction in Ribbon Blender 70
Figure 6-24: Powder Bed Surface at Various Fill Levels 70
Figure 6-25: Relative Mixing vs. Fill Fraction for Different Blenders 71
Figure 6-26: Actual VRR vs. Mean Residence Time in Ribbon Blender 72
Figure 6-27: Actual VRR vs. Markov-Predicted VRR in Ribbon Blender 73
Figure 7-1: Sample Set of Fill Weight Results over Mass Flow Rates 75
Figure 7-2: Fill Weight Results Converted to Estimated Fill Fraction 76
Figure 7-3: Space Time vs. Fill Fraction in Paddle Blender 77
Figure 7-4: Fill Fraction vs. Mass Flow Rate for Different Rotation Rates 78
Figure 7-5: Space Time vs. Fill Fraction for Different Rotation Rates 78
Figure 7-6: Fill Fractions for Different Excipients, Adjusted by Bulk Density 79
Figure 7-7: Space Times for Different Excipients 79
Figure 7-8: Mean Residence Time vs. Fill Fraction in Paddle Blender 80
Figure 7-9: Blade Passes vs. Fill Fraction in Paddle Blender 81

Figure 7-10: Comparison of Mean Residence Time across Different API 82
Figure 7-11: Comparison of Bodenstein number across Different API 82
Figure 7-12: Comparison of Mean Residence Time to Space Time 83
Figure 7-13: Relative Mixing vs. Fill Fraction in Paddle Blender 83
Figure 7-14: Actual VRR vs. Mean Residence Time in Paddle Blender 84
Figure 7-15: Actual VRR vs. Markov-Predicted VRR in Paddle Blender 85
Figure 7-16: Blending Performance by Blender and API 86
Figure 8-1: Multivariate Correlation of Parameters to VRR in Ribbon Blenders 88
Figure 8-2: Goodness of Fit with Experimental Level 88
Figure 8-3: Multivariate Correlation of Parameters to VRR, Fill Fraction Linearized 90
Figure 8-4: Multivariate Correlation of Parameters to VRR, Ribbon vs. Paddle Blenders 91
Figure 8-5: Multivariate Correlation of Parameters to VRR, Extending to Excipients 98
Figure 9-1: Overview of the Drug Development Process 102
Figure 9-2: Comparison of Revenue Growth vs. R&D Spending 104
Figure 9-3: Simple Linear Regression between Revenue Growth and R&D Spending 105
Figure 9-4: Goodness of Fit with Future Revenue Growth 105
Figure 9-5: Correlation between R&D Spending and Revenue Growth 106
Figure 9-6: Multivariate Analysis of R&D Productivity by Firm 107

1 Introduction

Pharmaceutical manufacturing has not changed drastically over the last century. In an industry fueled by waves of newer and better products, discovering the next blockbuster drug has always taken precedence over process innovation. Pharmaceutical innovation was focused on developing novel compounds and driving sales growth, rather than optimizing operations and reducing costs. In the years of high profit margins and seemingly limitless product opportunities, this was not a problem. More recently, cost pressures have mounted as traditional pharmaceutical giants face competition from both smaller biotechnology companies and generic manufacturers.

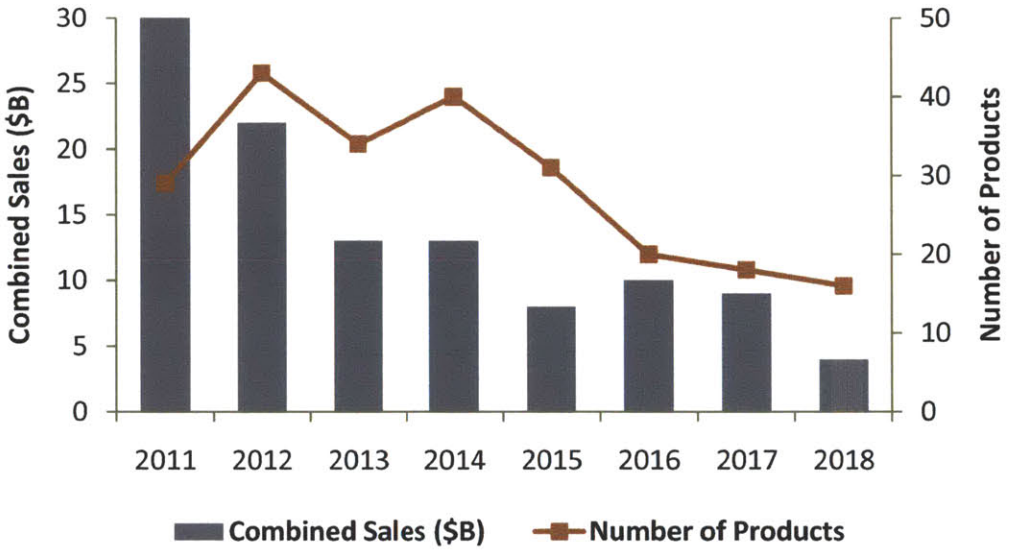

Figure 1-1: Branded Drugs Facing the Patent Cliff

In the next few years, patent protection on a host of blockbuster drugs is expected to expire, costing pharmaceutical companies billions of dollars in annual recurring revenue. The impending patent cliff will erode a stable base of sales for the industry, weakening growth prospects in the near-term. Figure 1-1 shows the anticipated losses over the coming decade, according to a Thomson Reuters report [1]. Pharmaceutical giants will lose patent protection on over 200 branded products that generated over $100B in combined global sales in 2010. Chief among these expiring blockbusters are Lipitor, Advair, and Seroquel, three of the top five prescription drugs by revenue. Given this stark industry outlook, pharmaceutical companies may renew their

focus on costs and operations. In this current climate, increased attention towards streamlining drug development and manufacturing may be a way to do more with less capital.

1.1 What Is Pharmaceutical Blending?

In traditional pharmaceutical manufacturing, the active pharmaceutical ingredient is embedded as a compressed dry powder in the final product, most commonly a tablet or capsule. This process can be split into two tasks – the API is chemically synthesized, then formulated with excipients to create the final drug product. The latter, often called secondary or downstream pharmaceutical manufacturing, involves a series of processing operations to convert the API into end user form. Figure 1-2 shows a typical sequence of pharmaceutical manufacturing processes. Common steps include crystallization, drying, granulation, blending, tabletting, coating, and packaging. Each unit operation is carefully calibrated such that the drug product conveys the appropriate usability and pharmacokinetic profile.

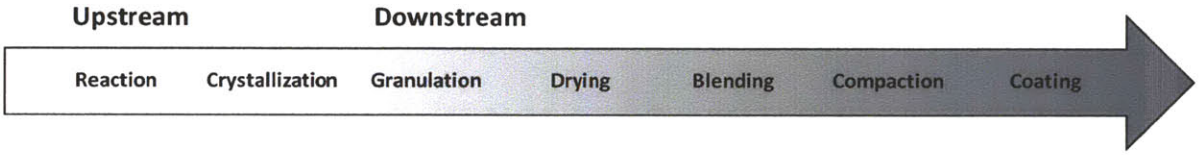

Figure 1-2: Process Schematic of Pharmaceutical Manufacturing

Blending is a pivotal step in maintaining the quality of secondary pharmaceutical manufacturing. During this process, the API is mixed with a pre-specified formulation of excipients designed to influence bulk density, dissolution properties, and flowability. After mixing, the drug product is locked in its final dosage form. Blending is then the last opportunity for product variance to be managed and minimized. Homogeneity is critical to drug quality as the local composition of materials in the formulation dictates its processing properties and pharmacokinetic profile. Most importantly, blending is responsible for controlling the accurate dosage of the API across the millions of tablets in each manufacturing run. As drugs become more potent and targeted, a robust blending operation becomes ever more critical to a safe and reliable drug production system [2]. Mixing is thus a key process to understand and streamline in any effort to improve pharmaceutical operations and reduce costs.

1.2 What Is Continuous Manufacturing?

Like other pharmaceutical processing steps, the majority of blending is currently conducted in batch mode. In batch operations, each step of the manufacturing process is run to completion as defined by a pre-specified performance metric. Material is then transported to the next step in a sequential and step-wise manner. Batch operations provide a number of advantages, primarily in reducing system complexity. Material can be tracked in distinct lots and batches since product is housed in distinct equipment units throughout the manufacturing process. This separation of equipment and material eases regulatory compliance and provides a natural buffer time between steps to check quality.

Recently, the pharmaceutical industry and the US Food and Drug Administration have pushed towards a continuous manufacturing paradigm [3]. The Consortium for the Advancement of Manufacturing of Pharmaceuticals has defined continuous manufacturing as the "processing of raw materials without interruption and with continuity of production over a sustained period of time". Continuous processing confers several advantages discussed below.

Steady-State Operation at Lower Scale

Continuous manufacturing is designed to run effectively at steady-state with little downtime. Using proper monitoring and control, operations can be performed on an extended schedule with minimal supervision. This allows a continuous process with a constant throughput to scale-up simply through longer run times. This scalability provides greater operational flexibility during drug development and clinical trials and also enables the target production rate to be achieved with smaller equipment. Continuous processing also eliminates accumulation of material during manufacturing, thus reducing work in process and material containment issues.

Reduced Capital Requirements

A corresponding advantage to the lower scale of operation is reduced capital requirements. The smaller sizing of equipment also reduces space and support requirements, allowing a plant to be constructed at a lower capital cost. The decrease in cycle time and work in process also yields lower working capital. Continuous processing promotes a lean manufacturing methodology which increases process efficiency and return on capital.

1.3 Current Challenges

At its heart, continuous pharmaceutical manufacturing can be viewed as an attempt to treat the processing of dry pharmaceutical powder in the same way as the processing of fluids. By moving material automatically and uniformly from step to step, queuing and transfer issues no longer arise. However, the imposition of movement along an organized production line necessitates a much deeper understanding of the process timing. In batch blending, a run which did not meet homogeneity standards could simply be repeated at the cost of a time delay. In continuous blending, the unmixed material would proceed through the manufacturing process, resulting in unusable product and wasted operating time. The greater consequences of a failed run mean that operations must be rigorously optimized for both robustness and performance.

Understanding of particle systems has been historically sparse compared to research into fluid systems. Bridgwater noted that while 60% of the products of the chemical industry are in solid form, chemical engineering undergraduate curriculums contain little on particle technology [4]. This discrepancy has been exacerbated by difficulties in characterization of solids processing. Prior to the advent of optical imaging methods, offline sampling of material was the industry standard for evaluating pharmaceutical blending. Recent analytical methods such as positron emission particle tracking, light-induced fluorescence, and near-infrared spectroscopy have been powerful improvements in peering into solids dynamics.

The opportunity then is to apply new frameworks for understanding and characterizing particle systems to solve the current challenges in pharmaceutical manufacturing. Research on continuous processing from the food and chemicals industries can be combined with new optical imaging methods to provide insight and elucidate design principles for continuous manufacturing in the dry powder context. These findings can then be used to improve the current inefficiencies in pharmaceutical manufacturing.

1.4 Thesis Outline

The thesis begins with an abbreviated literature review in Chapter 2 highlighting specific insight which informed the development of this work. Given the current state of blending research, Chapter 3 lays out the thesis objectives. Next, Chapter 4 presents theoretical simulations

conducted to establish a baseline understanding of blending dynamics. Chapter 5 describes the experimental methodology, including overall design rationale, types of experiments, and analytical techniques employed. The results are presented and discussed in the next 3 chapters. Chapter 6 focuses on findings from the double helical ribbon blenders, from fill weight data to residence time distribution data and variance reduction ratios. The same layout is repeated in Chapter 7 for the paddle blender. The whole data set is then aggregated for multivariate analysis in Chapter 8, followed by a discussion of the implications for future blender design and potential avenues for further work. The multivariate analysis is applied to an evaluation of pharmaceutical revenue growth with respect to research and development spending in Chapter 9, followed by conclusions in Chapter 10.

2 Literature Review

The research on powder blending has focused on developing a fundamental understanding of the mixing process to elucidate further improvements and enhance predictive power. Within this body of work, several reviews cover the theory and practice of powder blending over time. Fan et al. [5, 6] documented theoretical work to define mixing performance and surveyed the development of mixing mechanisms and models for specific blenders. Williams [7] detailed relevant applications to continuous drum mixers. Poux et al. [8] provided a review of practical distinctions between different mixing systems. Pernenkil and Cooney [9] summarized the state of work with a comprehensive list of modeling methodologies and monitoring techniques.

This review serves as a supplement to existing surveys, particularly the work of my predecessor Lakshman Pernenkil. Specific emphasis is placed on recent developments where technological advancements have yielded new contributions to conventional understanding of powder blending. The review is divided into three portions – 1) practical theoretical applications to continuous mixing, 2) the mechanics of mixing, and 3) recent experimental findings.

2.1 Models of Continuous Mixing

Two theoretical frameworks for continuous mixing are highlighted here – the axial dispersion equation and Markov chain theory. Due to current computational limitations in expanding up to experimental scale, discrete element method simulations are considered impractical for cohesive applications and not covered. Specifics of research implementation are discussed in detail in the experimental methodology.

2.1.1 Axial Dispersion Equation

When blending is transformed into a continuous process, forward axial motion is superimposed on top of convective and diffusive mixing in the radial and axial directions. This can be accomplished by designing to agitator to impart forward momentum. If loading fraction is to remain a variable parameter, the blender must have the capacity to carry powder at a faster rate than the throughput. Since the mixer length is usually significantly larger than the diameter,

mixing in the radial direction is simply assumed, while greater efforts are spent on ensuring axial homogeneity. Ghaderi [10] notes that particles that enter the system simultaneously should be delayed by different amounts of time in order to smooth out input axial fluctuation patterns.

This concept of axial mixing can be characterized using the general transport equation of the axial dispersion model [11-15]. As shown in Equation (2-1), both convective and diffusive terms are incorporated into transient transport in the axial dimension. When non-dimensionalized into Equation (2-2), the characteristic parameter is the Bodenstein number, the solid equivalent of the Peclet number for fluid transport, which relates convective to diffusive motion. Hence, low Bodenstein numbers indicate a high degree of axial mixing. When the equation is solved for closed boundary conditions, the concentration at the outlet of the blender yields the residence time distribution, plotted in Figure 2-1 for a wide range of Bodenstein numbers and normalized space times. The RTD can vary from the plug flow model for no dispersion to the continuously stirred tank model for infinitely high dispersion. In this one-dimensional model, the mean residence time, the average velocity, and the axial dispersion are the only metrics necessary to characterize blender dynamics.

$$\frac{\partial C}{\partial t} = -v\frac{\partial C}{\partial z} + D\frac{\partial^2 C}{\partial z^2} \tag{2-1}$$

$$\frac{\partial \Psi}{\partial \theta} = -\frac{\partial \Psi}{\partial \zeta} + \frac{1}{Bo}\frac{\partial^2 \Psi}{\partial \zeta^2} \tag{2-2}$$

$$\theta = \frac{tv}{L} \quad \zeta = \frac{z}{L} \quad \Psi = \frac{C}{C_0} \quad Bo = \frac{vL}{D}$$

The most direct measure of blending performance in literature is the variance reduction ratio, defined as the variance in the material of interest at the mixer inlet divided by the variance at the outlet. Equation (2-3) shows the relationship between VRR and the Danckwerts model, which postulates that the VRR can be calculated using the autocorrelation functions of the residence time distribution and the input feed profile. Note that for solids mixing, another term is appended to the Danckwerts model to account for the random mixture limit, an upper bound on physically achievable performance in the blending of dry solids.

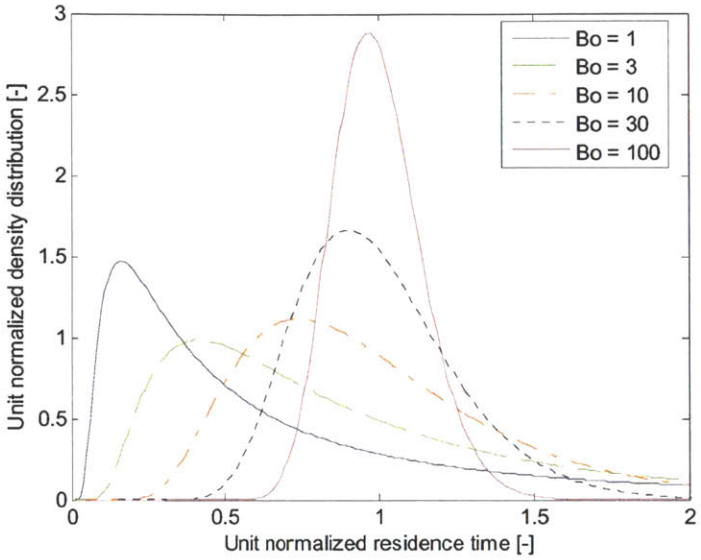

Figure 2-1: Residence Time Distributions for Varying Axial Dispersions

$$\frac{1}{VRR} = \frac{\sigma_{out}^2}{\sigma_{in}^2} = 2\int_{t=0}^{\infty}\int_{\tau=0}^{\infty} E(t)E(t+\tau)R(\tau)d\tau dt + \frac{\sigma_{out,ideal}^2}{\sigma_{in}^2} \qquad (2\text{-}3)$$

The homogeneity of the mixer output is thus dependent on both the blender performance and the input consistency. It is difficult for the blender to smooth out feeding variations that occur beyond the mean residence time – leading to the circuit analogy that blenders act like a low-pass filter. This concept can be tested by feeding the blender in a sinusoidal pattern and varying the oscillation frequency. For feed variations that are not perfectly sinusoidal, the same analysis can be conducted in the frequency domain by performing a Fourier transform on the input and output concentration profiles. The resulting power density spectrum can be used to calculate the VRR at each frequency by dividing the input value by the output value. The VRR can also be plotted against the period or the frequency of the feeding fluctuation to provide an indication of how robust the blending process is. The theoretical work of Danckwerts and the experimental data presented by Weinekotter and Reh [15] both suggest that the VRR can be improved by increasing the axial mixing, increasing the mean residence time, or by decreasing the perturbation frequency of the input feed. In the one-dimensional paradigm of continuous blending, these variables are the key to maximizing fundamental performance within a given design space.

2.1.2 Markov Chain Theory

One-dimensional axial movement along a blender can also be modeled via Markov chain theory, a theoretical construct wherein the system is sliced into discrete chambers and flow through the system is characterized as a series of probabilities of movement. For any given system profile represented by probabilities, inputs can be altered and outputs simulated in order to predict the system response. The advantage of Markov chain theory is the linear algebra framework, which makes the simulation analytically tractable in one- and two-dimensional models. As the unit of interest here is a chamber rather than a discrete particle, Markov models are easier to scale up compared to discrete element method simulations, which approach computational limitations in the 10^9 particle range [16].

Marikh et al. [17] applied a Markov model to experimental powder mixing data and validated its use in characterization of continuous mixing. The framework has also been extended to static mixers [18] and hybridized with discrete element method [19]. The model provides an alternative paradigm for characterizing a blending system, with greater flexibility to account for complex designs such as asymmetry or irregular shaft elements. However, Markov chains can still be reduced to the same number of independent parameters as the axial dispersion model with appropriate assumptions for system uniformity and powder dynamics. A deeper explanation of Markov chain theory is included in the theoretical work discussed in Chapter 4.

2.2 Mechanics of Mixing

Powder mixing is caused by relative differences in powder flow, leading to a rearrangement in particle positions. Mixing can occur through two mechanisms – convection refers to blending due to bulk movement of powder, while diffusion refers to random movement of powder across slip planes or free surfaces. It is important to note that the smallest unit in solid mixing is the particle, while the smallest unit in fluid mixing is the molecule. In this case, diffusion does not occur due to Brownian motion, but only through the input of mechanical energy to displace particles. In addition, agglomeration and deagglomeration can also have a significant impact on output homogeneity. Shear forces are thus another important mechanism to consider, given the impact of cohesion and adhesion of the interaction of pharmaceutical particles [20].

Powder flow can first be understood at simpler geometries, such as a rotating cylinder used in horizontal drum mixers. Mellmann [21] examined transverse bed behavior in a partially filled rotating cylinder and categorized the forms of motion based on rotation speed. At the slowest speeds, the bed constantly slides from the wall, causing the tube to rotate while the bed appears to rest at a slight angle of repose. As the rotation rate increases, the solid bed is elevated higher, causing intermittent avalanching to produce a slumping behavior. This motion transitions into a continuous flow of material down the free surface of the bed to yield a rolling action. At higher speeds, powder is lifted even higher and the bed surface begins to arch as cascading sets in. Eventually, more and more individual particles are flung up and out of the bed to produce the cataracting and centrifuging motions.

Sherritt et al. [22] determined that different degrees of axial dispersion were associated with each form of bed motion. Other significant parameters included rotation speed, degree of fill, drum diameter and particle diameter. Other material properties can also greatly impact mixing mechanics. Faqih et al. [23] explored the extent to which cohesive granular materials expand in response to mechanical agitation. In simple cylinders, the powder bed may dilate 10-40% depending on powder size and cohesion. The dilation effect during powder motion effectively reduces the bulk density of the formulation during mixing.

The process geometry has a significant impact on powder flow, and consequently, on the mixing mechanisms. Additional motion can be provided by the introduction of agitators – paddles, lifts, and ribbons designed to produce greater bulk movement. Malhotra and Mujumdar [24] explored the motion of powders in response to a single flat blade by visually tracking the displacement of a section of tracer particles from their original position. The influence of multiple flat blades in a cylindrical mixer was explored by Laurent and Bridgwater [25-29] using positron emission particle tracking. A batch was run for an hour with a radioactive tracer, and a positron camera captured the spatial coordinates and instantaneous velocities of the tracer over time. This allowed powder flow to be fully visualized in density bins and vectors, respectively, with root mean square displacements in the radial and axial directions broken down by particle position.

Laurent and Bridgwater found that the bladed agitator created loops of circulation. The center of the loop of circulation moves towards the shaft as the fill increases. The types of motion produced here are similar to those described by Mellmann in a rotating cylinder. The flow at 20%

fill is a combination of cascading and cataracting powder – some of the particles swept up by the blades roll down the free surface, while others are flung over the shaft. The flow at 60% fill is almost all cataracting, although some centrifuging is also evident. The advantage of using a rotating agitator is that proper design and operation allows an agitator to simultaneously produce several types of motion found in a drum mixer.

Since mixing occurs through relative differences in powder flow, a wide range of angular velocities provides mixing in the radial direction. Laurent and Bridgwater discovered that maximum radial displacement occurred between 40% and 50% fill, corresponding to the splitting of material over and under the shaft. This bifurcation of cascading and cataracting powder is due to the physical presence of the agitator shaft, which prevents more particles from being flung up as well. The blocking behavior alters the powder flow, resulting in a wide distribution of angular velocities. This is in sharp contrast to flow at 70% fill, when almost all of the particles are cataracting over the shaft. Since the powder is moving in the same loops of circulation, the lack of change in relative position yields little mixing. Thus, the loading fraction plays a large role in agitated powder flow as a certain amount of void space is required for several types of motion to occur simultaneously. The optimum fill is also dependent on the specific design of the agitator.

The same understanding of radial mixing can also be applied to axial mixing along the length of the cylindrical blender. Although the blades are flat, individual particles can be displaced axially during the sweeping of the blade, as they roll down the free surface, or as they cataract over the shaft. Similar to the blocking behavior in radial mixing, particles can also move axially as they bounce off the shaft. Once again, Laurent and Bridgwater found that fill levels between 40% and 50% provide the greatest axial dispersion. The presence of more blades produces more continuous particle motion, which also increases the amount of axial displacement.

2.3 Experimental Mixing

2.3.1 Powder Characterization

Many pharmaceutical ingredients are described as cohesive powders, which imply the material is highly sticky with poor flowability. This behavior is due to the dominance of inter-particle forces over gravitational forces, causing material to aggregate. Powder flow changes with the relative

importance of these forces. Particles larger than 400 μm are generally free flowing, while those on the order of 100 μm exhibit stick-slip flow [30]. Even the presence of such small particles in a wide size distribution may cause the whole powder to become cohesive [20].

The application of mixing literature on granular material to drug product formulation has been drastically limited by this key distinction – most experimental work is performed with free flowing material while most pharmaceutical ingredients are cohesive. This discrepancy is due to the fact that larger particles are easier to track and that most studies are not geared directly towards the pharmaceutical industry. Thus, it is pivotal to approach the literature below with a grain of salt and be aware of any deviations that may occur due to the cohesive nature of pharmaceutical powders.

A wealth of metrics has been used over the years to characterize powder flow in different industries. Historically, these indices were a way of empirically incorporating material properties into the operation of processes [31]. However, each value was specific to a given combination of granular material, flow geometry, and equipment design, making this characterization a poor method for understanding fundamental powder flow and predicting future behavior when parameters are varied.

Attempts have been made to standardize and consolidate powder characterization under the aegis of an umbrella metric. For instance, Kaye et al. [32] captured the rheological properties of cohesive powders by characterizing avalanching behavior in a rotating disc. Further research was conducted to unify this testing procedure with previously used indices [33-37]. The use of these intermediate proxies for material properties have aided R&D involving cohesive powders, but remains restricted due to the fragmented applicability of these techniques to different operations in the relevant manufacturing industries.

2.3.2 Analytical Setup

A typical method of characterizing batch mixing is to analyze multiple samples at each time interval, akin to monitoring the outlet concentration over time in continuous blending. The variance in concentration provides a metric for the degree of mixing. Blending usually causes an initial steep drop in variance, attributed primarily to convective mixing, and then a more gradual

decrease, due to diffusive mixing [38]. Since powders are a non-ordered system, the variance never reduces to zero, but reaches a minimum at the ideal random limit of mixing.

The biggest advance in analytical characterization of live processes was the movement from offline techniques such as standard spectroscopy to online monitoring through light-induced fluorescence and near-infrared spectroscopy. This evolution was made possible by technological progress in optical equipment, enabling rapid and instantaneous feedback on performance. This data-driven approach required greater statistical analysis but opened the doors to more quality-focused applications such as pharmaceuticals [39]. LIF was shown to monitor dry powder homogeneity non-invasively [40, 41] while NIR demonstrated potential in tracking quality in both blends and tablets [42-45].

2.3.3 Experimental Characterization

While a great body of literature exists on pharmaceutical batch blending and continuous mixing of non-cohesive particles, the intersecting field of continuous blending of cohesive powders has historically been underexplored due to the difficulties in addressing processing scale with rapid online analytical capabilities. In numerous batch studies, several authors [46-49] noted the effect of sufficient shearing and fill height levels on blending performance and the applicability of this relationship to continuous processing.

Earliest continuous blending research was conducted with cheap, industrial material from the food and chemicals industries. Weinekotter et al. [14, 15] investigated continuous mixing of Irgalite particle systems ranging from 0.2 to 100 μm at a maximum throughput of 300 kg/hr, using inline analytics to determine performance via the variance reduction ratio. Both theoretical and experimental work supported the relationship between VRR, the period of the input feed, the mean residence time, and the Bodenstein number. Portillo et al. [50] conducted similar convective powder mixing experiments using pharmaceutical material, noting flow patterns with respect to horizontal angle and the importance of the number of blade passes on performance. Berthiaux and Marikh et al. [51-53] designed a series of continuous blending experiments around both food and pharmaceutical mixtures, capturing the relationship between operating parameters and the hold-up weight, as well as the influence of a fluidized flow regime and the feed consistency on the variance reduction ratio.

Pernenkil [54] performed a larger set of pharmaceutical mixing experiments, identifying mean residence time and the time period of feeder fluctuations again as the key variables in predicting blending efficiency. A deeper analysis also found increased particle sizes lead to higher axial dispersion coefficients and thus increased performance. Pernenkil also made greater use of multivariate data analysis to distinguish collinear relationships between various variables and demonstrated its potential to characterize multicomponent blending systems.

Kehlenbeck [55] also conducted a rigorous exploration of the continuous blending of cohesive powders, integrating the results of axial dispersion model simulations with experimental data collected from large scale industrial mixers. The blending of calcium carbonate and maize starch was found to correlate closely with one-dimensional transport profiles and the ratio between the mean residence time and the period of the input feed fluctuations was concluded to be the key determinant of mixing quality. Kehlenbeck briefly sampled the effect of different weirs at the blender output and noted the importance of validating published results using other mixing devices and shaft designs.

3 Thesis Objectives

Most notable in recent continuous blending literature has been the lack of unifying frameworks for understanding the full parameter space during blender design and operation. As shown in Figure 3-1, the performance of continuous blenders can ultimately be attributed to one of three factors – the physical design, operating parameters, and material properties. Physical design encompasses variables that irreversibly set during the manufacturing of the blender and thus not easily adjustable during operations. The primary variables of interest in this category are the blender length and diameter as well as the details of the shaft design, from elements employed to specific positioning. Operating parameters include process variables commonly tuned during development and manufacturing to optimize performance, such as the shaft rotation rate, loading fraction of the blender, and throughput of the system. Material properties comprise key values inherent to the API and excipients employed in the formulation of choice, ranging from cohesion to particle size and shape distributions.

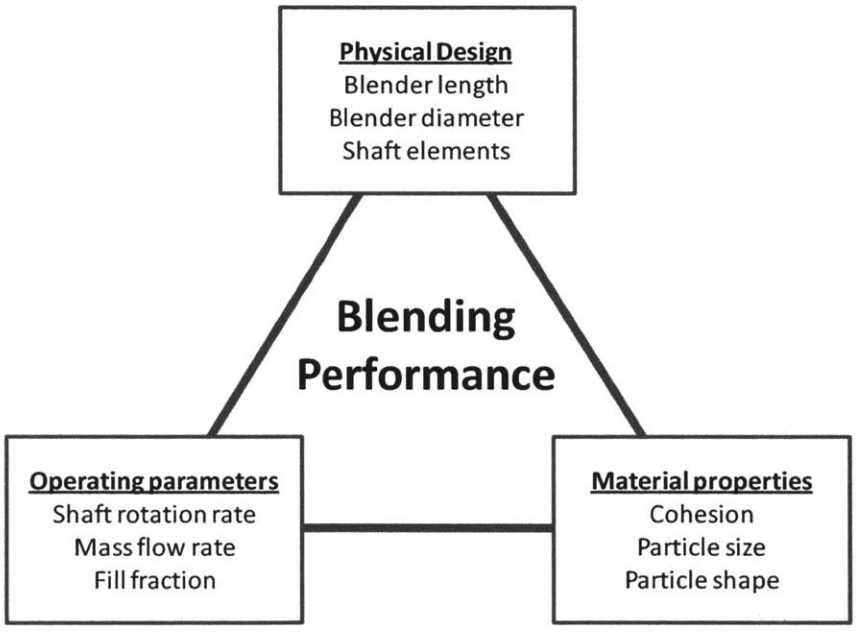

Figure 3-1: Design Framework for Continuous Blending

Following the advent of analytical techniques to effectively characterize blending in real time, research has focused on understanding the relationships between operating parameters and the optimal combinations for maximizing performance. While these works are quite comprehensive

for the chosen mixer and formulation, the absence of a holistic framework incorporating all three groups of factors makes comparisons difficult. This inefficiency in reconciling isolated data sets yields an incomplete picture of continuous blending, as differences in scale, equipment, and materials influence the findings reported and the conclusions derived. A common methodology and analytical framework for unifying related research is necessary in order to glean high-level design principles from experimental data.

The application of continuous blending to pharmaceutical mixtures has also been encumbered by the prohibitive cost of expending API for full scale manufacturing R&D. In the early stages of pharmaceutical drug development, API synthesis can be expensive and inefficient, making it a limiting factor during project management. At best, API committed to processing R&D subtract directly from sales and at worst, API shortages slow the clinical trial timeline and delay marketing approval. Care should be exercised in order to extract maximum information from a pharmaceutical design of experiments.

This thesis aims to establish an analytical and experimental framework for understanding and improving continuous pharmaceutical blending. This framework is meant to elucidate the mixing behavior of pharmaceutical powders and illuminate general design principles which may be applied in future blending research. The work extends efforts conducted by my predecessor, Lakshman Pernenkil. By applying multivariate statistical analysis, this proposed framework creates an iterative procedure for refining blending design and operation at minimal cost in terms of material wasted. The objective of this framework is to quantify the effects of various independent variables – blender design, operating parameters, and material properties – on overall blending performance and reconcile these findings with the current understanding of powder dynamics and continuous manufacturing.

The goal of this design of experiments then is to develop a full understanding of the relationships between various parameters, intermediate metrics, and of course the VRR. A key consideration throughout is the ability to leverage cheap and quick studies to inform higher-level experimental design. The extent to which these intermediate parameters elucidate blending performance is indicative of the processing efficiency gains which could be achieved through proper execution. This boost in R&D productivity would play no small part in the implementation of such a design strategy in the development of clinical stage drug candidates.

4 Theoretical Work

Previous theoretical work in powder blending was leveraged as a starting point for the design of experiments conducted in this thesis. Given the limits in the scalability of discrete element simulation, efforts centered on the axial dispersion equation and Markov modeling. Simulations were then conducted at the expected experimental scale as a baseline for understanding powder dynamics and blending performance in the given range. In this chapter, the specific implementation is described, followed by a discussion of simulation results and the consequences for experimental design.

4.1 Implementation of Markov Model

A one-dimensional Markov model was constructed based on the work of Berthiaux and Marikh et al. [16, 17]. In brief, a longitudinal blender was hypothetically broken down into a series of n chambers forming a single chain. Markov theory posits that discrete elements can move freely between the individual compartments in the chain with probabilities governed by the general format given by Equation (4-1). The matrix consists of a central diagonal with the probabilities of a particle staying in the same chamber during the time interval Δt, with adjacent diagonals above and below describing the probabilities of a particle moving back one chamber and forward one chamber, respectively. The final column is an absorbing state, representing the irreversible exit of a particle from the system.

$$P = \begin{bmatrix} p_{1,1} & p_{1,2} & 0 & \cdots & 0 & 0 & 0 \\ p_{2,1} & p_{2,2} & p_{2,3} & \cdots & 0 & 0 & 0 \\ 0 & p_{3,2} & p_{3,3} & \cdots & 0 & 0 & 0 \\ 0 & 0 & p_{4,3} & \cdots & 0 & 0 & 0 \\ \cdots & \cdots & \cdots & \cdots & \cdots & \cdots & \cdots \\ 0 & 0 & 0 & \cdots & p_{n-2,n-1} & 0 & 0 \\ 0 & 0 & 0 & \cdots & p_{n-1,n-1} & p_{n-1,n} & 0 \\ 0 & 0 & 0 & \cdots & p_{n,n-1} & p_{n,n} & 0 \\ 0 & 0 & 0 & \cdots & 0 & p_{n+1,n} & 1 \end{bmatrix} \quad (4\text{-}1)$$

This general model can be used to describe complex motion generated by different agitating elements of a blender and can also be adapted to incorporate the effect of weirs in interrupting free movement along the chain. For a blender with functionally equivalent chambers, this matrix of probabilities can be simplified considerably. That is, the central diagonal and the adjacent diagonals above and below can be represented by static probabilities of no movement, backward movement, and forward movement. These three parameters encompass all possible trajectories of a particle in the given time interval and thus must add to unity.

The mass or concentration of the material of interest along the Markov chain over time is modeled by the vector S. In combination with a feed vector describing the forced input of material into the system, the evolution of particle movement along each time interval can be simulated by Equation (4-2). Over time, these vectors document the flow of material as dictated by the given probability matrix and feed profile. In particular, the collection of concentration values in the last chamber approximates the profile of the material as it exits the system.

$$S(i+1) = P[S(i) + S_0(i)] \tag{4-2}$$

This one-dimensional Markov model was built in Matlab in order to conduct computational simulations around blending efficiency given feeding inconsistencies. Linear Markov chain theory implicitly assumes the fluctuations in the inflow are not significantly enough to disrupt the steady-state regime of the local hold-up and fill fraction, only the concentration of various materials therein. Since pharmaceutical focus is on the API as the material of interest and the low concentration of API in the overall formulation, this simplification was acceptable.

When the feed vector is simply a Dirac delta function, the resulting exit profile is an impulse response function, akin to an experimentally-derived residence time distribution. The simulations can be reconciled with experimental data derived from the axial dispersion equation by fitting Markov probability values to the given mean residence time and Bodenstein number. Figure 4-1 provides a sample experimental fit with the yielded Markov parameters. The model provided a good fit with the open-open one-dimensional axial dispersion equation, indicating an acceptable translation between Markov simulation data and residence time distribution experiments in terms of understanding axial blending performance. This enabled the model to predict the system response to any given input feed profile for the API.

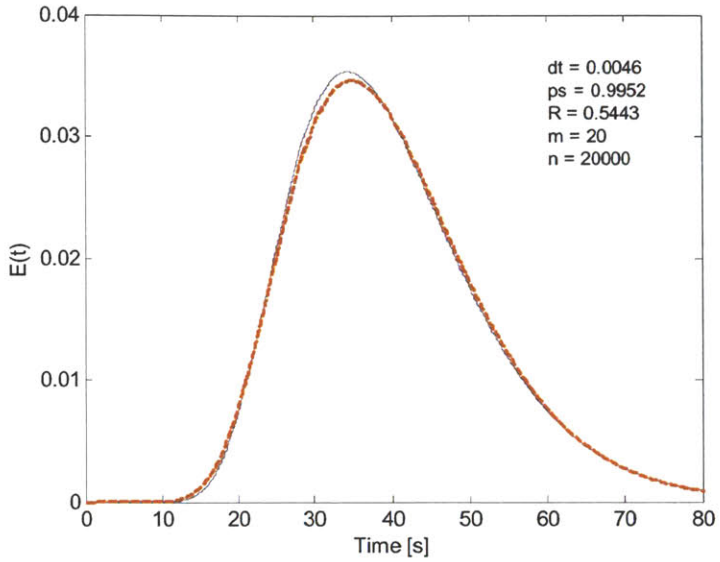

Figure 4-1: Fitting Markov Model to Axial Dispersion Equation

The Markov model thus served as a simulation package for predicting the effect of input feed consistency on the exit profile, for any given system characterized by axial dispersion or Markov probability parameters. The primary performance metric, variance reduction ratio, was evaluated against a range of values for mean residence time, Bodenstein number, and feed frequency period. Figure 4-2 shows a simulation of blending startup where the mean residence time is equivalent to the feed frequency period, for a normalized residence time of 1. After an initial induction lag to reach steady-state, the output profile began to follow the input feed profile, albeit with an amplitude attenuation (variance reduction) and a phase shift matching the mean residence time.

Figure 4-3 shows the same system with more frequent feed input variation, half the original wave period for a normalized residence time of 2. The resulting output was significantly less volatile, indicating a higher variance reduction ratio. As discussed in the previous chapter, a blender functions as a low-pass filter, dampening high frequency signals through homogenization but allowing low frequency feed variation to slip through. For a given mean residence time, it becomes increasing difficult to mix particles together the further apart they are in time and space.

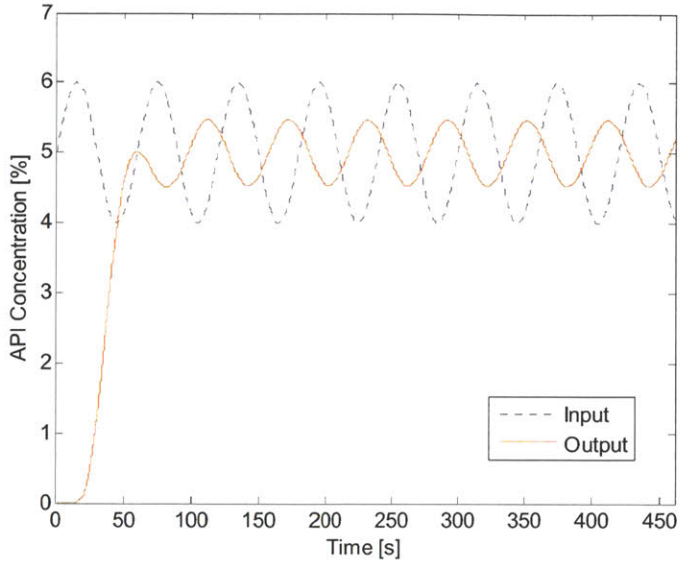

Figure 4-2: Markov Simulation, Normalized Residence Time = 1

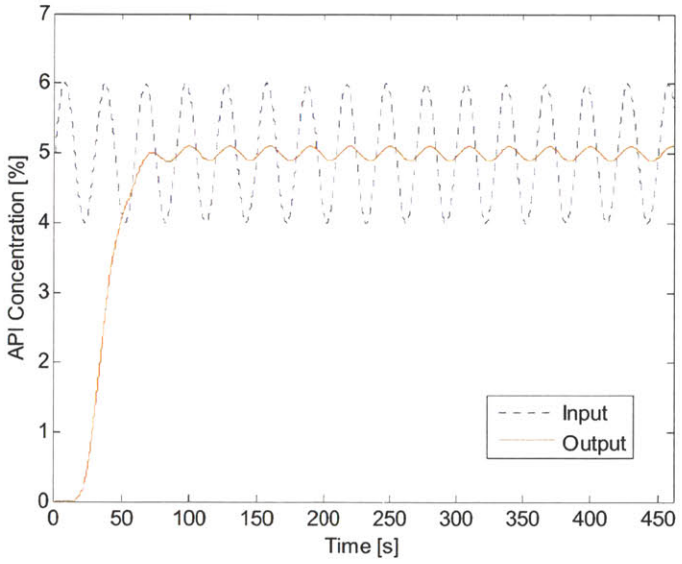

Figure 4-3: Markov Simulation, Normalized Residence Time = 2

The resulting variance reduction ratio at steady-state for each simulation was compiled to better understand the relationship between blending performance, normalized residence time, and the Bodenstein number. The results and consequences for blending and experimental design are discussed in the next section.

4.2 Markov Model Results

Markov simulations were conducted at a range of mean residence times, Bodenstein numbers, and feed input periods corresponding with the work of Pernenkil [54] in order to glean insights into blending performance. While literature has shown the general influence of each variable with respect to variance reduction [15, 16], the simulations performed here are specific to the range for potential experiments and the design space of interest.

Figure 4-4 shows blending performance for a blender with a mean residence time of 60 s and variable Bodenstein numbers and feed input periods. Variance reduction ratio was plotted against normalized residence time, the non-dimensional ratio between mean residence time and the feed input period. A semilog relationship between VRR and normalized residence time was found, with a performance gain of two orders of magnitude when the normalized residence time was increased from 1 to 2, the same range demonstrated in Figure 4-2 and Figure 4-3. Increases in blending efficiency diminish greatly beyond this range as the physical mixture hits the random mixture limit [8, 9]. This relationship re-emphasizes the importance of feeding consistency in blending performance and provides a simple first-order rule-of-thumb for sizing a blender once feeding equipment has been selected and its limits understood.

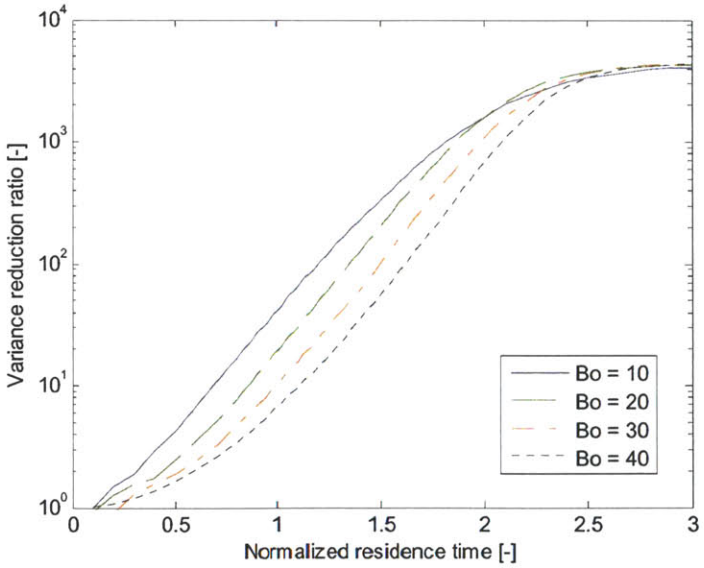

Figure 4-4: Variance Reduction Ratio during Markov Simulations

The blending performance curves were plotted separately for several Bodenstein numbers, representing relative differences in dispersive and convective motion within the blender. Here, the gains in performance were not as significant. Over the expected range of Bodenstein numbers, variance reduction increased by approximately half an order of magnitude, gains which were erased at the higher normalized residence times. The Markov simulations suggest that while higher dispersion can boost blending efficiency, higher normalized residence times may provide a more robust method of designing better blenders.

For another perspective, Figure 4-5 shows blending performance in terms of output relative standard deviation, given an API feed rate of 5% ± 1%. Again, the performance gains of lower Bodenstein numbers were completely absorbed at higher normalized residence times. The mean residence time had to be roughly equivalent to the input feed period in order to generate relative standard deviations below 6%, the FDA-mandated threshold for manufacturing quality. Tablet failure rates for a given bound of ±6% from mean concentration were plotted in Figure 4-6, assuming axial slices were directly punched into tablets. Failure rates dramatically fell to 0% around a normalized residence time of 1.

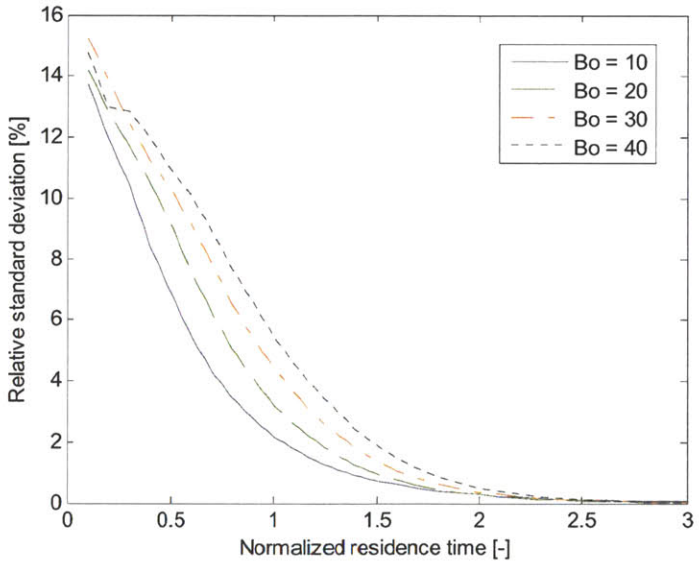

Figure 4-5: Output Relative Standard Deviation during Markov Simulations

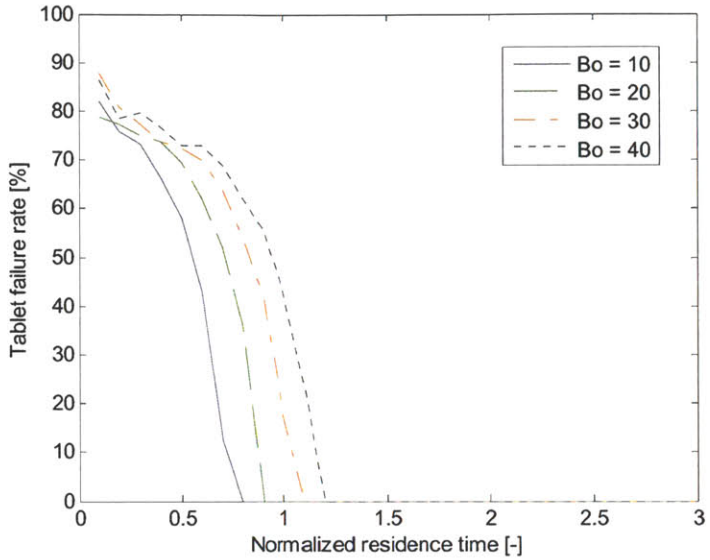

Figure 4-6: Projected Tablet Failure Rate during Markov Simulations

The Markov modeling provided a theoretical foundation for iterative design and experimental work. In sum, the simulations suggest that the mean residence time must be greater than the input oscillation period of the feeding equipment, with order of magnitude gains up to a normalized residence time of 2. While Bodenstein numbers can also have a positive effect on blending performance, the gains between higher mean residence times and lower Bodenstein numbers overlap and become redundant at higher normalized residence times. Thus, the Markov models indicate that higher mean residence times should be the focal point of improving VRR along the axial dimension.

5 Experimental Methodology

This chapter details the materials, equipment, and method of approach for blending experiments. Blender design, choice of API, and selection of excipients were based on literature research and standard protocol in the pharmaceutical industry, particularly the work of Pernenkil [54].

5.1 Materials

Pharmaceutical material for tablets is broadly split into two groups – the API, responsible for pharmacodynamic behavior, and excipients, which adjust the operational or pharmacokinetic properties of the tablet. Excipients can be sorted and added to the pharmaceutical recipe depending on the specific purpose. For example, fillers simply provide tablets with bulk, while lubricants coat the powder mixture to improve flowability during processing and manufacturing. Two API and five excipients were used during the course of this research, summarized below in Table 5-1. All materials were sealed from moisture during storage.

Material	Particle Size		Density
	μ (μm)	σ (μm)	(g/cc)
Acetaminophen	110	-	0.267
Caffeine	196	100	0.576
DCL11	100	50	0.595
DCL14	110	70	0.641
Parteck M200	160	110	0.568
Avicel PH-102	100	-	0.378
Avicel HFE-102	100	-	0.386

Table 5-1: Material Properties

5.1.1 Active Ingredients

Acetaminophen

Acetaminophen (also known as N-(4-hydroxyphenyl)-acetamide or paracetamol) is a common analgesic and anti-pyretic used in the treatment of headaches, pains, cold, and flu, perhaps better recognized as the main ingredient in Tylenol. Acetaminophen was obtained from Sigma-Aldrich as an anhydrous white powder. A slight tendency to clump during handling was observed.

Caffeine

Caffeine (1,3,7-trimethylpurine-2,6-dione) is a naturally occurring xanthine alkaloid and a well known psychoactive stimulant. Caffeine was obtained from Sigma-Aldrich as an anhydrous white powder. A pronounced tendency to clump during handling was noted.

5.1.2 Excipients

DCL11

Direct compressible lactose, grade 11 (DCL11) is composed of both amorphous and crystalline forms of lactose, a disaccharide derived from the glycosidic linkage of galactose and glucose. DCL11 particles have been spray dried to create spherical shapes, improve powder flowability, and reduce the need for lubricants. DCL11 was obtained from DMV-Fonterra Excipients.

DCL14

Direct compressible lactose, grade 14 (DCL14) also consists of spray dried lactose in both crystalline and amorphous forms. DCL14 has a larger mean particle size and a wider distribution of particle sizes than DCL11. DCL14 was also obtained from DMV-Fonterra Excipients.

Parteck M200

Parteck M200 is composed of mannitol ((2R,3R,4R,5R)-hexane-1,2,3,4,5,6-hexol), a naturally occurring sugar alcohol often chosen as an excipient due to its low solubility and sweet taste. Parteck M200 is a free flowing, high compactibility formulation of mannitol, obtained from EMD Chemicals.

Avicel PH-102

Avicel PH-102 consists of microcrystalline cellulose (MCC) in irregular shapes and sizes to promote compaction. Cellulose is a biopolymer chain of D-glucose units most commonly found in nature as the structural component of plant cell walls. In pharmaceutical development, MCC is a widely used as a filler and binder. Due in part to the particle shapes, Avicel PH-102 may not exhibit free flowing characteristics under a high moisture environment. Avicel PH-102 was obtained from FMC Biopolymer.

Avicel HFE-102

Avicel HFE-102 is composed of roughly 90% MCC and 10% mannitol, a novel blend intended to improve flowability and compactibility. Given the chemical composition, Avicel HFE-102 was expected and observed to possess powder characteristics similar to both Avicel PH-102 and Parteck M200. Avicel HFE-102 was also obtained from FMC Biopolymer.

5.2 Equipment

An overview of the hardware used in experiments is provided below. The section begins with a description of various elements of the blending devices, then details the powder feeder and the near-infrared spectrometer. More common devices employed in this methodology, such as the weigh scale and the tachometer, are not expanded here but discussed in experimental procedure.

5.2.1 Blender

A total of four blenders were constructed and utilized in the design of experiments. Blender parts were custom-designed and fabricated by the MIT Central Machine Shop. Each blender consisted of a shaft sitting inside a shell and capped by end plates. The blender assembly was mounted onto a vertical plate with a heavy base. The plate also houses a 24 V DC motor that was secured to the exposed shaft via interlocking joints. A near-infrared spectrometer was positioned next to the analytical ports in the shell to provide real-time monitoring. A depiction of the complete configuration is shown in Figure 5-1.

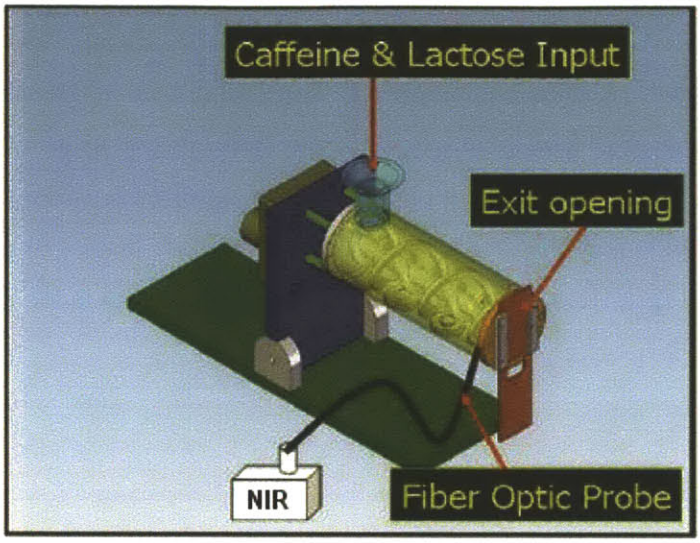

Figure 5-1: Physical Configuration of Blender

The shell and end plate are shown in Figure 5-2. The shell is composed of poly(methyl methacrylate), with an input port on the top of the upstream end and analytical ports on the bottom of the downstream end. The analytical ports are quartz panels which lay flat against the inner diameter of the shell, maintaining the operational integrity of the rotating shaft. The ends of the shell are threaded to affix the end plates. Both end plates include a central opening where the shaft will sit and centers the shaft for rotation within the shell. Ball bearings float between the each end plate and the shaft, enabling free rotation. The downstream end plate also contains two weirs that serve as the outlet ports of the blender.

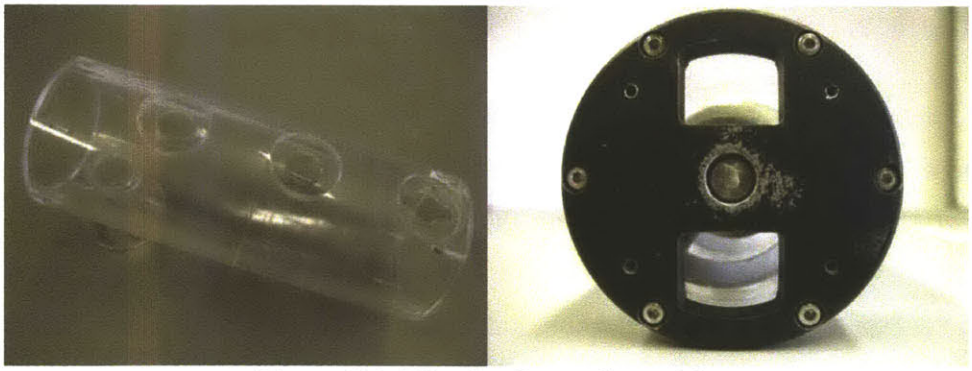

Figure 5-2: Blender Outer Assembly

Two types of shafts were designed for blending. The double helical ribbon shafts consist of two concentric helices with opposite pitching – the outer helix propels particles forward while the

inner helix pushes particles backward. The original shaft is 15 cm in length and 5 cm in diameter and made of polymeric stereolithographic resin, with steel pins connecting the ribbon structure to the central shaft. A clearance rate of 0.5 mm was set between the shaft and the inner wall of the shell to protect the shell from damage during operation. The same clearance rate was also used between the two concentric helices to create a free surface for powder movement. Two additional versions of the double helical ribbon shaft were also manufactured, both made of grade 17-4PH stainless steel. The double length version extends the shaft to 30cm in length while the half scale version shrinks the shaft to 7.5 cm in length and 2.5 cm in diameter.

The paddle shaft consist of a series of rectangular paddles jutting out of the central shaft at a 2° tilt to provide greater radial movement and impart a small net forward axial velocity, as proposed by Marikh et al. [52]. Each segment of the paddle shaft contains two paddles on opposite sides of the shaft, with each set alternating in a 90° configuration rotation from the adjacent segments. The paddle shaft was made at the original scale of 15 cm in length and 5 cm in diameter, with a total of 16 paddles. All four shafts are pictured in Figure 5-3.

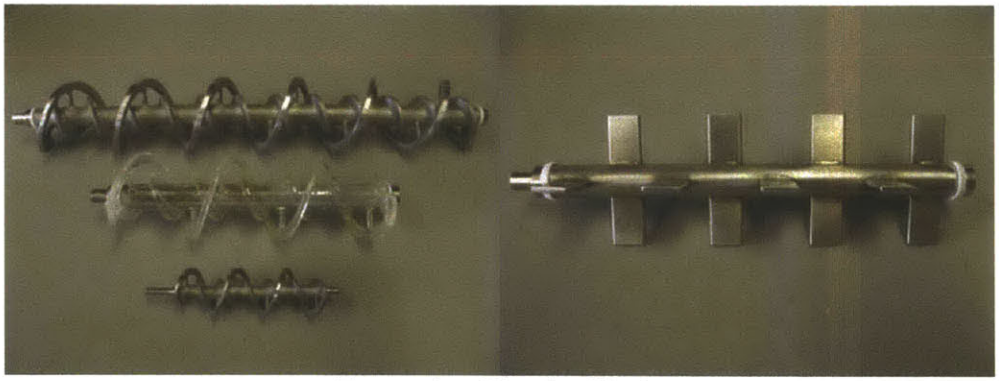

Figure 5-3: Blender Shafts

The four shafts and three shells can be combined to form four different blender assemblies – the original scale ribbon blender (Figure 5-4), the double length ribbon blender (Figure 5-5), the half scale ribbon blender (Figure 5-6), and the original scale paddle blender (Figure 5-7). In all four figures, material enters through the inlet port on the left and is propelled through the blender by the action of the shaft. Particles pass by the analytical ports where real-time measurements are collected before exiting through the weirs in the outlet end plate.

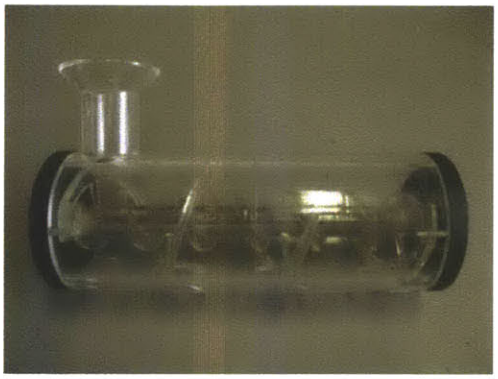

Figure 5-4: Original Scale Ribbon Blender

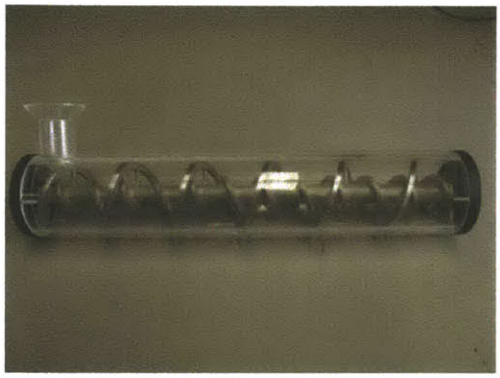

Figure 5-5: Double Length Ribbon Blender

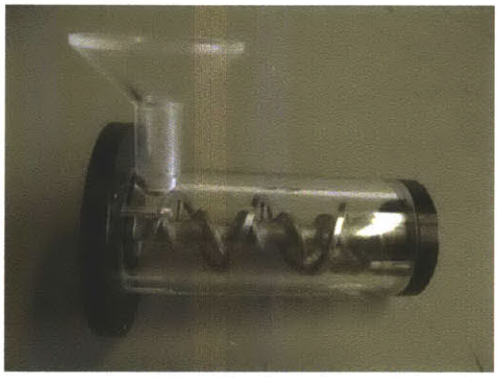

Figure 5-6: Half Scale Ribbon Blender

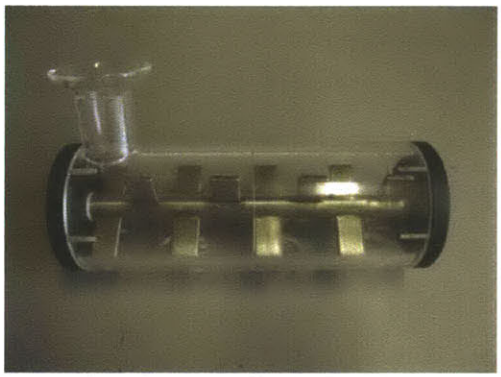

Figure 5-7: Original Scale Paddle Blender

5.2.2 Feeder

A Schenck AccuRate feeder (Tuf-Flex Series 300) was used to deliver excipients to the blender. The feeder consisted of a hopper funneling down to a nozzle where a rotating helix or screw dispensed powder out. The feeder sat on top of a counterbalance scale and was linked to a feedback control system. The loss-in-weight during feeding was actively measured, allowing the PID algorithm to adjust the shaft rotation rate to match a set mass flow rate. Using different screws or helices, flow rates ranging from 0.1 to 15 kg/hr were achievable.

Figure 5-8: Schenck AccuRate Feeder

5.2.3 Near-Infrared Spectroscopy

The majority of experiments relied on near-infrared spectroscopy for analysis. When molecules are excited by light, relaxation from higher vibrational states occurs through emission of electromagnetic radiation in the near-infrared range. The absorbance of NIR wavelengths provides a signature of the composition of matter in the analytical space, containing information on both chemical identity and physical positioning. An Axsun NIR Analyzer was used to collect NIR data in the 1350-1850 nm range. The spectrometer consists of a Class 1 laser with a flexible detection platform and microelectromechanically tunable optical filters to rapidly measure NIR spectra over discrete ranges.

While the NIR spectra provide indirect chemical and physical information, calibration samples and multivariate statistical analysis are necessary to translate the readings to relevant parameters of interest. Projections to latent structures are necessary to distill the large number of X variables (in this case, absorbance data for 501 wavelengths) in order to glean the Y variable of interest (in this case, the API%) from a small number of observations. Section 5.3 will cover the application of multivariate data analysis to this thesis is broader terms, while Section 5.4.2 below will detail the specifics of leveraging statistical techniques to translate NIR data.

5.3 Multivariate Data Analysis

Scientific research is the process of collecting observations about variables. In traditional data collection, a large number of observations are made regarding a relatively small number of independent variables. This creates data sets commonly described as "long and lean" – more rows

of observations than columns of variables. Such a data set lends itself well to classical methods of statistical analysis, such as linear regression and analysis of variance. When the data is statistically powered and variables are independent, the common scientific method of developing correlations and models is widely accepted.

However, this luxury is not always affordable. In the age of increasingly sophisticated analytical technology and massive servers of data, problems at hand may not be tractable with traditional analytical tools. In particular, "short and wide" data sets are becoming prevalent – statistically underpowered data with more columns of variables than rows of observations. Such data sets occur often in chemometrics, the field of extracting information from analytical data on chemical systems. As in the case of NIR spectroscopy, hundreds of variables (such as 501 wavelengths of absorbance) may be employed to detect a single underlying chemical property (such as the API% by mass). The data is expected to be noisy and variables exhibit different degrees of correlation with respect to the primary Y variable of interest and other X variables.

Problems such as dimensionality and multicollinearity have been discussed for decades [56-58]. Advances in statistical analysis and computing power have allowed a variety of multivariate tools to address such issues. Two key methods, principal component analysis and projections to latent structures, are described in brief below. Further exploration in the literature is higher encouraged to develop a stronger sense of the material [57-59].

5.3.1 Principal Component Analysis

Principal component analysis is a mathematical transformation which converts a set of variables into principal components which capture the data in fewer dimensions. PCA was first proposed by Pearson [60] and can be used to simplify and visualize multi-dimensional data in order to discover correlations, trends, and outliers. For a given set of data, PCA determines "the lines and planes of closest fit" by identifying the linear combinations of the variable space which yield the least squares for the PCA fit. These orthogonal principal components explain the spread of data while reducing the dimensionality, stripping out noise and revealing which variables move together through their composite interaction with the principal components.

The fundamental mathematical foundation of PCA is represented in Equation (5-1). The data set X can be separated into three factors – pre-treatments, principal components, and noise. A

given set of data is first pre-treated to give equal weighting to each variable and objectively shape the data for analysis. Common techniques include unit variance scaling and mean-centering. The principal components are represented by the matrix TP', where T are the scores which map the relationship between the observations and the principal components while P' are the loadings which carry the weighting of the variables in the principal components. This matrix contains the least squares PCA model, while the matrix E contains the residual noise.

$$X = 1\bar{x}' + TP' + E \tag{5-1}$$

PCA is a flexible statistical process and forms the basis of numerous derivative multivariate analytical methods, including projections to latent structures.

5.3.2 Projections to Latent Structures

Projections to latent structures leverages the mathematical foundation of PCA to find the relationship between a set of factors X and a set of responses Y. Rather than determining the scores and loadings which maximize the explained variance in X, PLS seeks to maximize the explained covariance between X and Y. The PLS model builds on top of the PCA framework through the addition of Equation (5-2), where the scores matrices T and U and linked through an inner relation. PLS thus utilizes the principal components of X in order to best explain the variability in Y.

$$Y = 1\bar{y}' + UC' + F \tag{5-2}$$

$$U = T + H$$

PLS has two separate applications in this current research. First, PLS was used to construct NIR calibration models translating NIR spectral data to chemical composition. Specifically, PLS modeled the relationship between absorbance values at 501 wavelengths and the API mass percentage. Second, PLS was employed to explore the correlations between experimental variables, such as design characteristics, operating parameters, material properties, and performance metrics. In this application, PLS serves more as an identification tool for determining key variables of interest which should receive greater focus in blending optimization

efforts. Both statistical methods are necessary for this work given the large number of variables available and the limited number of observations, as detailed below in Section 5.4.

5.4 Experimental Procedure

A series of experiments were used to collect data on blending performance. The relationship between these studies is shown in Figure 5-9. At the lowest level, fill weight experiments were conducted by running pure excipient through the various blenders at different operating parameters. This non-destructive processing technique gave quick estimates of space time, the amount of time a particle spent in the blender, and fill fraction, the percentage by volume of the blender occupied by material. At the next level, residence time distributions were conducted by adding an impulse shot of API to a steady-state stream of excipients to determine the system response to the API. This yielded data on the mean residence time, the average amount of time an API particle spent in the blender, and the Bodenstein number, a measure of the variability in mean residence time. Finally, full blending experiments were also conducted where a continuous signal of API over time was fed to a steady-state blender to determine the VRR. When the blending studies were repeated with different frequency feed inputs, the frequency response provided another dimension of data on blending performance.

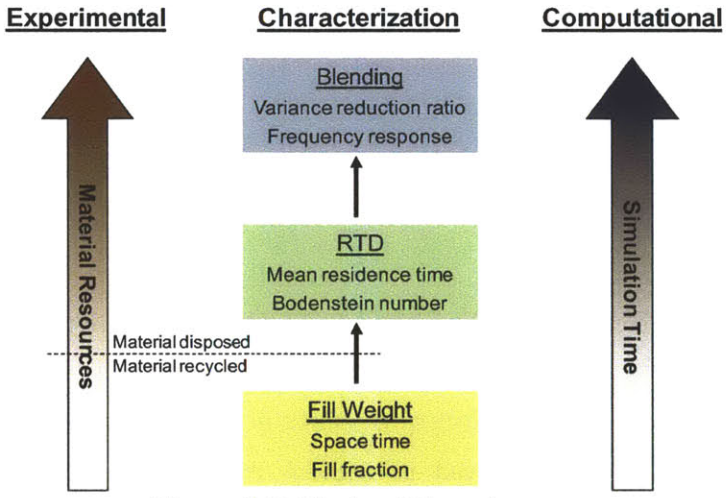

Figure 5-9: Chain of Experiments

This chain of experiments yielded a host of metrics by which to evaluate the performance of the blender in any given configuration of design, operational, and material parameters. As indicated

in Figure 5-9, these metrics can be reached with differing degrees of technical complexity, time, and cost. While fill weight studies can be done economically and rapidly with no unsalvageable loss of material, the intermediate metrics it provides may be less relevant to the primary metric of concern, the VRR. On the other hand, full blending experiments give direct results but can be prohibitively expensive to run at manufacturing or in a rigorous design set, especially with new API that is still in development and only available in rare quantities.

This hierarchical approach to design space exploration produced data sets on primary parameters, intermediate metrics, and the VRR, which could be collated to develop a deeper understanding of the complex interrelationships in this process system. As proposed in the thesis objectives, this longitudinal structure enables correlation studies between all variables of interest. Multivariate analysis can be employed here to disentangle multicollinearity and highlight key parameters to leverage for improving blending performance.

5.4.1 Fill Weights

Fill weight experiments were conducted by placing the blender assembly on top of a weigh scale and running pure excipient through the system to reach steady-state operation. Mass flow rate was adjusted through the feeder controller while the shaft rotation rate was tuned by manually correcting the voltage supplied to the motor in order to match the reading on the tachometer. Care was taken to configure the fill weight system such that the material interfaces were free of direct physical connections to eliminate variability in the weigh scale readings. For any given set of operating conditions, the weight of material in the blender was measured once steady-state was achieved. To attain results in triplicate, steady-state was disrupted and allowed to resettle again. The average weight was then used to calculate both the space time and the fill fraction. A linear correction was applied to the space time to account for the relative lengths of the blender from end to end and from input to the analytical port. This adjustment made the values more directly comparable to those parameters ascertained from near-infrared spectroscopy.

5.4.2 NIR Calibration

Higher-level metrics were computed through API% over time, as determined via near-infrared spectroscopy. This characterization technique requires calibration with known samples in order to

accurate interpret the spectral results. NIR calibration was conducted in each instance with samples of the API-excipient combination that had been mixed in a V-shaped blender for 30 minutes to reach homogeneity, as per Ngai [46]. Samples ranged from 0% to 50% according to API% by mass. NIR reflectance values were collected from each sample at 501 different wavelengths (1350 to 1850 nm). The spectra was prepared for data analysis, following general chemometric protocol as per Brereton [58] – conversion to unit variance scale, then application of an 11-point first-derivative Savitzky-Golay filter and a standard normal variate transform. This data treatment reduces noise in the chemometric signal while removing the effect of density and ambient light on the data. The top half of Figure 5-10 shows the processed signal for a complete set of calibration samples for caffeine and Avicel PH-102. Due to differences in the chemical signature of the API versus the excipient, the spectra diverge in the near-infrared range as API concentration is varied, although the extent of divergence depends upon the relative resonance between each wavelength and the various compounds.

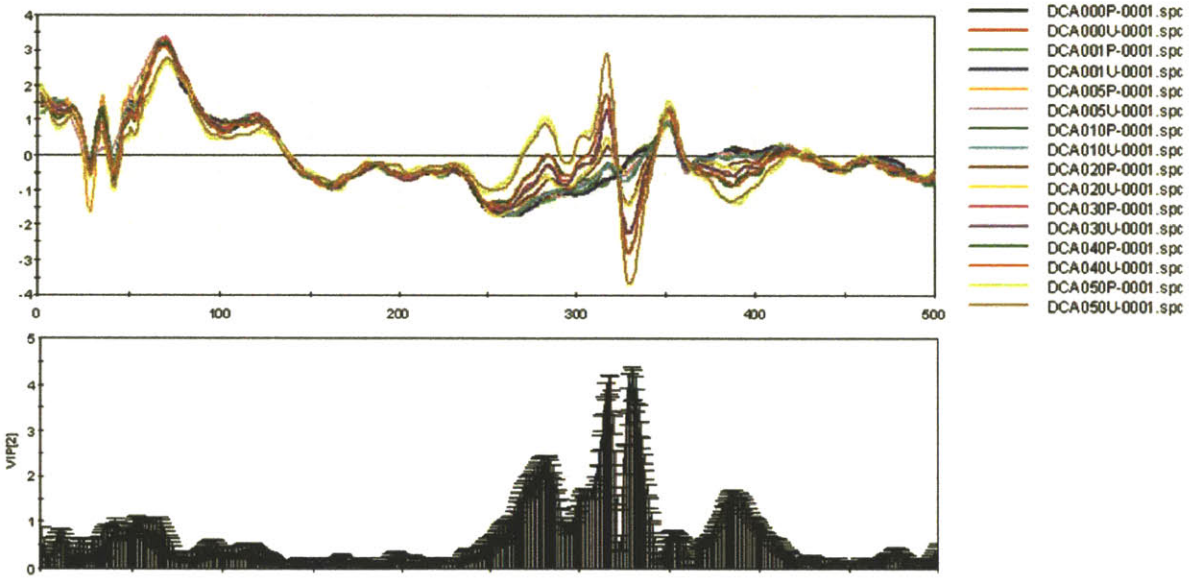

Figure 5-10: Intermediate NIR Data Processing

A PLS model was assembled in SIMCA-P+ using the processed NIR data and the API% values of the known samples. The PLS model was built using the preset algorithms to quantify the importance of each variable to the metric of interest. The bottom half of Figure 5-10 shows the variable importance plot for the same wavelengths. Notice that the spectra for the calibration samples diverge more at certain wavelengths that resonate more with the chemical identity of the

API than the excipient. The PLS model attributes greater weighting to those wavelengths in the statistical regression with respect to API%.

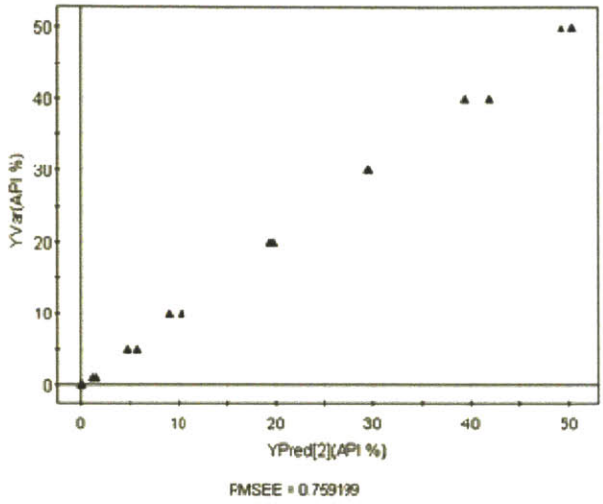

Figure 5-11: PLS NIR Calibration

The result is a PLS calibration shown in Figure 5-11. The calibration can be evaluated by several statistical metrics, including R2Y (the amount of Y variability explained by X) and Q2 (predictive ability of the model as checked by statistical cross-validation). PLS models of NIR samples yielded R2Y and Q2 values above 0.95 for all calibrations used in data collection, indicating strong correlation and translation of NIR spectral data to API% values.

5.4.3 Residence Time Distribution

Residence time distributions were obtained by monitoring the outlet API% after an impulse shot of API was administered to a steady-state stream of excipient flow. The quantity of the shot was set to be 10% of the average weight observed at the same operating conditions during the fill weight studies to ensure a strong data signal. NIR spectra was recorded at the analytical port every 2 s by automated Axsun software. The duration of the experiment was set to a minimum of twice the relevant space time to ensure the full residence time distribution was captured. Figure 5-12 shows the sample NIR output upon PLS translation in blue dots.

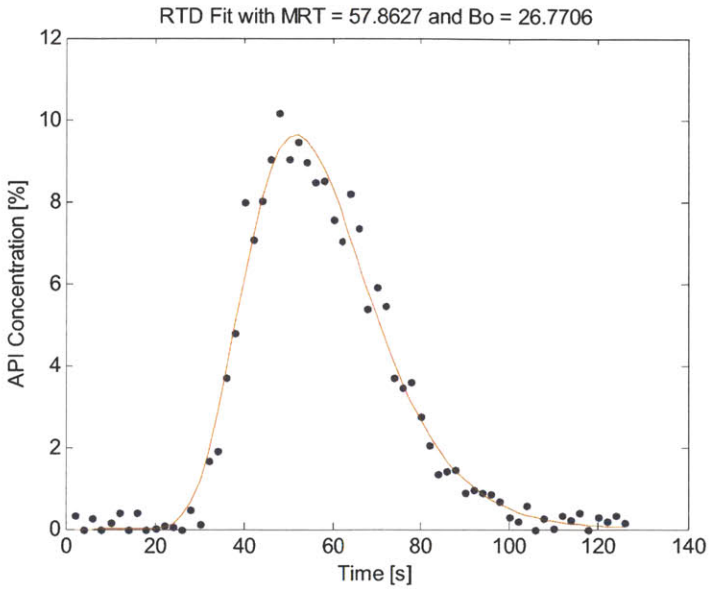

Figure 5-12: Fitting of RTD Data to Axial Dispersion Model

Blending in an axially mixed system can be modeled as one-dimensional axial dispersion using the Fokker-Planck equation, shown earlier as Equation (2-1). When non-dimensionalized, key parameter Bo indicates the Bodenstein number, a measure of velocity versus dispersion and the solid equivalent of the Peclet number for liquids.

Along the length of interest, from the inlet port to the analytical port where NIR spectra is collected, dispersion occurs both immediately upstream and downstream, resulting in tractable open-open boundary conditions. Fogler [61] derived the solution to be Equation (5-3):

$$E(\theta) = \sqrt{\frac{Bo}{4\pi\theta^3}} \exp\left(-\frac{Bo(1-\theta)^2}{4\theta}\right) \tag{5-3}$$

The open-open solution to the one-dimensional axial dispersion model was used to characterize the residence time distribution via two parameters – the mean residence time and the Bodenstein number. A sample fitting in shown in Figure 5-12, where the red line delineates the axial dispersion model overlaid on the NIR data. Mean residence time averages the duration of a particle in the blender, while the Bodenstein number indicates the width of the distribution and the amount of variability in particle duration over the entire range of probabilities.

5.4.4 Blending

In full blending runs, API is constantly fed at a given frequency to a steady-state stream of excipients in order to characterize the system response to an input signal. At these small scale manufacturing rates, feeder technology is not yet capable of delivering an input with any more sophistication than a constant rate. In order to reconcile the experimental work with previous theoretical understanding, API feed was delivered manually to mimic the sine wave signals from the Markov simulations. Four dosages were fed sequentially in ascending and then descending order, producing a cycle of six shots – 25%, 40%, 50%, 40%, 25%, then 0%. The dosage was set such that an overall API mass of 5% was maintained in the blender at steady-state. In the 60 s feed frequency, API shots were 10 s apart, while in the 30 s feed frequency, API shots were 5 s apart. Table 5-2 provides the API feed schedule for given excipient flow rates.

Excipient	30 s Feed Frequency				60 s Feed Frequency			
Flow Rate	Mass of API per Feed (g)				Mass of API per Feed (g)			
(kg/hr)	0%	25%	40%	50%	0%	25%	40%	50%
2	0.00	0.14	0.22	0.28	0.00	0.28	0.44	0.56
5	0.00	0.35	0.56	0.69	0.00	0.69	1.11	1.39
10	0.00	0.69	1.11	1.39	0.00	1.39	2.22	2.78

Table 5-2: API Feed Profiles for Blending

Feeding during blending runs continued for a minimum of 5 minutes to ensure enough cycles at the new steady-state. Figure 5-13 shows a representative sample output, with the same ramp-up to steady-state as the Markov simulations and a ramp-down once API feeding is discontinued. Based on the Markov work, data collection for VRR calculation began after two mean residence times (based on the relevant residence time distribution experiment) had elapsed. Only full cycles of data were incorporated for VRR calculation. The red lines in Figure 5-13 mark the sample data used in this instance to determine the output variance.

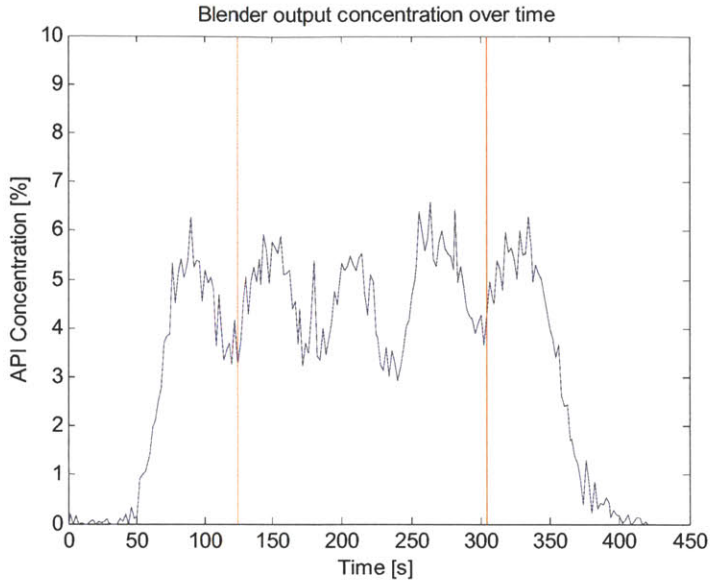

Figure 5-13: Sample of Full Blending Data

The resulting VRR could then be recorded along with other intermediate metrics determined for the same operational setting – fill fraction, space time, mean residence time, and the Bodenstein number. These metrics, along with the original design characteristics, operating parameters, and material properties, will be evaluated through close juxtaposition and multivariate data analysis in the following chapter detailing the experimental results.

6 Double Helical Ribbon Blending Results

The experiments described in the previous chapter were conducted on three double helical ribbon blenders. The results of each procedural set are first discussed separately with respect to intermediate parameters of note. Data was then aggregated for multivariate analysis.

6.1 Fill Weight Experiments

Fill weight experiments were conducted over a range of mass flow rates and rotation rates, using five excipients and three ribbon blenders. The steady state hold-up weight of powder in the blender during continuous operation enabled calculation of the fill fraction and the space time. The effect of design and operating parameters on these values is discussed below. Initial results focus on 30 rpm fill weight studies conducted with Avicel PH-102 in the double length blender, and then expand to include more data sets as more parameters are presented.

Effect of Mass Flow Rate

A sample output from fill weight experiments over the feasible range of mass flow rates is shown in Figure 6-1. Three runs were conducted at each experimental setting, with each run result plotted as an individual data point. Hold-up weights and mass flow rates exhibited a strong positive linear correlation and the values were in close agreement after repeated trials. An increase in the mass flow rate filled the blender at a faster pace, causing the fill weight and fill fraction to increase as well. When the powder bed height rose, more powder was exposed to the mechanical motion of the shaft, until a new equilibrium was reached.

For the given bulk density of each excipient and free volume of each blender, the fill fraction of powder within the blender could be estimated. The action of the ribbon blender resulted in a net forward movement of powder in the axial direction, sufficient to carry powder downstream as new material was introduced into the blender. As a result, the fill fraction level was observed to be relatively even along the length of the blender. The same experimental set from Figure 6-1 was used to plot fill fraction over mass flow rates, shown in Figure 6-2. A similar positive trend was noted the two variables. Although the estimated fill fraction neglects the effect of powder dilation due to agitation, the resulting values seemed to fit with visual evidence. The maximum

mass flow rate at which continuous steady state operations could be maintained consistently yielded fill fractions of approximately 90%. The remainder was attributable to powder dilation and overhead necessary to accommodate movement of material along the length of the blender.

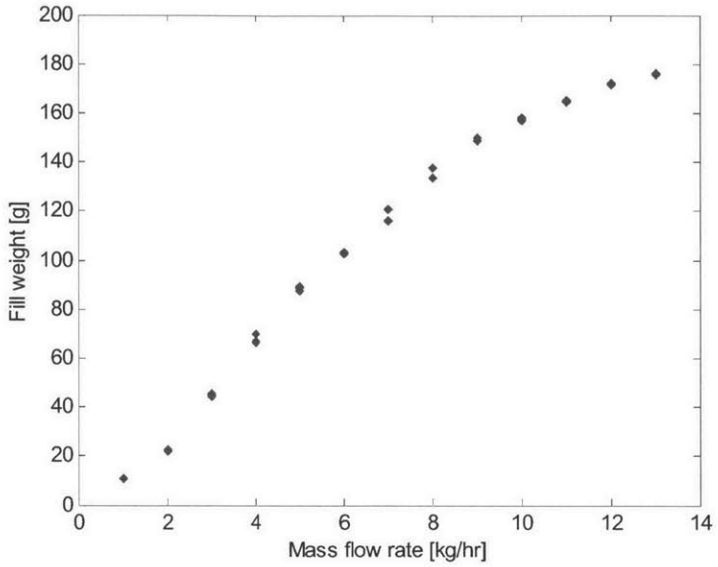

Figure 6-1: Sample Set of Fill Weight Results over Mass Flow Rates

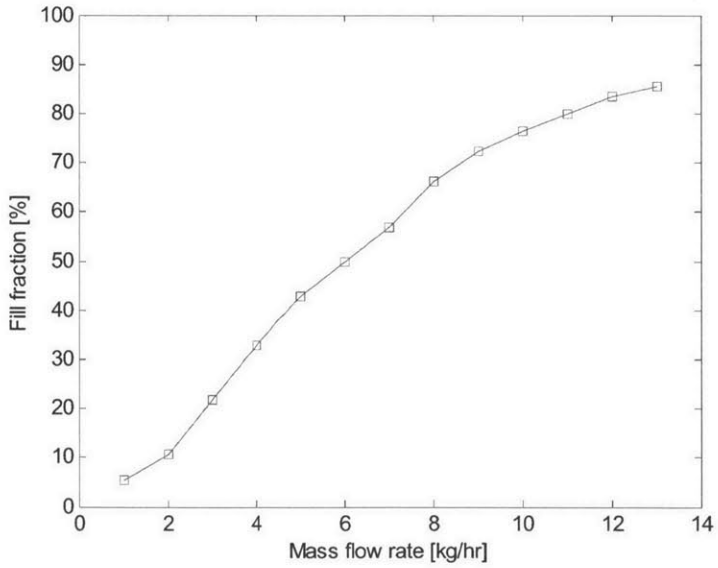

Figure 6-2: Fill Weight Results Converted to Estimated Fill Fraction

For the given mass flow rate and hold-up weight, the space time was also calculated. The space time indicated the average amount of time each excipient particle spent in the blender. The resulting values were plotted against fill fraction, as shown in Figure 6-3. Space times were lowest at low fill levels, where the powder bed was only exposed to the movement of the outer ribbon, which pushed powder forward towards the blender exit. At moderate levels of fill, powder was also in contact with the inner ribbon, which pushed powder upstream, yielding a lower net forward axial velocity and increasing the space time. At high fill fractions, the powder surface saw more of the top edge of the outer ribbon, once again increasing net forward axial velocity and decreasing the space time. Space time reached a broad, stable peak at around 40% fill fraction.

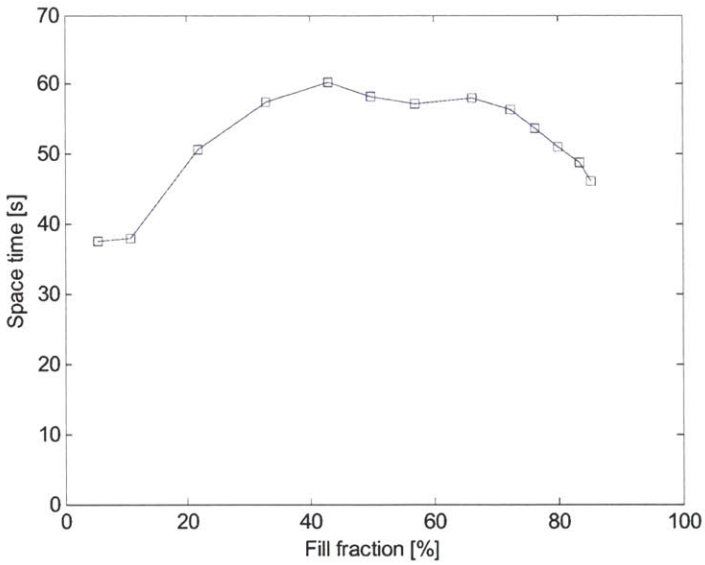

Figure 6-3: Space Time vs. Fill Fraction in Ribbon Blender

Effect of Rotation Rate

Fill weight studies were extended to incorporate the effect of various rotation rates of the internal shaft. Figure 6-4 includes fill fraction values at two additional slower rotation rates. With reduced mechanical input, powder in the blender experienced a lower net forward axial velocity. At the same mass flow rate, this resulted in an increase in the fill fraction. Since lower shaft speeds caused the blender to fill up faster as mass flow rate increased, lower rotation rates produced a smaller range of mass flow rates for feasible continuous operation.

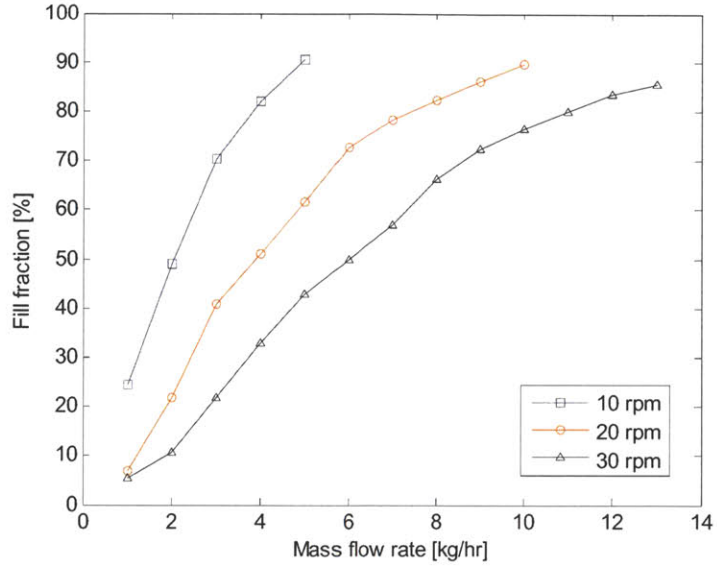

Figure 6-4: Fill Fraction vs. Mass Flow Rate for Different Rotation Rates

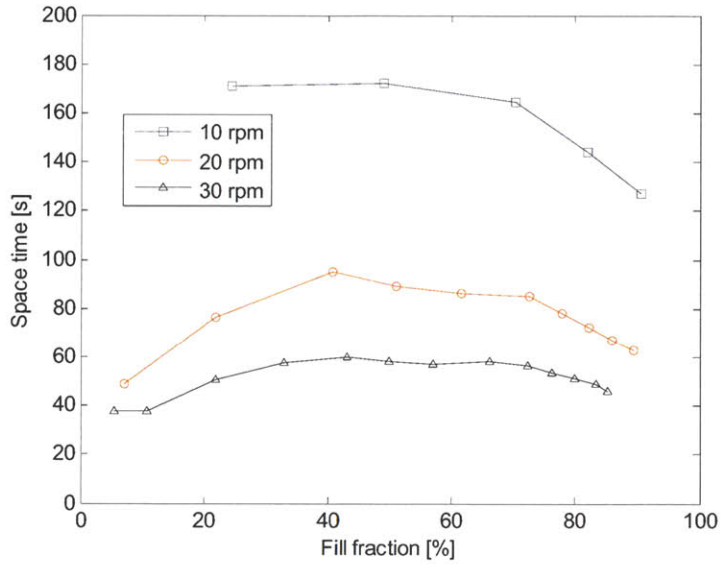

Figure 6-5: Space Time vs. Fill Fraction for Different Rotation Rates

The space time for different rotation rates is plotted in Figure 6-5. The same trend described earlier persists – low space times at low fill fractions, with a broad peak achieved at a fill fraction of 40%. However, the lower rotation rates induce a smaller net forward axial velocity, causing the space time curve to move upwards. Space time thus increases as rotation rates are reduced.

The results discussed so far can also be compiled into three-dimensional graphs of estimated intermediate parameters versus operating parameters. Fill fraction is shown in Figure 6-6 while space time is shown in Figure 6-7. Again, fill levels increase with higher mass flow rates and lower shaft rotation rates. Space times are relatively stable with respect to mass flow rates but increase significantly at lower shaft rotation rates.

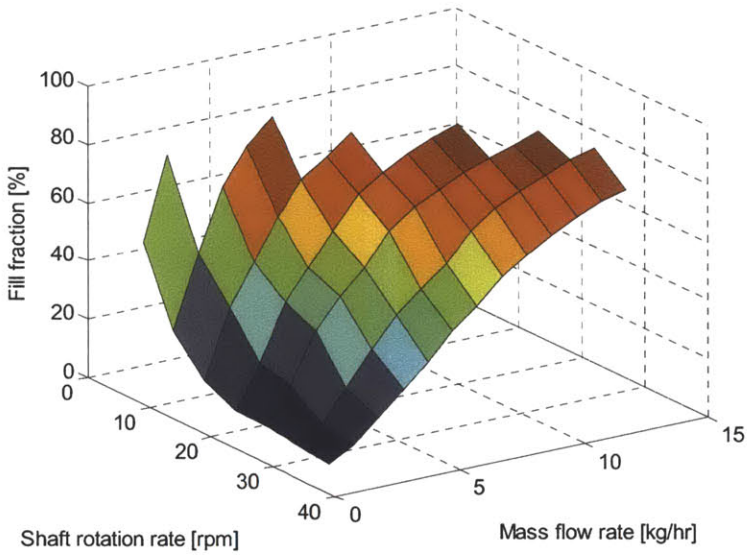

Figure 6-6: 3D Plot of Fill Fraction vs. Operating Parameters in Ribbon Blender

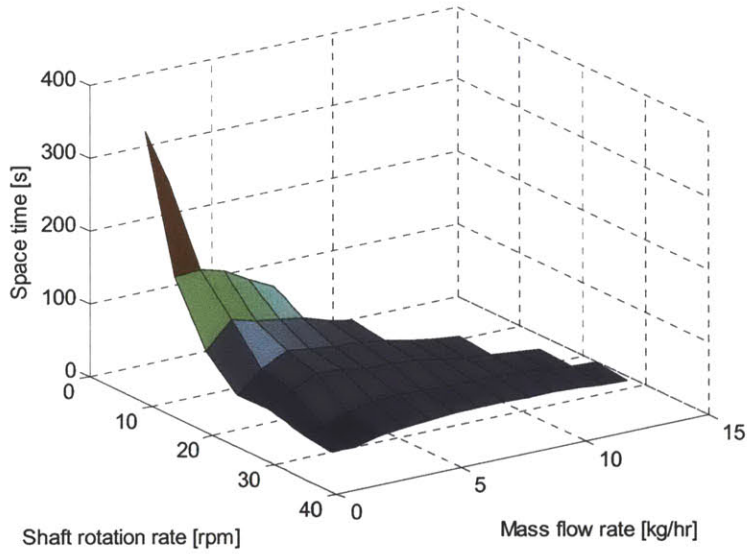

Figure 6-7: 3D Plot of Space Time vs. Operating Parameters in Ribbon Blender

The results discussed so far can also be compiled into three-dimensional graphs of estimated intermediate parameters versus operating parameters. Fill fraction is shown in Figure 6-6 while space time is shown in Figure 6-7. Again, fill levels increase with higher mass flow rates and lower shaft rotation rates. Space times are relatively stable with respect to mass flow rates but increase significantly at lower shaft rotation rates.

Effect of Excipients

The variance in bulk density across the five excipients necessitated a normalization of the mass flow rate to yield the volumetric flow rate. Figure 6-8 shows fill weight data for all excipients plotted as fill fraction against volumetric flow rate. Space times across all excipients are shown in Figure 6-9. The resulting trends were in agreement across all the excipients tested. This indicated that the first order effect of different excipients on blending dynamics could be accounted for by correcting with the bulk density of the given material. The aggregation of fill weight data also revealed a kink in the fill fraction curve and a more prominent peak in the space time curve at fill levels of 40%. This was due to the double helical nature of the shaft design. The relative exposure of powder to the reverse-pitch ribbon was maximized around 40%, causing an inflection point in blending dynamics with respect to both fill fraction and space time.

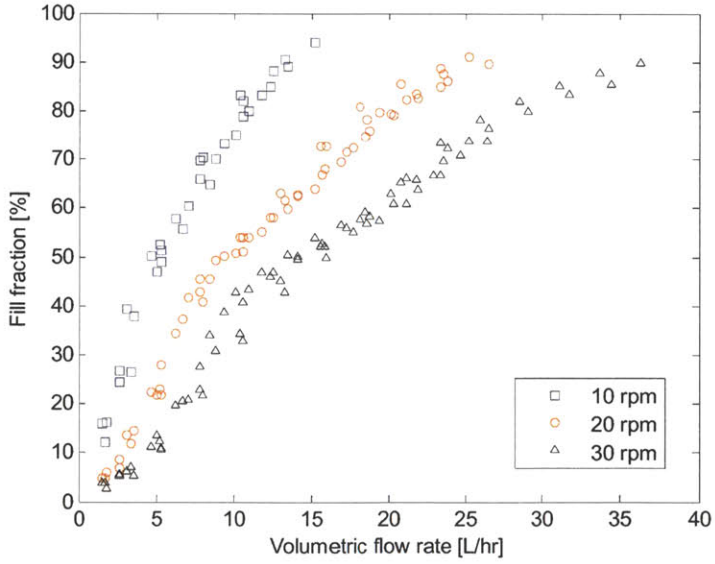

Figure 6-8: Fill Fractions for Different Excipients, Adjusted by Bulk Density

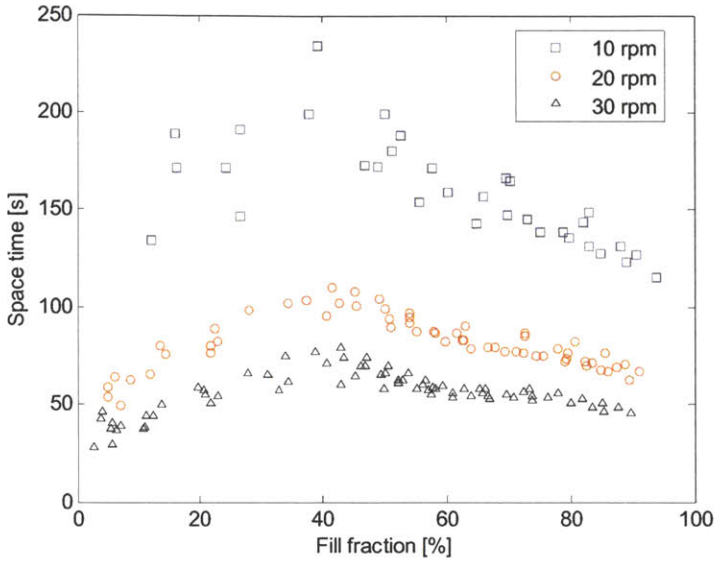

Figure 6-9: Space Times for Different Excipients

Effect of Length

The fill weight data for both the original blender and the double length version was overlaid to examine the effect of length on fill weight experiments. Figure 6-10 shows fill fraction versus volumetric flow rate with both sets of results at various rotation rates included. The effect of length on fill fraction was minimal, as the positive correlation with respect to volumetric flow rate and negative correlation with respect to rotation rate are still apparent, albeit less discernible. The variability in the fill weight data was greater for original blender studies, likely due to the smaller scale of the experiments, which magnified the effect of noise on blending dynamics and error on fill weight data collection.

For a more direct comparison of the effect of length on fill fraction, fill weight studies at the same operating parameters were cross-tabulated across both blender data sets to produce Figure 6-11. Regardless of which blender was used, fill fractions were relatively consistent. A slight tendency toward higher fill fractions in the double length blender was noted. This may be due to minor manufacturing variability between the two shafts, and was not considered to be a significant effect in the multivariate analysis.

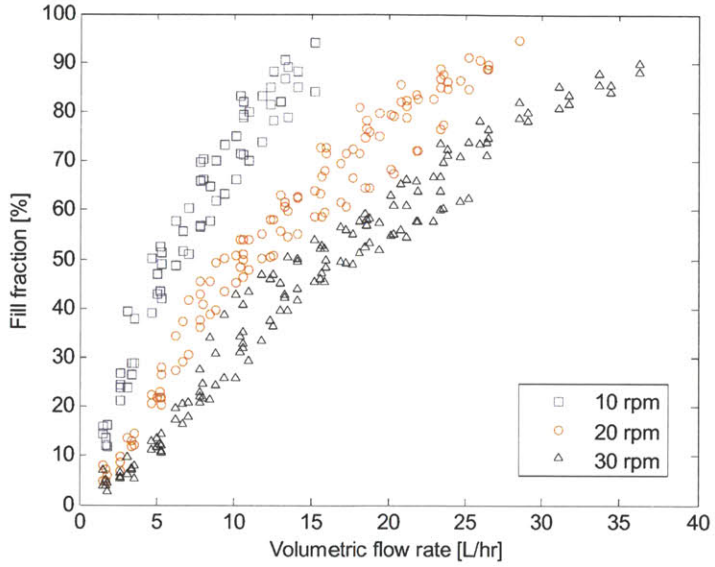

Figure 6-10: Fill Fraction vs. Volumetric Flow Rate for Different Blender Lengths

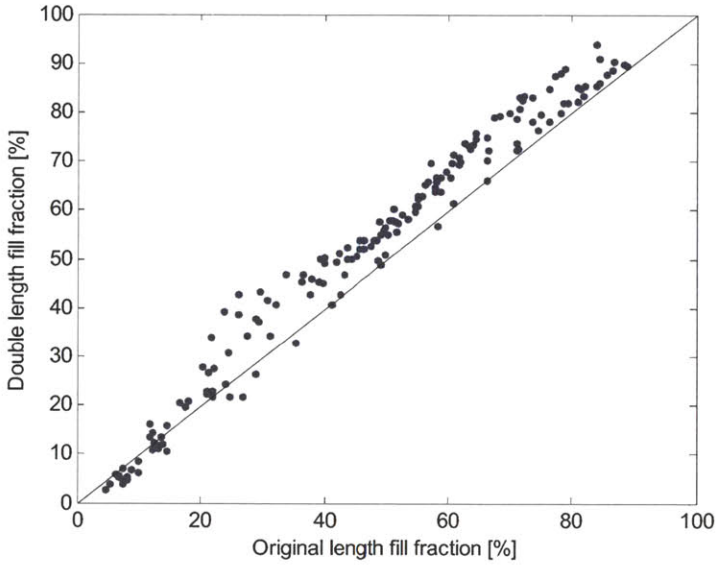

Figure 6-11: Comparison of Fill Fraction across Different Blender Lengths

The effect of operating parameters on space time for the original blender is shown in Figure 6-12. Space times were roughly half the value of those in Figure 6-9, as the length of the blender was halved. Again, more variability was observed within this data set, although the slight peak at 40% fill fraction was still visible. The same comparison is shown in Figure 6-13, where space times from the original blender were linearly extrapolated with length to predict space times in

the double length blender. A strong 1:1 correlation was also observed, indicating the effect of length was linear for fill weight experiments.

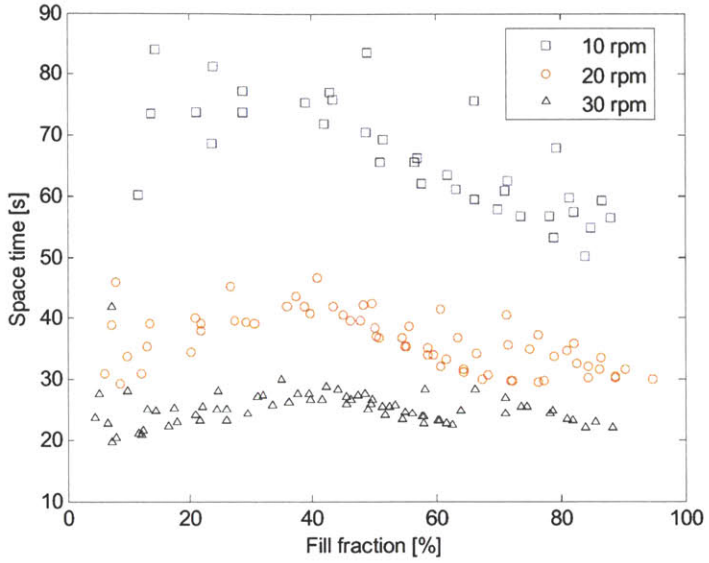

Figure 6-12: Space Time vs. Fill Fraction for Original Blender

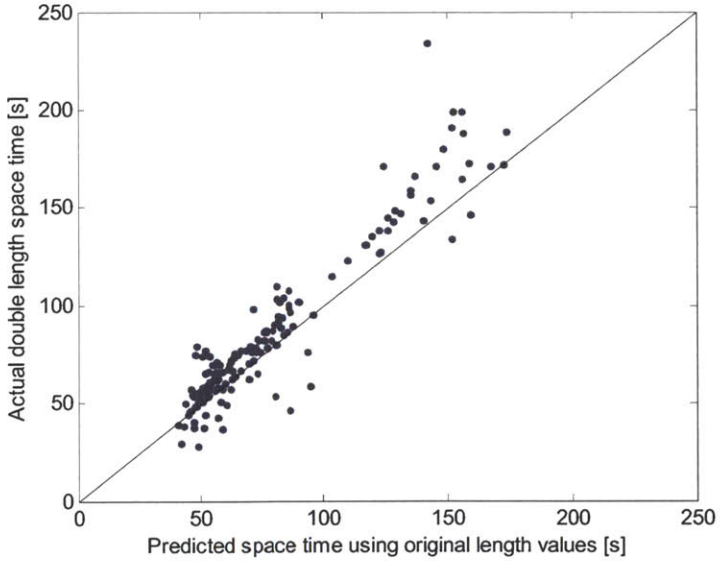

Figure 6-13: Comparison of Space Time across Different Blender Lengths

6.2 Residence Time Distribution Experiments

Near-infrared spectroscopy was used to characterize the impulse response over a similar range of operating parameters for two APIs, five excipients, and three ribbon blenders. The resulting residence time distributions were fitted to a closed-boundary, one-dimensional axial dispersion equation in order to determine the mean residence time and Bodenstein number. Estimated fill fractions from fill weight studies at the same experimental setting were leveraged to analyze residence time distributions. This convenient proxy for volumetric flow rate provides a more intuitive understanding of blending dynamics and enabled comparison across different excipients and blenders. The effect of design and operating parameters, along with the materials used, is discussed below.

Effect of Operating Parameters

Figure 6-14 shows the mean residence time with respect to fill fraction and rotation rate. The trends bore a striking resemblance to those of Figure 6-5, with mean residence time in place of space time. A peak was observed once more at the 40% fill level. This result was expected as both parameters are simply hold-up times; the former for the API and the latter for the excipient.

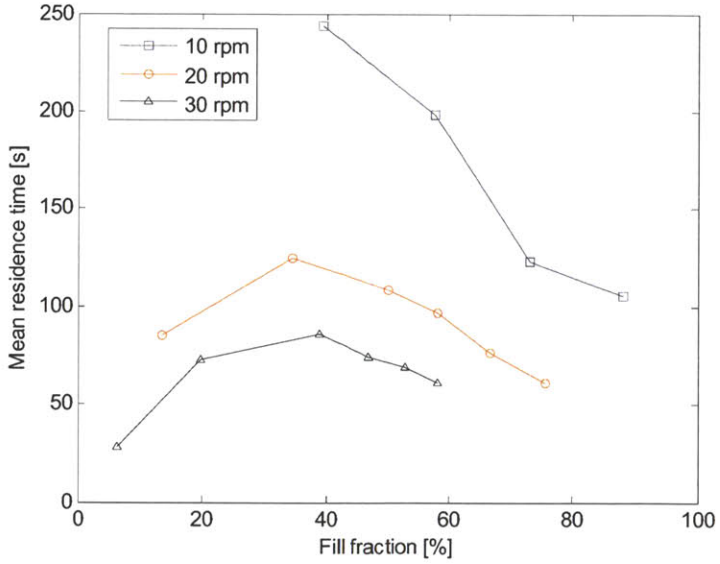

Figure 6-14: Mean Residence Time vs. Fill Fraction in Ribbon Blender

Effect on Shear Rate

Determination of residence time distributions also enabled calculation of the number of blade passes, the product between mean residence time and rotation rate, which reveals the average number of shaft rotations experienced by an API particle passing through the blender. This parameter provides a rough estimate of the amount of mechanical shear. Figure 6-15 shows the number of blade passes with respect to fill fraction. A peak was observed around the 40% mark. At the given shaft rotation rates, increases in blade speed were offset by decreases in the mean residence time, resulting in a similar number of blade passes.

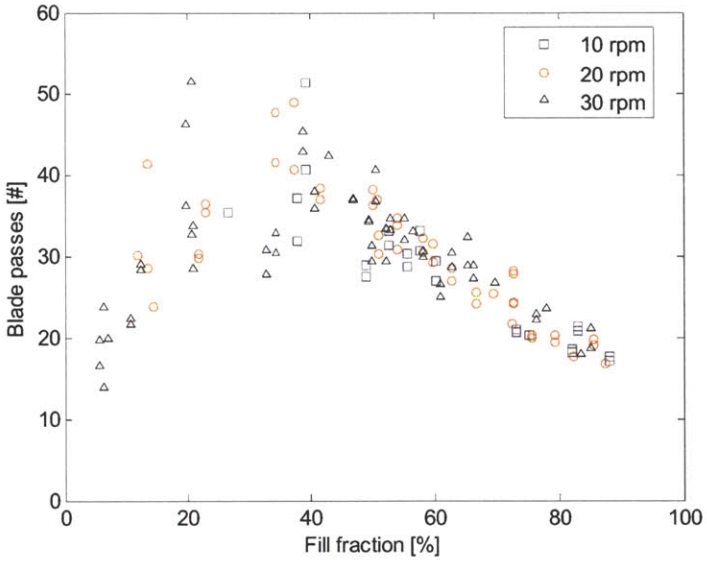

Figure 6-15: Blade Passes vs. Fill Fraction in Ribbon Blender

Effect of Excipients

The results for all excipients were aggregated to examine the effect of different excipients on residence time distributions. No correlation was found with respect to the Bodenstein number. The influence of fill fraction on mean residence time is shown in Figure 6-16. The trends were in agreement with those of space time in Figure 6-9.

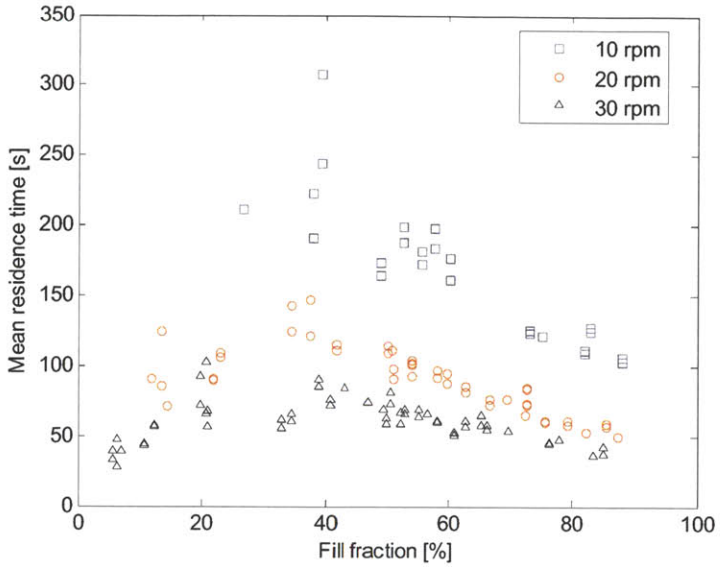

Figure 6-16: Mean Residence Time vs. Fill Fraction for Different Excipients

Effect of Length

Similar results are presented for the original blender in Figure 6-17. Mean residence time values were approximately half of those from the double length blender, reflecting the linear effect of length on transport time. The original blender results again exhibit greater variability, reflecting the difficulties of operating a solid continuous process at smaller scales.

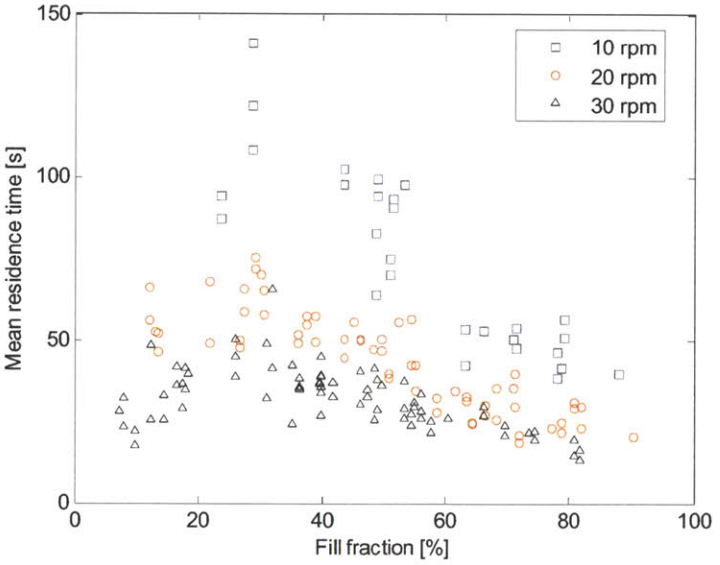

Figure 6-17: Mean Residence Time vs. Fill Fraction for Original Blender

A direct comparison across the two blenders is shown for mean residence time in Figure 6-18 and for the Bodenstein number in Figure 6-19. Just as with space times, mean residence times exhibited a strong 1:1 correlation with respect to length. On the other hand, Bodenstein numbers do not seem to correlate strongly with length either.

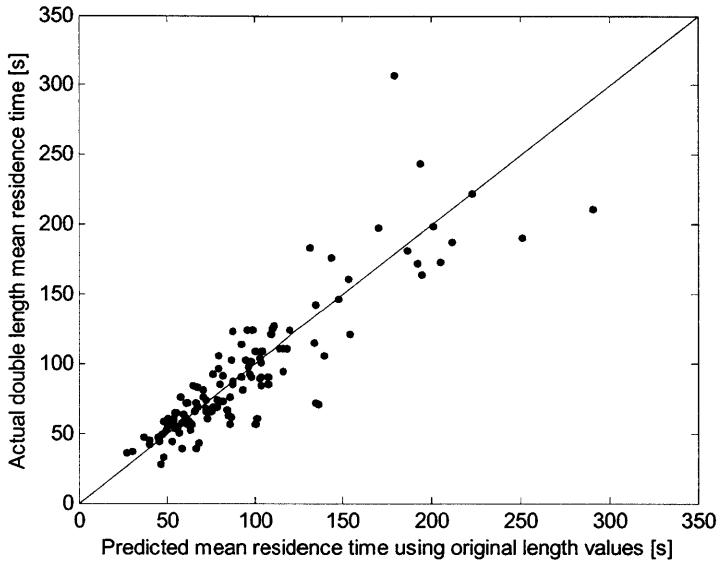

Figure 6-18: Comparison of Mean Residence Time across Different Blender Lengths

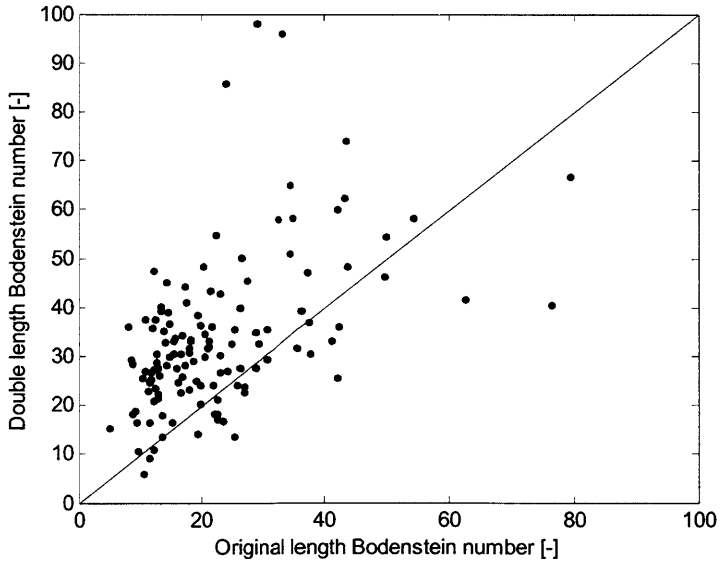

Figure 6-19: Comparison of Bodenstein number across Different Blender Lengths

Effect of API

Comparisons of mean residence time and Bodenstein number with respect to the two APIs used are shown in Figure 6-20 and Figure 6-21, respectively. A strong correlation for mean residence time and a weak correlation for the Bodenstein number were again observed.

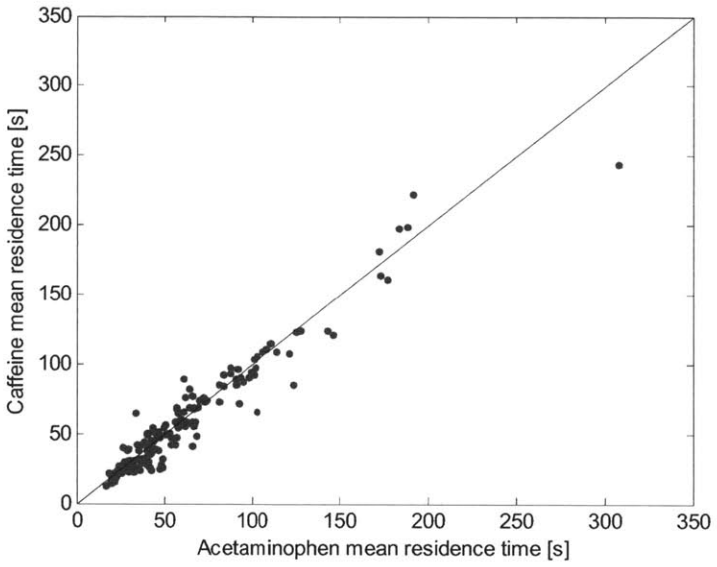

Figure 6-20: Comparison of Mean Residence Time across Different API

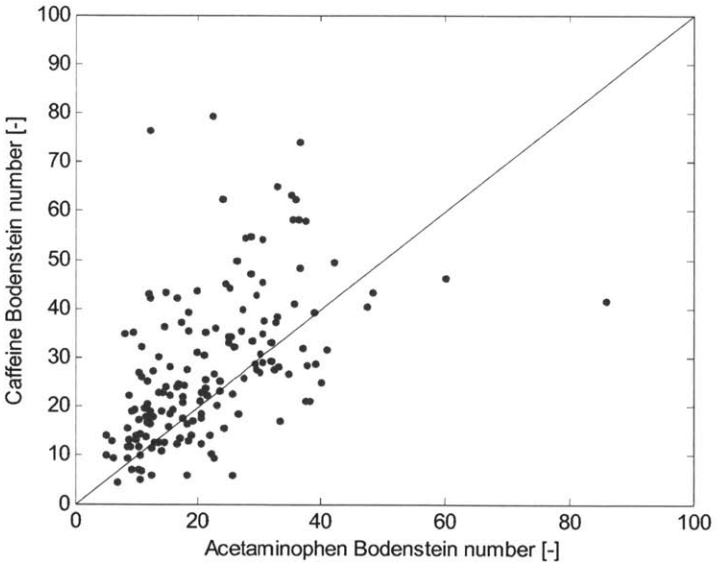

Figure 6-21: Comparison of Bodenstein number across Different API

While the mean residence time appears to scale relatively well, the Bodenstein number does not. This implies that the parameters and ranges used in this design of experiments provide little control over the Bodenstein number. For the given technology, this may be a necessary casualty of attempting to operate with cohesive material at such small scales.

Comparison to Space Time

Mean residence times and space times were compared in Figure 6-22 to determine the linkage between fill weight studies and residence time distribution experiments. As expected, a linear correlation exists between the two hold-up parameters.

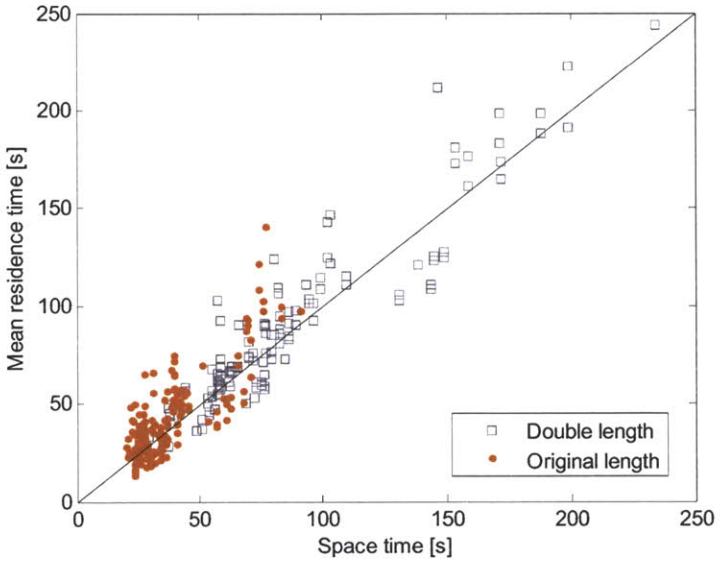

Figure 6-22: Comparison of Mean Residence Time to Space Time

This relationship indicates that space times may provide a reasonable estimate for mean residence times, provided the API% is relatively low or the bulk density of the formulation is similar to the bulk density of the excipient. The potential exists for fill weight experiments to yield first order characterization of blending dynamics without excessive use of material resources. The ability of space time to predict the mean residence time can be captured through a relative mixing index shown in Equation (6-1).

$$RelMix = \frac{Mrt - Spt}{Spt} \tag{6-1}$$

A positive relative mixing value signifies that the API has spent more time in the blender than the excipient, while a negative relative mixing value implies the API has spent less time. Higher relative mixing was expected to indicate incremental improvement in mixing performance in blending experiments. Figure 6-23 shows how this evaluative parameter varied with respect to fill fraction. At low fill levels, relative mixing was positive on average but fluctuated greatly. As fill level increased, both the value and the variability of the index decreased.

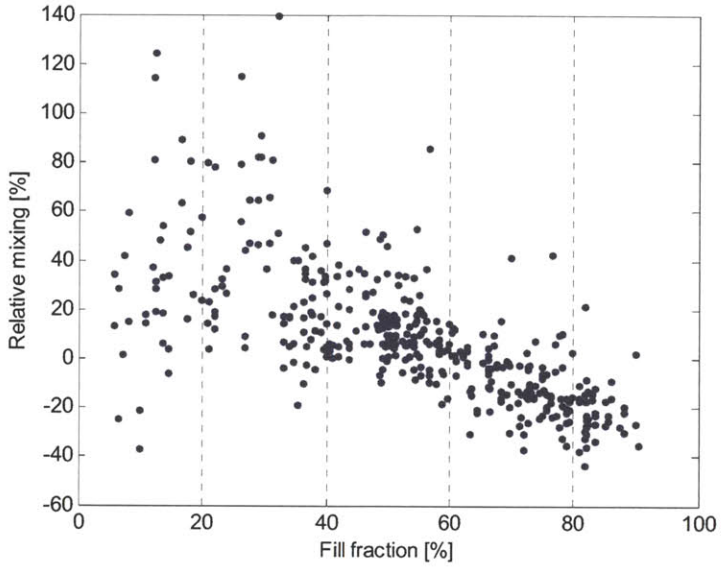

Figure 6-23: Relative Mixing vs. Fill Fraction in Ribbon Blender

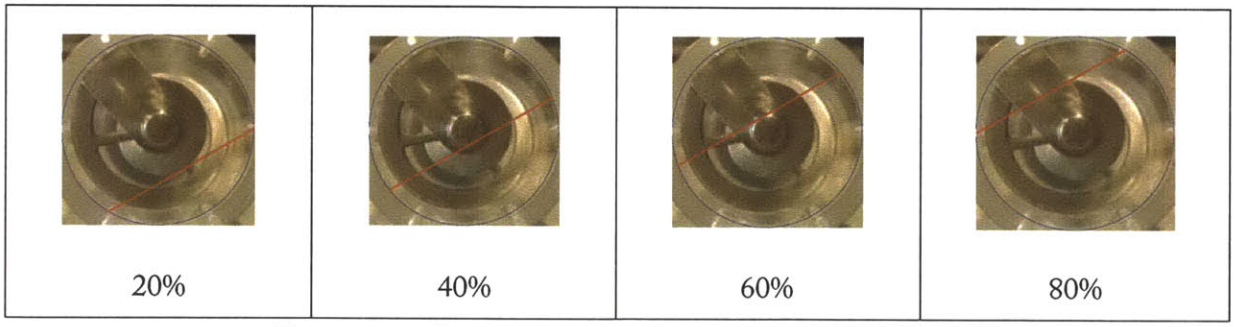

Figure 6-24: Powder Bed Surface at Various Fill Levels

The influence of fill fraction on the relative mixing index may be attributable to the position of the powder bed surface during the impulse response. Figure 6-24 overlays the location of the free surface (at an observed bed angle of 30°) on a cross-sectional image of the ribbon blender for fill fraction values marked in Figure 6-23. Since the API impulse was delivered to a steady state

continuous operation, the location of the free surface determines the initial position of the API particles and thus significantly influences their trajectory through the blender.

At fill levels of 20%, the free surface is adjacent to the lower edge of the inner ribbon. Particles above the powder bed are more likely to be exposed to the reverse-pitch of the inner ribbon, pushing them further upstream. This causes an increase in retention time for API within the blender, leading to higher relative mixing values. As the fill fraction increases, the amount of contact between the impulse shot and the inner ribbon decreases relative to excipient particles, bringing the mean residence time back in line with the space time. Relative mixing begins to decrease and turns negative when the API impulse experiences the top edge of the forward-pitch outer ribbon.

Figure 6-25 splits relative mixing values by blender type. As noted for space times and mean residence times, smaller scale blenders exhibited greater variability in repeat experiments due to the relatively larger effect of noise and error. The largest blender maintained the greatest consistency in relative mixing values across the range of fill fractions.

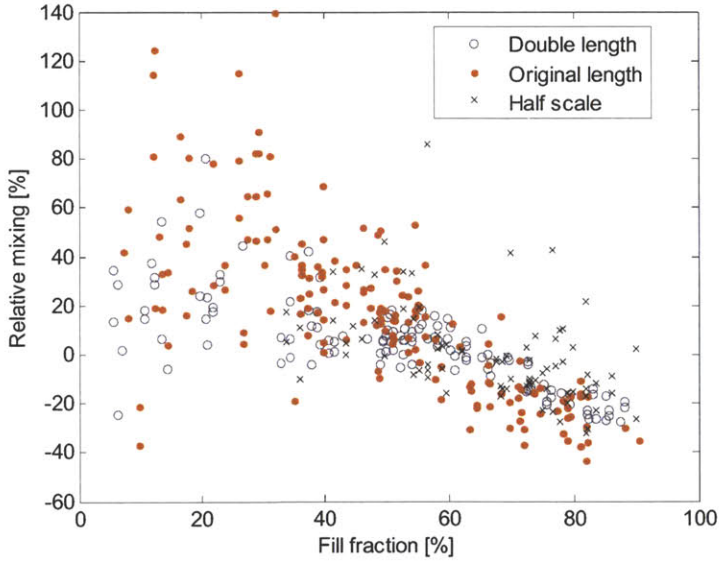

Figure 6-25: Relative Mixing vs. Fill Fraction for Different Blenders

6.3 Blending Experiments

API was fed as a sinusoidal input to a steady state continuous system in order to determine the variance reduction ratio. Blending experiments were conducted over a range of operating parameters with two APIs and three blenders, using Avicel PH-102 as a representative excipient. Results are discussed with respect to input frequency and API before multivariate analysis is employed to quantify the effect of various key parameters on blending performance.

Variance Reduction Ratio

The ratio of input to output variance in API% over time yields the variance reduction ratio, the key metric of blending performance. Figure 6-26 plots the actual VRR for blending trials versus the mean residence time, with splits accordingly to the input frequency. The correlation between VRR and mean residence time was relatively weak, given the impact predicted by previous Markov modeling results. Variability had a greater effect on VRR than the mean residence time, although a negative correlation with input frequency was observed.

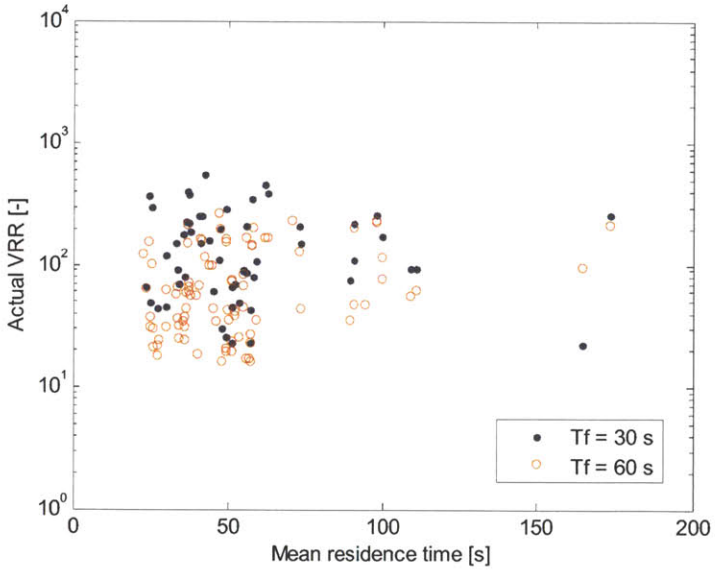

Figure 6-26: Actual VRR vs. Mean Residence Time in Ribbon Blender

The mean residence time, Bodenstein number, and input frequency of each blending experiment was input into the Markov model to produce a predicted VRR. Figure 6-27 shows the actual VRR versus predicted VRR with different APIs noted. Again, the correlation between VRR and

the key parameters highlighted by the Markov model was much weaker than expected, indicating that other influences may have dominated in this experimental space. The choice of API itself had a significant impact on blending, with acetaminophen runs outperforming caffeine runs by roughly half an order of magnitude. The fact that API could be mixed better suggested that radial mixing or shear rate should be explored. The weakness of the one-dimensional axial model may be the failure to incorporate other relevant parameters. This hypothesis is explored in the next section on the paddle blender.

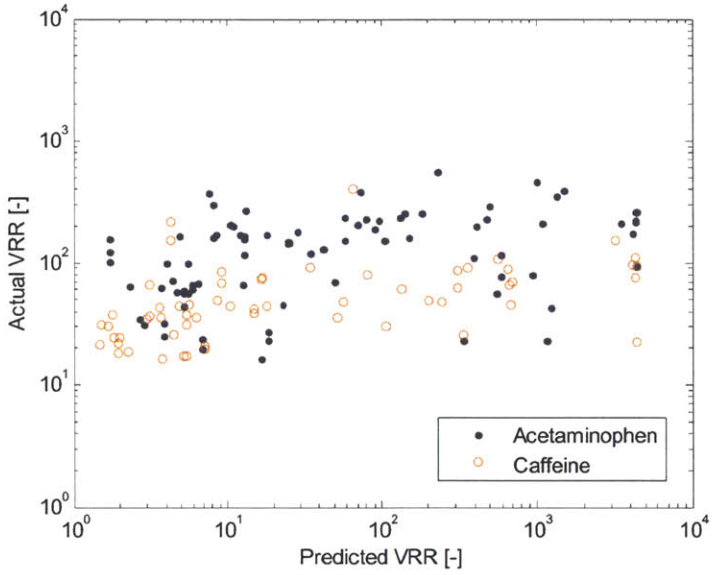

Figure 6-27: Actual VRR vs. Markov-Predicted VRR in Ribbon Blender

7 Paddle Blending Results

A subset of the experiments performed with the double helical ribbon blenders was repeated with the paddle blender. Intermediate results are discussed in the same sequence as the previous section before data analysis is aggregated at the multivariate level.

7.1 Fill Weight Experiments

Fill weight experiments were again conducted over a range of mass flow rates and rotation rates using the same five excipients. Due to the lower forward axial velocity provided by the paddle blender, shaft rotation rates were increased to 40-60 rpm in order to maintain the same scale of operations. Initial results focus on 60 rpm fill weight studies performed with DCL14 and then expand to include other parameters already introduced.

Effect of Mass Flow Rate

A sample output from fill weight experiments over the feasible range of mass flow rates is shown in Figure 7-1. Three runs were conducted at each experimental setting and individually plotted.

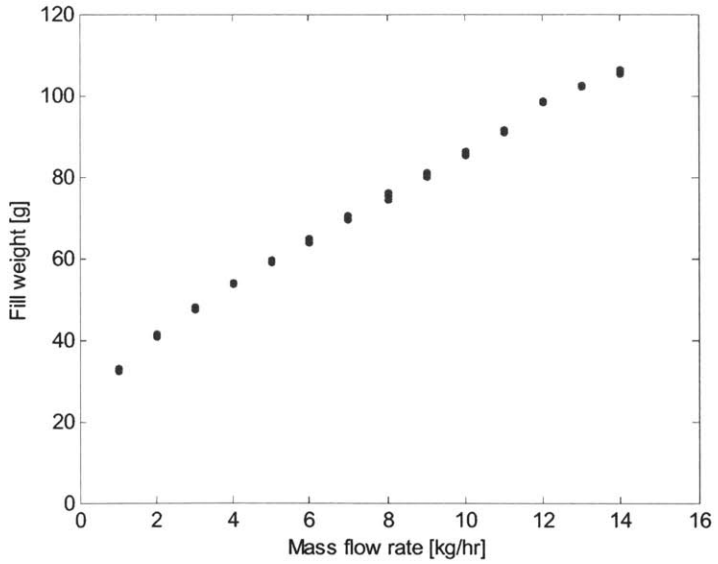

Figure 7-1: Sample Set of Fill Weight Results over Mass Flow Rates

Mass flow rates and hold-up weights once again demonstrated a strong positive correlation. Yet for the same blender dimension as the original double helical ribbon blender, the paddle blender accommodated a narrower range of fill fractions. In Figure 7-2, fill fraction maximizes at approximately 60%, compared to nearly 90% in all three double helical ribbon blenders. The lower net forward axial velocity of the paddle blender limits its flexibility in handling different scales of operation.

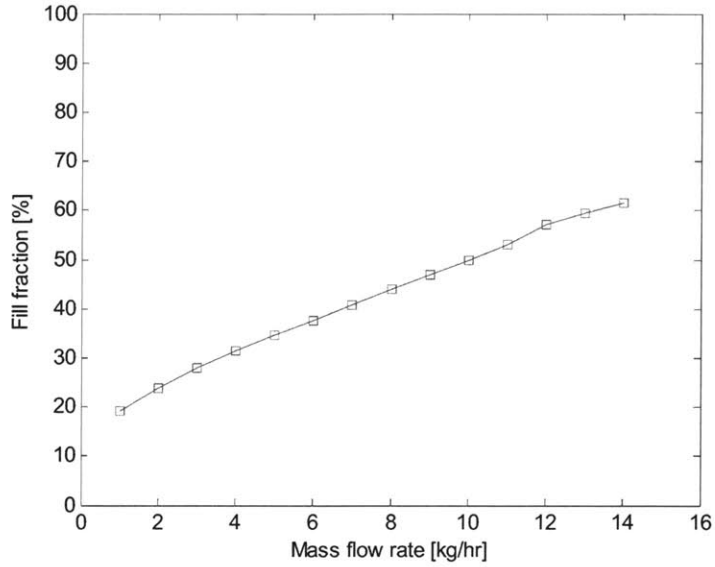

Figure 7-2: Fill Weight Results Converted to Estimated Fill Fraction

While the double helical ribbon design was able to maintain a constant bed height during steady state, the free surface was noticeably higher at the entrance of the paddle blender and fell linearly along the axial length, reaching a minimum at the exit weir. The ceiling for mass flow rate was reached when the paddles were no longer able to push particles forward fast enough to keep the local fill fraction under control and the powder bed below the input port was clogged. Due to transport rate limitations at the entrance, the maximum fill fraction of 60% denotes unutilized processing capacity downstream. This could be corrected in future iterations by increasing the pitch of upstream paddle blades to provide more forward push early in the blending process.

Space time was plotted against fill fraction in Figure 7-3. The simpler nature of the paddle design yielded simpler blender dynamics. Since the blade pitch is consistent with respect to axial length and bed height, higher forward velocities are achieved through greater exposure of powder

to paddles. The more particles available to be carried downstream, the faster the overall rate. Thus, space time decreases as fill fraction increases. Without an inner ribbon pushing material in the opposite direction, no broad peak exists as in the double helical ribbon profile. Space times in the paddle blender are significantly higher at low fill fractions, approximately equivalent to the ribbon blender in the 20-30% range and lower at higher fill fractions.

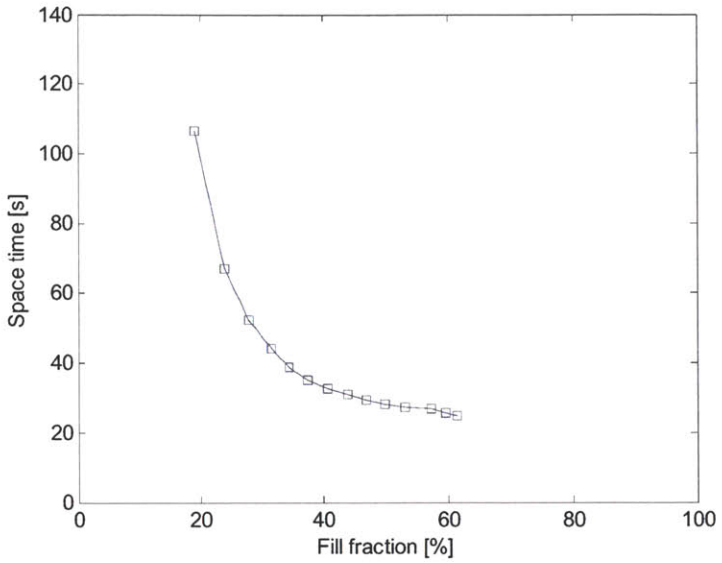

Figure 7-3: Space Time vs. Fill Fraction in Paddle Blender

Effect of Rotation Rate

Fill weight results are plotted according to shaft rotation speed in Figure 7-4. The lower net forward axial velocity imparted by the paddles necessitated higher rotation rates to maintain the same manufacturing scale and reduced the sensitivity of fill fraction to shaft speed. As a result, fill fractions showed a significantly weaker response to changes in rotation rate, as compared to the double helical ribbon spread in Figure 6-4. The same mechanical difference is also the cause of the tightly clustered space time curves in Figure 7-5. For the given 2° tilt of the paddles on the paddle shaft, a wider range of shaft rotation rates was not possible. This shaft design limits the potential design space to a narrow combination of fill fraction, flow rate, and space time, metrics that are strongly influenced by the convective capacity of the shaft. Since the paddle shaft emphasized radial mixing over axial mixing, flexibility in varying these parameters was lost but could be partially restored using paddles with a wider tilt.

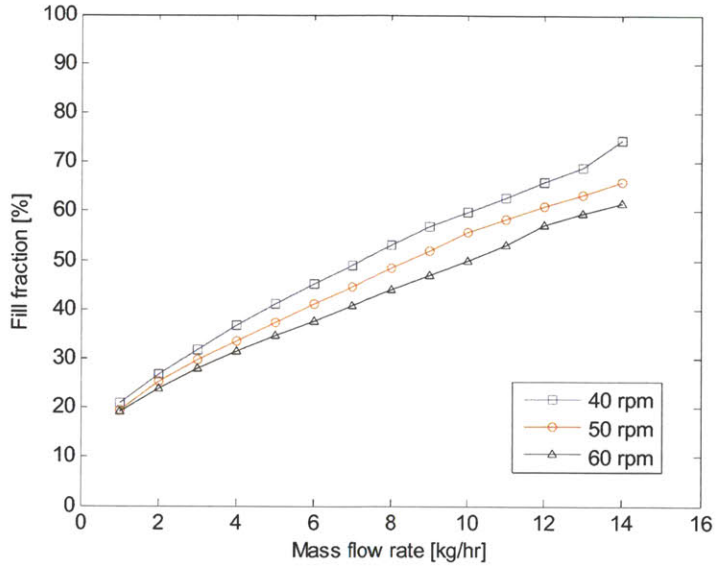

Figure 7-4: Fill Fraction vs. Mass Flow Rate for Different Rotation Rates

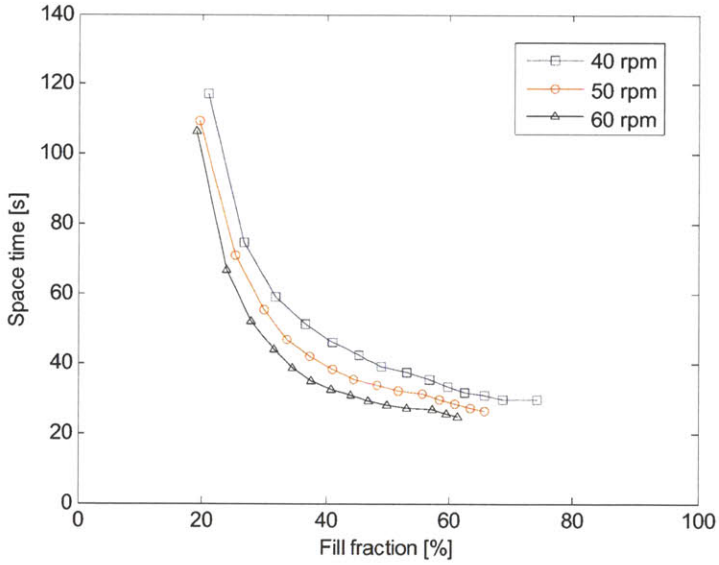

Figure 7-5: Space Time vs. Fill Fraction for Different Rotation Rates

Effect of Excipients

The volumetric normalization conducted in Section 6.1 was repeated for paddle blender results across five excipients. The resulting fill fraction and space time plots are shown in Figure 7-6 and Figure 7-7, respectively.

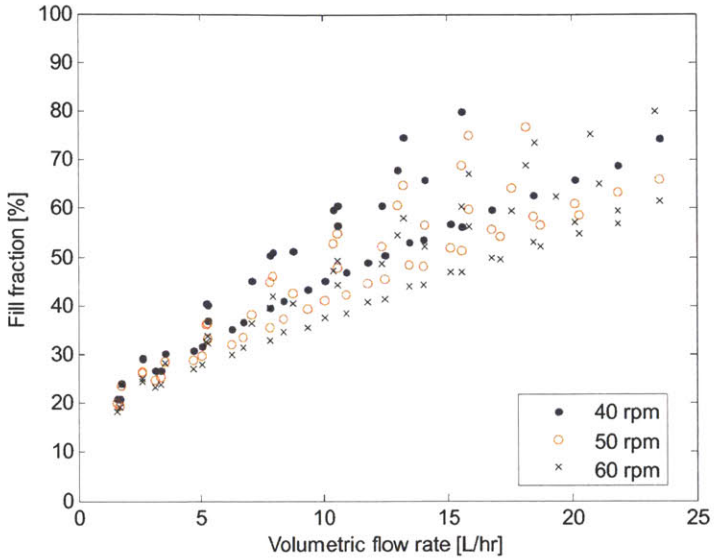

Figure 7-6: Fill Fractions for Different Excipients, Adjusted by Bulk Density

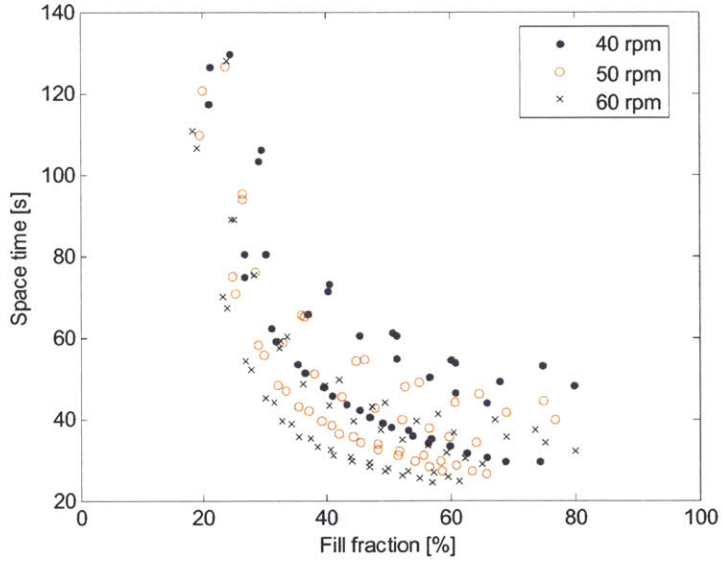

Figure 7-7: Space Times for Different Excipients

In this instance, the effects of shaft rotation rates and excipients were not as easily distinguishable. This may be due to the tighter grouping of intermediate metrics caused by lower net forward axial velocity as well as the greater effect of powder dilation in this system. The positioning of the paddle blades to increase radial motion will also increase powder dilation, decreasing the effective bulk density of the passing material. To the extent to which different

excipients experience different degrees of dilation, different blending dynamics would occur. The clustering of results indicates that bulk density values and any parameters derived thereof would be less reliable in paddle blending models. The reduced sensitivity of intermediate parameters to easily adjustable macro-scale parameters once again leads to weaker control of the system.

7.2 Residence Time Distribution Experiments

NIR was employed to characterize impulse responses for both caffeine and acetaminophen in Avicel PH-102 over a range of operating parameters. Mean residence times and Bodenstein numbers were compiled against calculated fill fractions from the fill weight studies presented above. Key relationships are discussed below while the entirety of the data set was abstracted into the multivariate analysis to follow.

Effect of Operating Parameters

Figure 7-8 shows the mean residence time with respect to fill fraction. As with the space time plots in Section 7.1, mean residence times decreased with increasing fill fraction. The lack of reverse axial motion led to a narrower range of observed values than found with the ribbon blenders. No strong correlation was observed with respect to the shaft rotation rate.

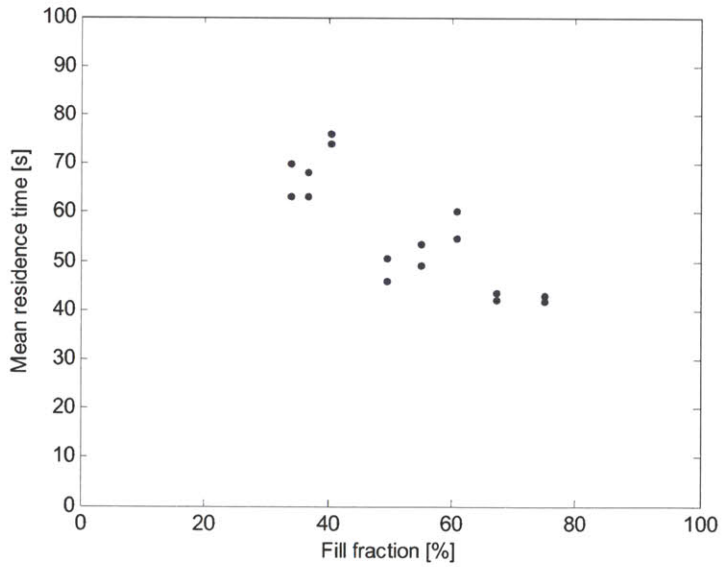

Figure 7-8: Mean Residence Time vs. Fill Fraction in Paddle Blender

Effect on Shear Rate

In Figure 7-9, blade passes are negatively correlated with fill fraction. The higher number of blade passes at lower fill fractions is attributable to the longer mean residence times, which exposes API particles to more shearing during the blending process. The linear response is again due to the simpler nature of the paddle design. Without the complex dynamics of the double helical ribbon, the number of blade passes can now be increased by lowering the mass flow rate. This feature provides an operational hedge as the system ramps up to steady state – material flowing through during a transient state (at lower fill fractions) will experience more shearing and mixing in the radial direction. Despite a lower range of mean residence times than the ribbon blenders, the paddle blender generally produced a higher number of blade passes due to higher operating shaft rotation rates.

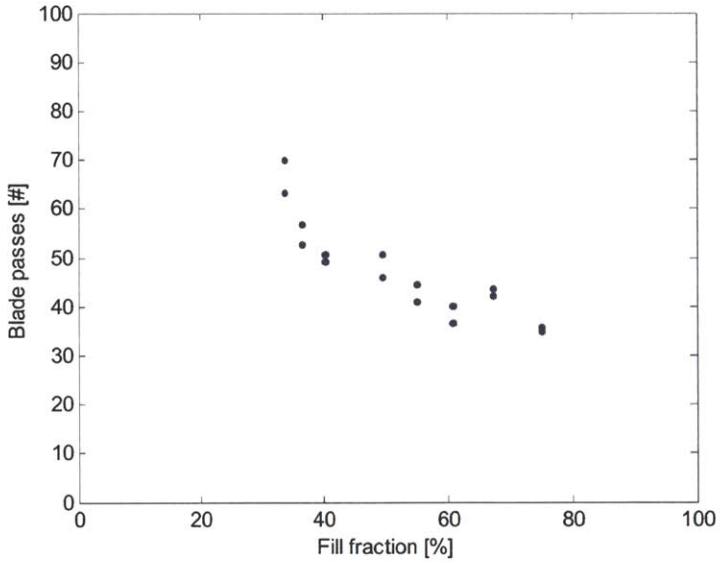

Figure 7-9: Blade Passes vs. Fill Fraction in Paddle Blender

Effect of API

Juxtaposition of mean residence times and Bodenstein numbers with respect to caffeine and acetaminophen are shown in Figure 7-10 and Figure 7-11, respectively. Similar to the findings in Section 6.2, a strong correlation was observed for mean residence time and a weak correlation for the Bodenstein number. Mean residence times were more consistent regardless of API used. This

independence between API and axial dispersion seemed to be evident in both the ribbon and paddle blender designs.

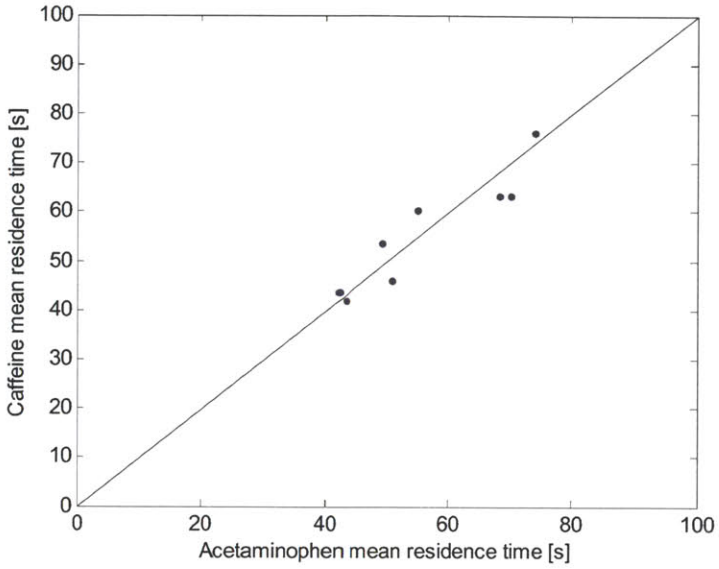

Figure 7-10: Comparison of Mean Residence Time across Different API

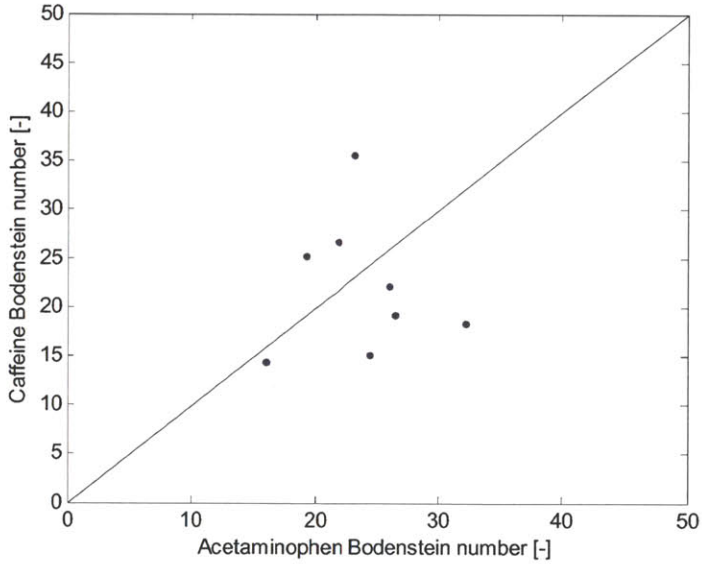

Figure 7-11: Comparison of Bodenstein number across Different API

Comparison to Space Time

Mean residence times and space times were fairly consistent, as shown in Figure 7-12. The relative mixing index was also calculated and plotted against fill fraction in Figure 7-13.

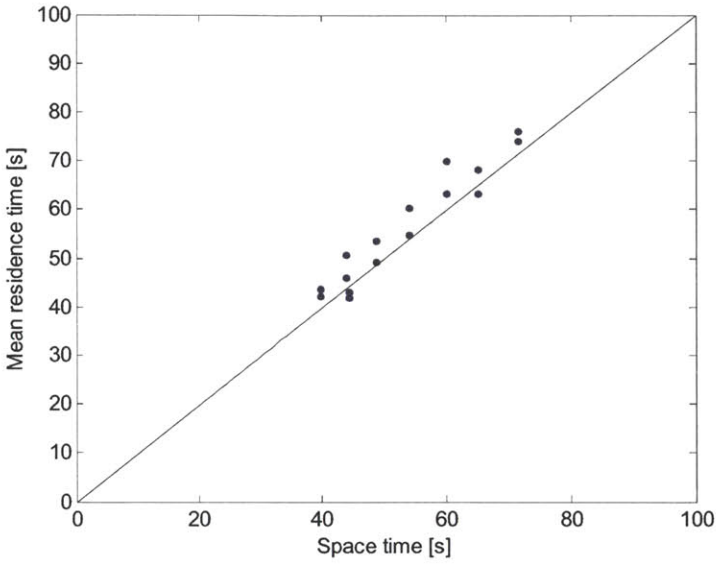

Figure 7-12: Comparison of Mean Residence Time to Space Time

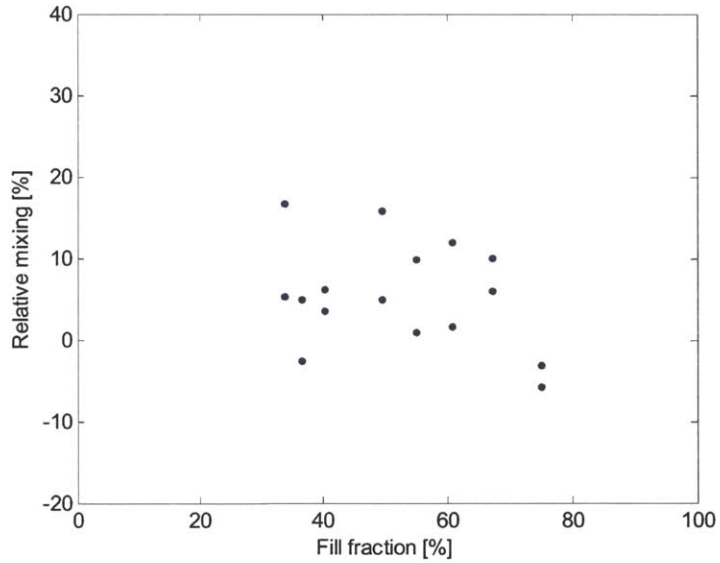

Figure 7-13: Relative Mixing vs. Fill Fraction in Paddle Blender

The relative mixing index indicates that the paddle blender produced less drastic differences between space times and mean residence times. While the index ranged from under -40% to over 100% in the double ribbon design, paddle blender experiments yielded values between -10% and 20%, a much smaller range of variation. The absence of an inner ribbon significantly reduced the dependence of the relative mixing index on the fill fraction.

7.3 Blending Experiments

Variance reduction ratio experiments were conducted with caffeine and acetaminophen, again using Avicel PH-102 as a representative excipient. A cursory two-dimensional analysis is shown in this section, while a higher level statistical examination is presented in the next chapter.

Variance Reduction Ratio

Figure 7-14 plots the experimentally derived VRR values against mean residence times obtained at the same settings, with data subdivided by shaft design. As noted earlier, the ribbon blenders produced a much wider range of mean residence times with a more limited effect on the actual VRR than expected from Markov modeling. The paddle blenders, on the other hand, were able to produce blending performance on par with the ribbon blenders even within the narrower band of mean residence times allowed by the operating parameters, as shown in Figure 7-15.

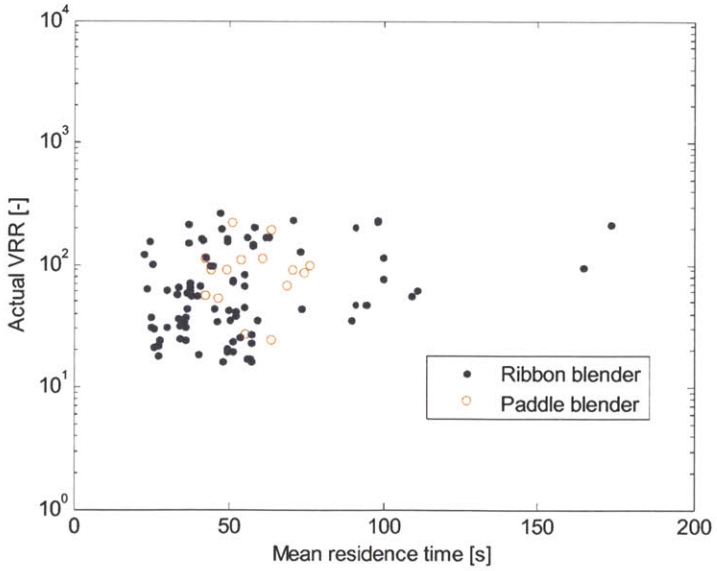

Figure 7-14: Actual VRR vs. Mean Residence Time in Paddle Blender

This once again suggests that the parameters of the Markov models – mean residence time, Bodenstein number, and period of input feed fluctuations – were insufficient to characterize these continuous blenders. Given the one-dimensional nature of the axial dispersion framework and the drastic difference in radial mixing between the ribbon blenders and the paddle blender, the inability of models in literature to incorporate shear into predictions appears to be a significant weakness in the current context.

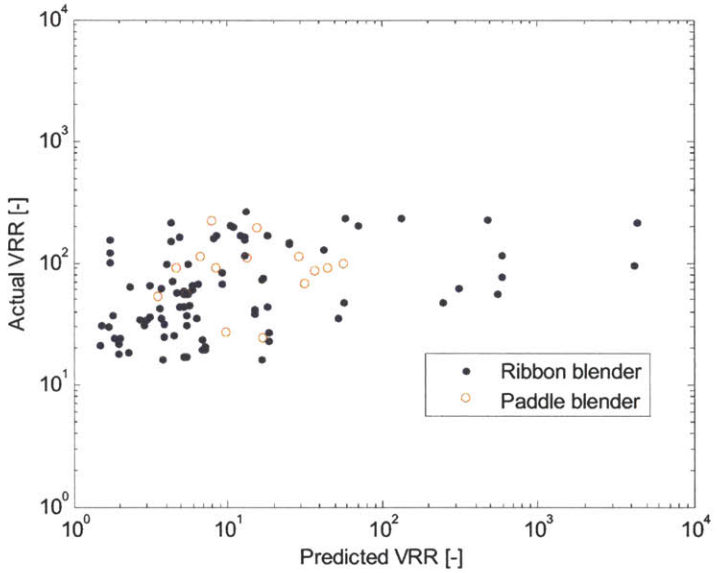

Figure 7-15: Actual VRR vs. Markov-Predicted VRR in Paddle Blender

Figure 7-16 summarizes the same data set with respect to blender type (ribbon vs. paddle on the same original scale) and API (acetaminophen vs. caffeine). The bar height indicates average VRR obtained across all operating parameters within the blending group while the spread shows the standard deviation. As discussed in Section 6.3, the ribbon design produced significantly better blending performance when acetaminophen was the API rather than caffeine. The paddle design was able to match blending performance with acetaminophen and also raise the VRR in caffeine experiments up to a similar level. This suggests that the paddle blender provides a more robust platform for handling the differences between caffeine and acetaminophen. The increased radial mixing and greater number of blade passes appear to correlate with better blending performance in multiple APIs.

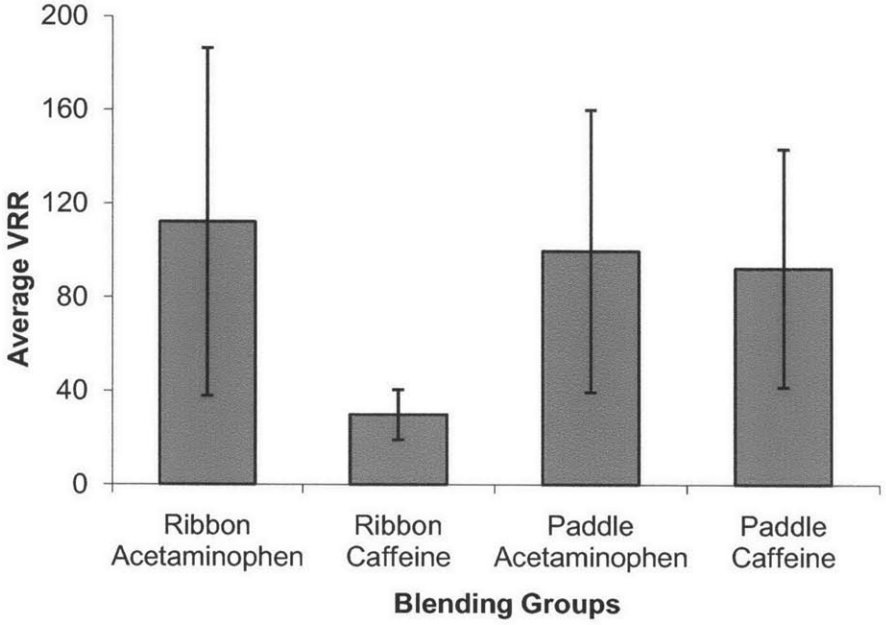

Figure 7-16: Blending Performance by Blender and API

8 Implications for Process Design

This chapter explores the implications of the presented results on process design in continuous pharmaceutical blending. First, multivariate analysis was performed to parse the effect of various variables on mixing performance and characterize the influence of physical design, operating parameters, and material properties on blending. Next, the findings are encapsulated into a design framework for future research. Finally, potential applications for this work are detailed.

8.1 Multivariate Analysis

The large data set and the exhaustive number of parameters render traditional two-dimensional graphical analyses incomplete. Variables of interest such as the Bodenstein number and the number of blade passes could not be controlled during the design of experiments due to its complicated interaction with parameters that were directly adjusted. In order to isolate the effect of any one factor, other variables must be corrected for. Multivariate analysis was used to separate overlapping influences and identify the extent of correlation between each individual parameter and the primary metric of performance, VRR. Figure 8-1 provides the degree of linear correlation between relevant variables and the log-adjusted VRR for all double helical ribbon blending experiments. Unit variance was employed to normalize the range of values of each parameter during the set of experiments.

This technique quantifies the effect of each parameter through multivariate linear regression to determine the individual contribution to blending performance. The correlation value, along with the error bars, provide a first order estimate of blender sensitivity to each variable over the range used in the experimental data set. The result is a normalized comparison which allows an "apples to oranges" translation with respect to the key performance metric – variance reduction.

The parameters are sorted from greatest positive correlation to greatest negative correlation. When variables on the top increased in value, the variance reduction ratio tended in increase as well. When variables on the bottom increased in value, the VRR tended to decrease instead. Parameters in the middle of Figure 8-1 exhibited comparatively little net effect on blending performance. The greatest influence on blending dynamics was the choice of API. The use of

acetaminophen rather than caffeine resulted in a statistically significant increase in VRR, reiterating the finding of Figure 6-27. Other parameters which demonstrated a strong correlation included the relative mixing index, the Markov-predicted VRR, the number of blade passes, the Bodenstein number, and the input feed frequency.

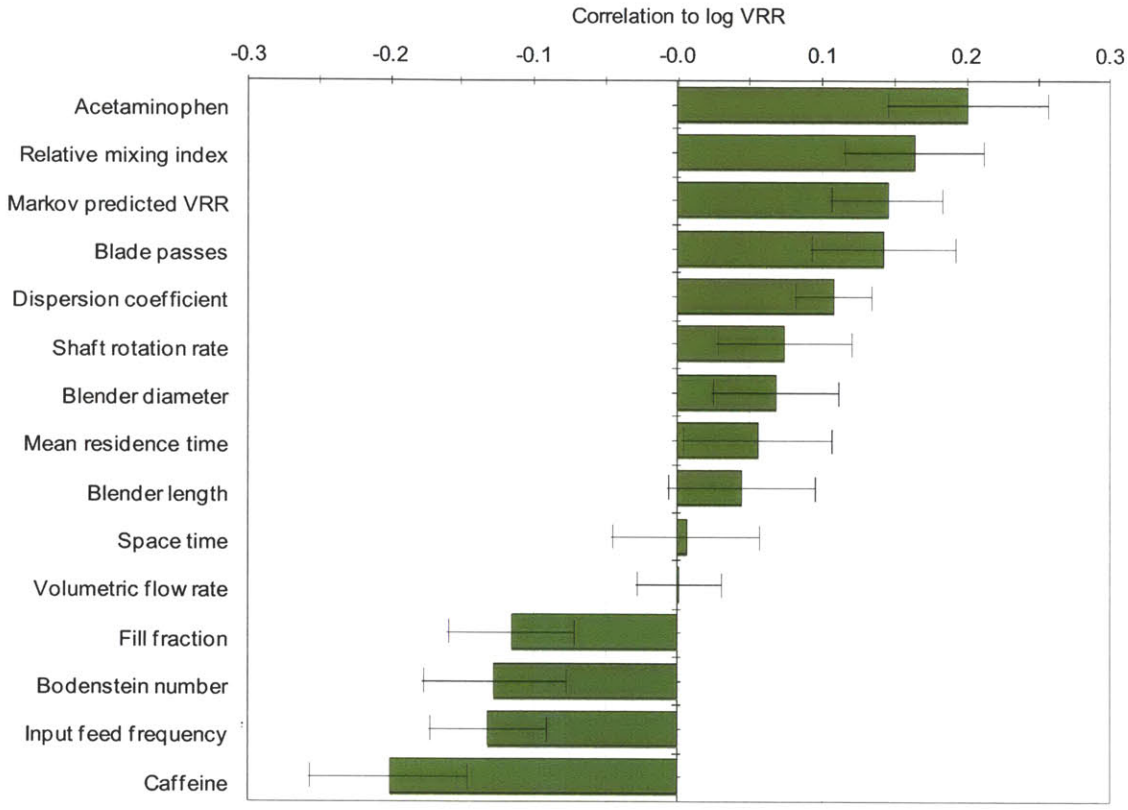

Figure 8-1: Multivariate Correlation of Parameters to VRR in Ribbon Blenders

Experimental level	Components	R2X	R2Y	Q2(cum)
Fill weights	1	20.2%	26.3%	22.3%
Residence times	2	38.8%	53.7%	45.1%
Blending	1	19.3%	62.9%	59.3%

Figure 8-2: Goodness of Fit with Experimental Level

Multivariate analysis improves as the proxy experiment approaches the complexity of the actual process. Figure 8-2 shows the goodness of fit to the primary metric as data from additional experimental levels are included in the analysis. The correlative strength of the data, represented by both R2Y (amount of Y variability explained by X) and Q2 (predictive ability of the model as checked by statistical cross-validation), increases significantly. With the entire data set employed, multivariate analysis explains approximately 60% of all variability observed in the VRR. While this value appears low when contrasted to standard two-dimensional correlations, it is quite comparable to other applications of multivariate analysis, especially given the number of parameters involved and the reliance on a spectroscopic model.

Note that although lower level experimental data (fill weights and residence time distributions) did not sufficiently account for the variation in blending performance, each level of experiments added significantly to the correlative strength of the data set. Indeed, many of the influential factors identified in multivariate analysis – the relative mixing index, the Bodenstein number, the number of blade passes, and the Markov-predicted VRR – were available for characterization with a relatively small expenditure of API. This suggests that once a general process framework has been established, key intermediate metrics may be used to improve process performance in a more timely and cost-effective manner.

Following standard protocol for projections to latent structures, the model provides a broad glimpse of the first-order effect of each parameter on the VRR. However, it is worth noting that the mathematical manipulations in this model inherently assume linear correlations between both X and Y variables. To the extent to which nonlinearities exist, systematic inaccuracies will be embedded within the resulting calculations. Care should be taken to linearize parameters whenever foresight allows. For instance, the VRR was log-adjusted for multivariate analysis due to correlations noted in the Markov computations. Another example is the fill fraction, where nonlinearities were observed in the ribbon blender data as shown in Figure 6-23. A quick dummy variable such as Equation (8-1) can be constructed as a substitute for multivariate modeling. Figure 8-3 shows the analysis repeated with a linearized fill fraction parameter.

$$Fill_{linear} = |Fill - 40\%| \tag{8-1}$$

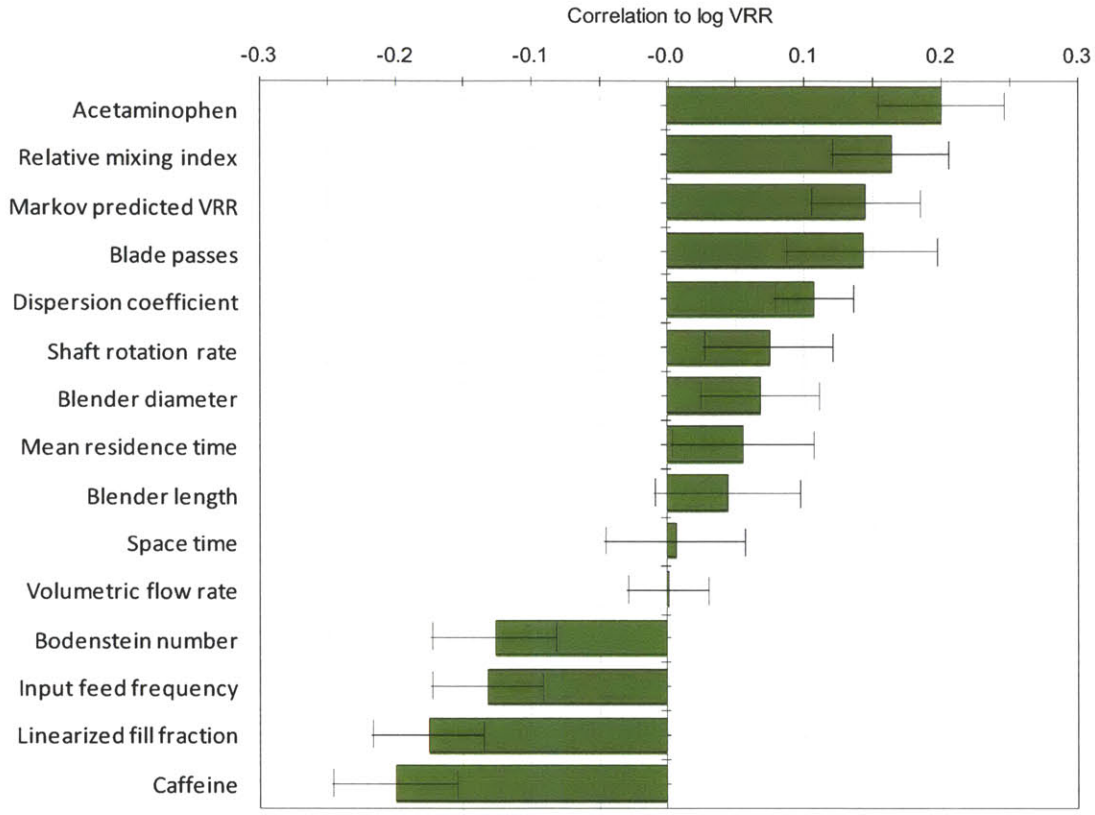

Figure 8-3: Multivariate Correlation of Parameters to VRR, Fill Fraction Linearized

With this dummy linearization, the correlation of the fill fraction to the VRR increases by approximately 50%. The original nonlinear scale of the fill fraction understated its true effect on blending performance. The all-encompassing nature of PCA and PLS analysis enables the observer to easily determine directionality and parse first-order effects, but this simple check demonstrates that further scrutiny is always recommended. Multivariate analysis serves as a key statistical tool, but the shotgun approach does not replace the precise experimental scalpel.

The paddle blender results were added into the multivariate analysis to produce Figure 8-4. While most parameters maintained a similar relationship to log VRR, the use of the paddle shaft correlated with a small boost in blending performance while the ribbon blender correlated with a decrease in VRR. This finding agrees with the earlier analysis summarized in Figure 7-16, which showed that the paddle design improved blending performance of caffeine experiments.

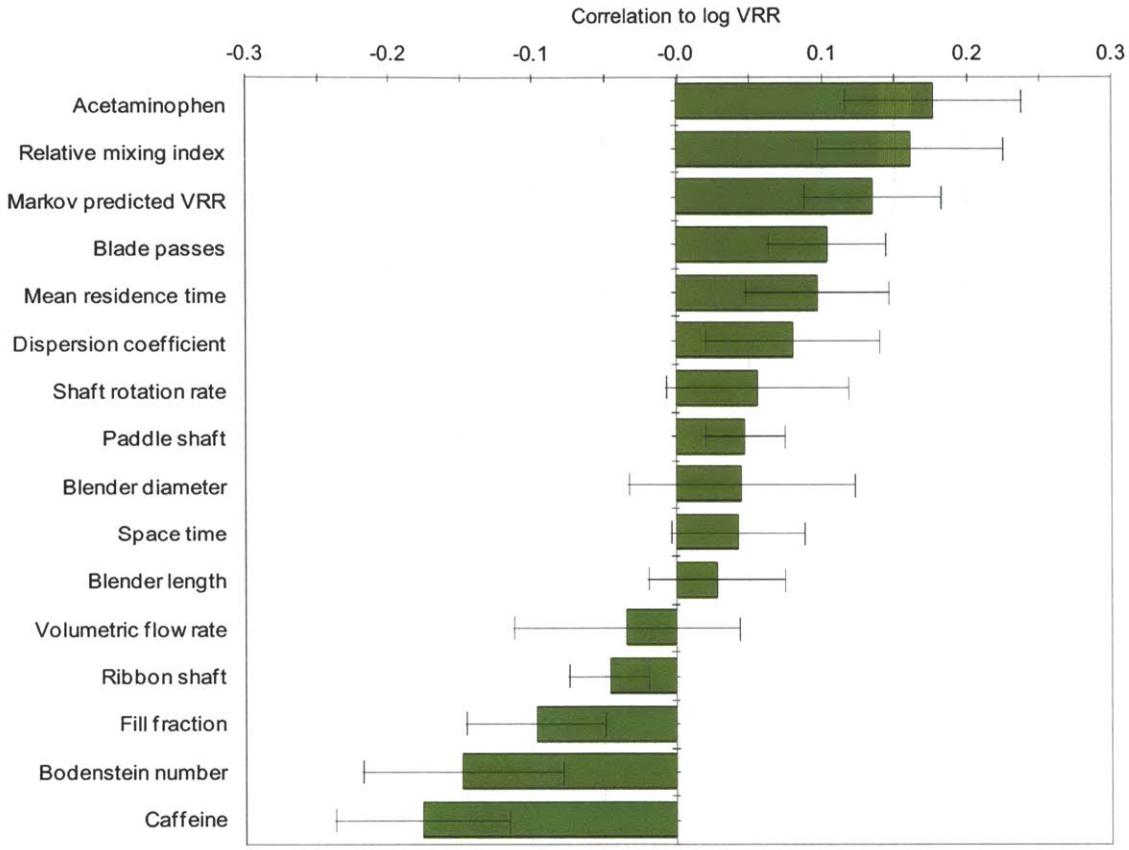

Figure 8-4: Multivariate Correlation of Parameters to VRR, Ribbon vs. Paddle Blenders

Overall, the correlations calculated through multivariate analysis support the two-dimensional relationships observed earlier. The Markov-predicted VRR and the input feed frequency had a significant correlation with the actual VRR, as anticipated by the Markov model. The design of experiments elucidated a number of other key parameters, including the choice of API, number of blade passes and fill fraction. Moreover, the multivariate analysis revealed the quantitative relevance of each variable, providing a standard for comparison and a basis for further design improvements. The relationships tested served as a roadmap for increasing blending performance. By increasing positively-correlated parameters and reducing negatively-correlated parameters, a similar design of experiments can strategically and systematically boost the efficiency of any given blender.

8.2 Design Principles for Continuous Blending

The results presented above suggest several design principles for improving continuous blending in the pharmaceutical context. This section outlines key findings from this research and the potential implications for future blending design and optimization. The following discussion attempts to summarize principles which may be applied in the range of conditions explored.

8.2.1 Physical Design

Experimental literature commonly employs one-dimensional models such as the axial dispersion equation and Markov chains as a theoretical basis of comparison against empirical data. Given computational limitations on applying more sophisticated techniques such as discrete element method simulations, this represents the current state of practical analysis. These frameworks can also serve as predictive models during initial design of continuous blenders. While the emphasis on mean residence time as a design metric was shown here to be prudent, caution should taken to ensure radial mixing is adequate when theoretical models are often blind to this requirement. When possible, multivariate analysis of experimental data can augment theoretical frameworks in the absence of a tractable three-dimensional model of mixing.

Focus on Mean Residence Time

Chapter 4 detailed simulations exploring the effect of input feed frequency, mean residence time, and the Bodenstein number on mixing performance within the one-dimensional Markov chain and axial dispersion paradigm. The results indicate that periods of input feed fluctuation are a significant detriment to blending homogeneity. Both the mean residence time and the Bodenstein number can improve performance, although any gains due to lower Bodenstein numbers can also be captured at higher mean residence times. In particular, the mean residence time should be 2-3 times greater than the longest expected time period of input feed inconsistency in order to maximize the variance reduction ratio.

This finding was validated by multivariate analysis highlighting the positive correlation of mean residence time and the Markov-predicted VRR with actual VRR from experimental runs. The rule of thumb has also been supported in previous literature [15, 55] and easily determined due

to the current emphasis on one-dimensional axial models. Nonetheless, a proper understanding of feeding limitations would allow mean residence time to be a primary design metric.

Residence time distribution results in Sections 6.2 and 7.2 also noted difficulty in reproducing Bodenstein numbers at the same operating parameters in different blenders with different API, suggesting that the Bodenstein number is also a harder target metric to control in processing. This may be a result of employing cohesive particles at a smaller manufacturing scale. Improved radial mixing may address this issue and make the Bodenstein number less unwieldy to manage, unlocking its potential as a design metric.

Radial Mixing for Robust Processing

The ability of the paddle shaft to yield more robust performance with respect to different API indicates the importance of radial mixing in the context of cohesive pharmaceutical powders. Given the use of one-dimensional characterization techniques, this factor may be overlooked. In the shorter operating timeframes of continuous blending, radial mixing is equally critical to achieving adequate performance. Abel [62] noted in smaller scale discrete element method simulations the drastic difference in radial mixing and performance between paddle blenders and ribbon blenders.

When simulations of radial motion are not available, this principle needs to be over-engineered into the blender design. Adjustable attachments such as paddles can be calibrated to provide enough radial movement without sacrificing too much axial convective capacity. This would require experimental optimization using operating metrics. The number of blade passes was shown in this research to be a useful proxy for extent of shear and a strong positive influence on blending performance.

Iterative Design using Multivariate Analysis

While design principles cannot be applied in every context, the tools employed in this research can be deployed in any processing design space or range of conditions. Multivariate analysis has been effective in characterizing systems with a large number of highly correlated variables and costly experiments, a common problem in pharmaceutical R&D. In this research, multivariate analysis has validated the use of the paddle shaft to reduce performance variability with respect to API and highlighted several parameters with the greatest effect on overall blending.

In this design space, material properties and operating parameters were found to have a more significant effect on performance than design factors such as blender length and diameter. This presents an opportunity to boost processing in the short-term by changing the formulation or making operational adjustments, but the same path to optimization may not be true in a different design space. Multivariate analysis provides first order system mapping to understand the context and implications of the parameter space in question.

8.2.2 Operating Parameters

While various operating parameters have been studied extensively in blending literature, this research has gathered both practically adjustable parameters and intermediate metrics in an effort to understand the interdependence between these variables and their overlapping effect on the performance of the blender. Fill fraction was found to be an easy metric to optimize, while other metrics such as the relative mixing index and number of blade passes were determined to be valuable proxies for understanding powder dynamics. Most importantly, these parameters can be characterized without full blending runs, limiting the use of API in the high-cost environment of pharmaceutical R&D.

Optimize Fill Fraction to Maximize Performance

Chapters 6 and 7 detailed the effect of fill fraction on space time, mean residence time, and the number of blade passes and noted that peaks occurred. In the ribbon blenders, these parameters reached their maximum at a fill fraction of 40-50%, where the powder bed surface experiences agitation from both the inner and outer helix. In the paddle blender, a lower fill fraction of 20-30% achieved more shear. Given the influence of mean residence time and the number of blade passes on blending performance, it was not surprising to see that fill fraction also had a significant effect.

The proper fill fraction to maximize mixing depends on the mixing elements in the blender. In low-shear systems such as the ribbon blender, the appropriate fill fraction has been found to be near the 50% mark, as Laurent and Bridgwater [25-29] demonstrated the importance of the central shaft in bifurcating powder movement. In high-shear systems such as the paddle blender, the optimal fill fraction is expected to be at the lower end where axial velocity is lower and the

frequency of blade passes is higher. In any case, the fill fraction can be adjusted via the mass flow rate and shaft rotation rate and the optimal level determined through fill weight studies.

Intermediate Metrics Provide Cost-Effective Insight

Strong correlations were observed between blending performance and several intermediate metrics – mean residence time, relative mixing index, and number of blade passes. These variables provide insight into powder motion through the blender but also serve as metrics for optimizing operating conditions. These metrics can be characterized with minimal use of API as residence time distribution experiments are performed rather than full blending runs. In fact, space times could be used in lieu of mean residence times for even greater savings. The research conducted suggests that these intermediate proxies are effective from both an experimental and cost perspective.

The utility of intermediate metrics demonstrates the potential of lower level experiments as substitutes for larger processing runs in the face of time or cost constraints. Fill weight studies, in which only excipients are used and recycled, and residence time distribution experiments, where only a small bolus of API is necessary, were shown to characterize system performance relatively well in the absence of actual VRR data. This suggests that intermediate metrics may become an acceptable characterization shortcut once a design space framework has been established.

8.2.3 Material Properties

While physical properties such as bulk density can be measured and accounted for in blending operation, other material properties cannot be addressed so easily. The ability of macro-scale parameters to adjust for micro-scale differences depends on a holistic understanding of their interrelationship with respect to blending performance. The choice of API had a clear effect on VRR during ribbon blender experiments but was found to be minimized by the use of the paddle blender. This suggests that the iterative design framework discussed above can be a powerful tool for both identifying and addressing the influence of material properties on blending.

Robust Design Reduces Variability Due to Material Properties

The choice between caffeine and acetaminophen was the most influential variable in the performance of the ribbon blender, as noted in Section 6.3 and the multivariate analysis above.

Given the small particle sizes and cohesive nature of pharmaceutical powders, factors such as agglomeration may be of greater import here than in continuous operations in the food or chemicals industry. This problem has been compounded by the wealth of metrics used to reconcile the micro-scale parameters of materials with empirical data, resulting in confusion and poor comparability.

However, multivariate analysis can address this performance variability by quantifying the extent of the problem and identify potential parameters to mitigate the effect. This creates two distinct methods of improving the design – improve the robustness of the operation by incorporating a safety factor to offset the performance drop or devise new shaft elements which may boost the values of those positive parameters. In this research, longer blenders and the use of the paddle shaft both improved the robustness of the blending operation with respect to the API used.

Processing as a Viable Characterization Technique

Beyond the use of multivariate analysis to troubleshoot and optimize operations, the established data set also seeds further exploration of the effect of material properties on blending. The sophistication of multivariate data analysis allows for continual iteration and refinement in the design of experiments to characterize higher order effects. Once the physical effect of blender design and operating parameters have been benchmarked, the additional impact of choices in API and excipients on mixing performance can be understood. In the same way that NIR data enables the multivariate analysis conducted above, these correlations serve as a second layer of foundation for aggregating the effect of other variables on the primary metric of interest. In a highly interdependent system with collinear parameters, a multivariate approach creates highly levered experiments when fully independent single-variable searches may not be possible.

Once the fundamental physical relationships have been resolved, new designs of experiments can fix key parameters such as fill fraction, volumetric flow rate, and the number of blade passes in order to minimize their effect on blending performance and facilitate experimental expansion into new variables of interest such as different excipient formulations. These higher order effects can now be discerned with the clearer resolution provided by the data discussed in the previous chapters. Multivariate analysis thus yields a more direct form of characterization methodology – the quantitative effect of the material on the end metric in question. This technique requires a higher degree of statistical rigor, but ultimately provides a stronger bridge between various

characterization and performance metrics in cost-sensitive fields such as pharmaceutical research and development.

8.3 Research Expansion Strategies

The design principles outlined above can be applied and extended in future research in the field of pharmaceutical blending. The high-level roadmap serves as a powerful structure for expanding the parameter space to include newer and more sophisticated variables. Moreover, existing data can be leveraged as a statistical foundation for multivariate analysis, allowing later experiments to be conducted with greater cost-efficiency. Potential avenues for future work are discussed below.

Optimize Physical Design with Intermediate Metrics

Given the statistical linkages between blending performance and intermediate metrics such as space time, mean residence time, and the number of blade passes, optimization of physical design parameters can be conducted at faster speeds with fewer resources. The use of fill weight and residence time distribution experiments as the primary methodology enables greater recycling of pharmaceutical material and reduces the use of API in process R&D. In this paradigm, full blending runs would be performed only as confirmation of design space optimization.

This strategy can be extended to specific details of physical design, such as the selection and exact positioning of shaft elements. The design structure proposed in this thesis creates a framework which enables the exploration of the increasing minutiae of continuous pharmaceutical blending while maintaining a rigorous methodology with a theoretical and empirical basis. This line of research would thus bridge the gap between experimental blending and sophisticated simulations such as discrete element method.

Characterize the Effect of Material Properties on Processing

As an example of statistical leverage, a small course of experiments was designed to focus on the effect of other excipients on blending performance. Using the correlations for design and operating parameters built above, Figure 8-5 shows the additional effect of these materials on the VRR. Here, the Markov-predicted VRR and the input feed frequency continue to have a similar effect on performance, but the effect of acetaminophen and caffeine has been muted by the larger impact of switching excipients. Avicel HFE-102 appears to have a positive influence on mixing,

while DCL11 has a negative effect and DCL14 was net neutral to blending performance. This suggests that certain material properties of Avicel HFE-102 promote mixing while some of those inherent to DCL11 do not. This design space study thus guides further exploration of potential interaction between material properties and processing metrics, providing a quantitative yardstick against which characterization data can be better understood.

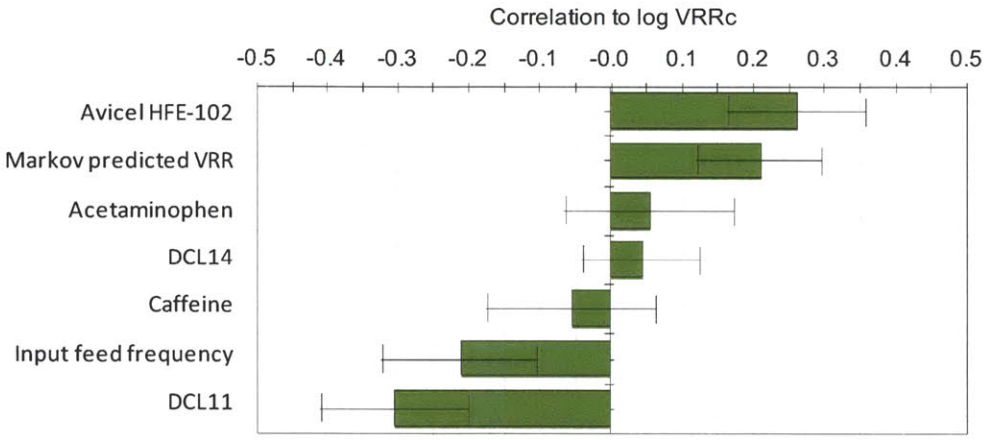

Figure 8-5: Multivariate Correlation of Parameters to VRR, Extending to Excipients

This iterative approach towards a deeper system mapping of higher order effects demonstrates the power of multivariate analysis. This statistical implementation broadens the design space by covering a greater number of variables and values and deepens the understanding of complex system relationships by untangling dimensionality and multicollinearity problems. This strategy can be employed to tackle more discrete effects of material properties – such as the difference in performance caused by changes in particle size distribution or cohesion. The statistical leverage provided by this multivariate methodology enables proper experimental design to characterize the individual effect of these micro-scale parameters in a rigorous manner.

Extend Research Methodology to Other Mixing Processes

While the focus of this thesis has been on dry powder pharmaceutical blending, other processes in pharmaceutical manufacturing can have a significant positive or negative impact on drug quality and overall homogeneity. The theoretical and experimental methodology presented in this thesis can be extended to similarly characterize these processes. In particular, melt extrusion and material transport are two pharmaceutical steps where the transition from batch to continuous

operations may have critical implications for API homogeneity. Both can benefit from a more rigorous understanding of the influence of design parameters on drug quality.

Bell recently explored the potential of applying melt extrusion to pharmaceutical manufacturing [63]. In a series of experiments with a novel pharmaceutical API, Bell noted that the twin screw design of the commercial extruder imparted a mixing motion during the melting process and used residence time distributions to model temperature-driven degradation. While the potential exists for melt extrusion to eliminate other mixing steps, further research is necessary in order to examine the consistency of homogeneity at the scale of interest and the process robustness within a larger design space that includes other formulations.

9 Multivariate Analysis of Pharmaceutical R&D

With the continued difficulties of the pharmaceutical industry (briefly outlined in Chapter 1), recent discussions about the future of the industry have centered on the role of research and development spending. The increasing cost of drug discovery (on both an absolute and per new molecular entity basis) has led to a myriad of opinions and approaches. In February 2011, two leading chief executives announced divergent strategies in their annual earnings conference calls [64]. Merck CEO Ken Frazier refused to make cuts to drug R&D, citing a focus on long-term profitability, while Pfizer CEO Ian Read promised to slash spending on internal R&D and instead repurchase outstanding stock. In the days after those statements, Merck stock dropped 2.7% while Pfizer shares rose 5.2%. Investors appeared to punish Merck for maintaining R&D spending and reward Pfizer for cutting its drug discovery budget.

9.1 Background

The product development process in the pharmaceutical industry is long and costly. Due to the regulatory hurdles necessary to protect consumer safety, the branded prescription drug industry is viewed as one the most capital-intensive sectors of the market. Figure 9-1 outlines the drug development process as per the Pharmaceutical Research and Manufacturers of America [65]. Potential drug candidates are first identified through chemical targeting and testing, then sent through preclinical trials in animals to gauge safety and efficacy in an indication of interest. If the initial results are promising, an Investigational New Drug application is submitted to the FDA. Following clearance, clinical trials begin in humans. Over three phases of clinical trials, the pharmaceutical company attempts to statistically prove the safety and efficacy of its candidate in the population segment the proposed indication is geared towards. Upon completion of these trials, the data is compiled and submitted in a New Drug Application for FDA review. An approved drug will then be manufactured at scale and marketed for sale.

Drug development is expensive due to the chance of regulatory failure and the cost of clinical trials. Of the host of drug candidates identified in early discovery, only a miniscule portion makes it to the market. In 2003, DiMasi et al. collected data from 10 pharmaceutical firms, calculated the success rates and costs of clinical trials, and determined the price of drug development to be

$802M per new drug [66]. In 2011, Adams and Brantner replicated the costing methodology with publicly available data and reached an updated figure of over $1B per new drug [67].

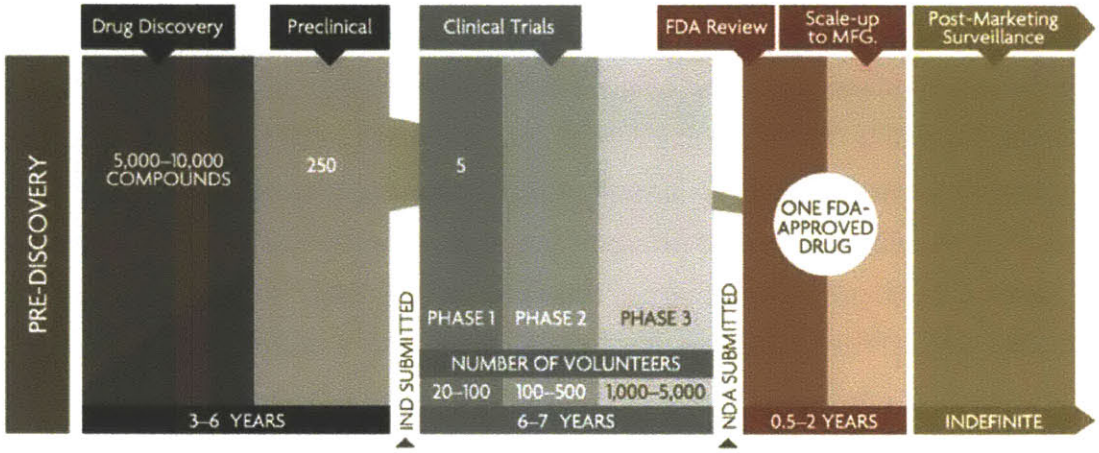

Figure 9-1: Overview of the Drug Development Process

The high cost of clinical trials has significant ramifications for drug development. Vernon [68] noted that costs have increased as Phase III clinical trials are increasingly designed to detect statistically significant efficacy differentials between a drug candidate and a comparator, rather than against a placebo. This higher standard requires greater statistical power in the form of more patients, adding to R&D investment and lowering profit margins and R&D intensity.

Despite the soaring costs of research and development, clinical trials are a necessary financial burden in order to obtain marketing approval for a new drug. A new product often experiences a ramp-up in sales for several years following launch before reaching a peak level. This peak level can be sustained for a number of years before competition from newer products and patent expiration cause a ramp-down in sales. This natural life cycle of a drug product leads to high sales and profits for a relatively short window. Sengoku [69] notes the prevalence of this cycle even as R&D productivity may decrease. Pharmaceutical companies must thus continually bring drug candidates out of the pipeline and into the market in order to maintain profitability.

9.2 Scope

Did the market respond appropriately to the Merck and Pfizer R&D spending announcements? In this chapter, multivariate analysis is conducted on historical financial data in order to quantify

the influence of R&D spending on industry growth. This work looks at the broad sector perspective in an effort to understand how investors should react to management guidance on R&D spending. The focus of this analysis is on historical correlations between R&D and firm performance and potential signals conveyed by changes in the drug discovery budget.

While financial performance can be measured in a variety of ways (price to earnings multiple, profit margin, and market capitalization come to mind), the most direct impact of research and development on financial metrics is support and growth of revenue levels over time. As R&D sustains the drug pipeline and brings new products to market, this effect will be recognized in new sales which either bolster flagging brands reaching patent expiration or boost revenue to even higher levels. Thus, the annual growth rate in revenue is an appropriate reflection of the success of a company pipeline and ultimately the choice to invest in R&D, although selection of promising candidates and differing rates of R&D productivity will also have an impact.

Given that R&D expenditure is necessary in order to bring a drug product to market, the relationship between R&D spending and revenue growth for a small pharmaceutical firm with only one or two drug candidates is self-evident. This correlation is expected to be strong during the growth phase of any pharmaceutical firm. The multivariate analysis thus focuses on mature companies with a diversified portfolio of drug products which need to be replenished over time. As these firms budget their R&D spending each year, does the resulting allocation have an effect on financial performance in the years to come?

9.3 Methodology

Pharmaceutical and biotechnology companies were identified by market capitalization and screened for financial stability and revenue maturity. Recurring revenue growth rates of over 40% per year indicated that a firm had a relatively small product portfolio and was in a growth phase as a few new products ramped up in sales. These timeframes were excluded from the analysis as discussed in the scope. Firms with a recurring history of significant mergers and acquisitions were similarly excluded as organic revenue growth due to successive drug approvals was difficult to determine as financial statements were consolidated.

A total of 11 large-cap pharmaceutical and biotechnology firms met the established criteria. Financial data from the selected group was collected from publicly available SEC filings – annual

reports, 10-K forms for domestic firms, and 20-F forms for foreign firms – going back 20 years to 1991. R&D spending was determined as a percentage of net revenue in the given year while compound annual growth rates (CAGR) of revenue were calculated along several time horizons, from one to seven years. The resulting data set was analyzed using SIMCA-P+ as per the statistical methodology outlined in Chapter 5.

9.4 Results

Figure 9-2 shows R&D spending as a percentage of net revenue against revenue growth in the following year for all the selected firms in the given time period. R&D spending ranged from roughly 8% to 31% while revenue growth ranged from -18% to 29%. While any sudden decrease in R&D spending is not expected to have an immediate impact on financial data, the data suggests a weak positive correlation between R&D spending and 1-year revenue growth.

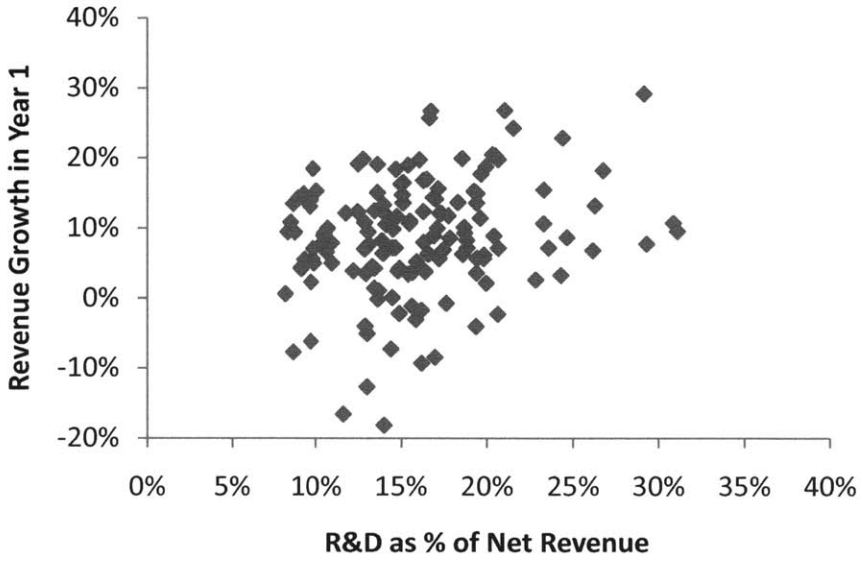

Figure 9-2: Comparison of Revenue Growth vs. R&D Spending

Next, R&D spending was compared to revenue growth over increasingly longer time horizons. Figure 9-3 shows the first order relationship between annual growth and R&D spending from the 1-year period to the 7-year window. In the year after the given drug discovery expenditure, revenue growth increased by 0.45% for every additional percent of net revenue spent on R&D. Over longer time horizons, this ratio increases gradually up to 0.834 for the 7-year revenue

CAGR. This trend suggests that R&D spending has an increasing influence on future revenue, as expected due to the extended timeframe of drug development and approval. The regressions indicate that R&D spending correlate well with top-line performance even 7 years out.

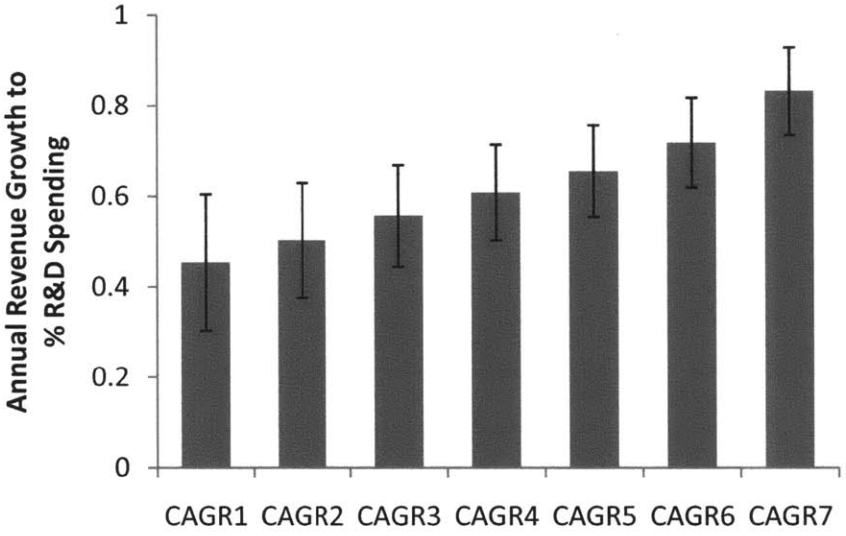

Figure 9-3: Simple Linear Regression between Revenue Growth and R&D Spending

Multivariate analysis was conducted with PLS models of each CAGR constructed around R&D spending data, with the year accounting for annual differences in pharmaceutical consumption and dummy variables representing each company to incorporate differences in pipeline success and productivity. The goodness of fit of these PLS models is summarized in Figure 9-4.

Model	Components	R2X	R2Y	Q2(cum)
CAGR1	1	12.6%	18.7%	10.0%
CAGR2	1	13.3%	27.9%	20.7%
CAGR3	1	13.9%	37.8%	32.9%
CAGR4	2	25.7%	49.7%	42.0%
CAGR5	2	25.8%	58.3%	51.2%
CAGR6	2	30.5%	67.4%	62.1%
CAGR7	2	30.9%	77.6%	72.7%

Figure 9-4: Goodness of Fit with Future Revenue Growth

R2Y (amount of Y variability explained by X) and Q2 (predictive ability of the model as checked by statistical cross-validation) both increased at longer time horizons, indicating high correlative strength between parameters. The specific correlation of each CAGR model to R&D spending is shown in Figure 9-5. The data again suggests a high degree of statistical correlation between R&D spending and revenue growth over the next 7 years.

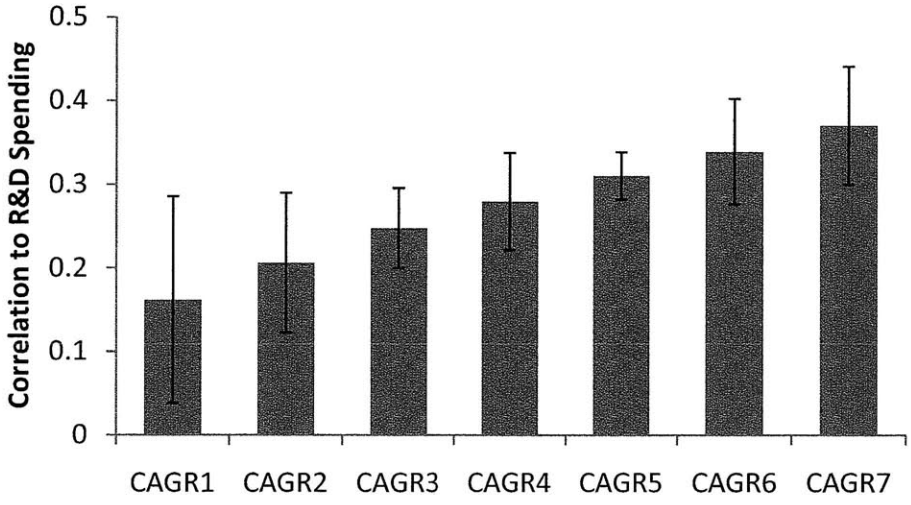

Figure 9-5: Correlation between R&D Spending and Revenue Growth

Differences between individual firm performance and the sector-wide relationship between revenue growth and R&D spending were attributed to each firm through lumped parameters in the PLS model. Figure 9-6 shows the correlation between pharmaceutical firms and revenue performance once R&D spending was accounted for. These values of correlative strength are comparable to those of Figure 9-5 and indicate that companies used their R&D expenditure to obtain very divergent financial results.

These correlations can be interpreted as R&D efficiency with respect to revenue growth, a gauge of research productivity over the last 20 years. The R&D productivity metric can vary with the success rate of pipeline candidates, a function of positive trial selection and effective scientific application, but also varies with the attractiveness of the market opportunity in the targeted product indications. For instance, Amgen and Biogen Idec both scored high on productivity at least in part due to their focus on biotechnology products, a newer segment with less competitive pressure and more commercial opportunities for novel therapeutics.

Pharmaceutical Firm	R&D Productivity
Amgen	0.263
Biogen Idec	0.094
Novo Nordisk	0.088
Novartis	0.028
Eli Lilly	0.009
Abbott	-0.007
Merck	-0.039
AstraZeneca	-0.044
Sanofi	-0.094
GlaxoSmithKline	-0.101
Bristol-Myers Squibb	-0.200

Figure 9-6: Multivariate Analysis of R&D Productivity by Firm

On the negative end of the spectrum, Bristol-Myers Squibb has shown poor productivity by this metric. While R&D spending has steadily increased from 9.3% in 1991 to 19.4% in 2009, revenue has stagnated in the last decade for an overall CAGR of 3.3%. The PLS models also noted a slight negative correlation of -0.071 with respect to year, a potential reflection of declining R&D productivity across the industry.

9.5 Discussion

The correlation between R&D spending and revenue growth appears to be historically strong. Higher R&D spending has on average yielded greater top-line growth over the last 20 years, with the effect persisting past time horizons of over 7 years. The implications of these findings are discussed in this section.

Signaling Effect of Higher R&D Spending

As it should often be said, correlation does not imply causation. Higher expenditure does not automatically lead to revenue growth, as the R&D productivity metric above illustrates. A budget must still be utilized wisely in order to generate returns in the form of increased commercial success. More likely, the correlation between R&D spending and revenue growth may be a leading signaling effect demonstrating management confidence in the near-term pipeline. Each

pharmaceutical firm relies on its own internal process for evaluating the probability of clinical trial success and the potential commercial opportunity of a marketable product. The risk-reward tradeoff must necessarily clear a prescribed hurdle for a drug candidate to proceed to the next stage of development. Higher R&D spending may simply reflect an excess of such candidates in the upcoming pipeline, motivating management to spend more in order to advance these drugs to the next phase of clinical trials. In this signaling theory, increased R&D expenditure would imply a perceived abundance of "shots on goal" in the near future and a determination to proceed with costly late-stage clinical trials, the final steps towards FDA approval. For the attentive investor, an increased guidance on R&D spending should then be accompanied by aggressive schedules for Phase 3 trials and patient recruitment.

Influence of External R&D on Growth

The focus of the previous analysis on research and development costs booked in the income statements neglects the potential of licensing, mergers, and acquisitions to boost revenue levels. Rippy [70] documented the prevalence of licensing and M&A in the recent economic climate and Getz et al. [71] determined that R&D spending generally remains flat after a merger or acquisition then begins to increase after 4 years. These external paths to top-line growth would not be reflected in the R&D productivity metrics developed above, hence the selection of companies with a greater focus on organic growth for analysis. While licensing and M&A both reduce the risk of trial failure by obtaining pipeline assets that are further along in the regulatory approval process, this de-risking usually results in a price premium for the counterparty, to acknowledge the higher value of the drug candidates being traded. A more systematic analysis of R&D productivity may incorporate the cost of external R&D into the data set in order to adjust for companies with a penchant for inorganic strategies.

Lack of Sensitivity to Product Margins

The focus on revenue growth as a performance metric does not mean to ignore the importance of profitability on the financial outlook. While pharmaceutical and biotechnology products routinely yield high gross margins, some variability in product margins may affect the viability of this multivariate analysis. For instance, customized immunotherapy drugs such as the prostate cancer vaccine Provenge, which requires the extraction of white blood cells from each patient followed by propriety incubation and on-site re-infusion for treatment, would be expected to

generate a lower profit margin regardless of its price tag. The presence of wide variation in other relative costs may skew this analysis of R&D productivity.

9.6 Summary

This chapter provides some historical support for higher R&D spending. Multivariate analysis of the revenue of mature pharmaceutical firms over the last 20 years has shown a strong correlation between R&D spending and revenue growth, particularly over long time horizons of 7 years or more. This correlation was found to be greater than any attributable to the R&D productivity of particularly successful drug companies. The strong relationship between R&D spending and future top-line growth may be due to internal hurdles to increasing research expenditure, causing such decisions to be signals of confidence from management about the prospects of candidates in the upcoming pipeline. Since past performance is not a guarantee of future results, only time will tell when Merck CEO Ken Frazier or Pfizer CEO Ian Read made the right call.

10 Conclusion

Blending is a pivotal step in pharmaceutical manufacturing, ensuring consistent drug quality. With recent advances in processing and analytical technology, an opportunity exists to transform current batch practices to continuous manufacturing, thereby reducing the scale of operation and improving quality control. This switch necessitates a rigorous understanding of the system, as the timing of each process becomes crucial to factory operation. This thesis established an analytical and experimental framework for characterizing and improving continuous pharmaceutical blending. By investigating the relationship between process parameters and mixer performance, this work reconciled previous continuous blending research with the pharmaceutical context and developed general design principles for maximizing the variance reduction ratio.

A design of experiments was constructed to determine blending performance with respect to physical design, operating parameters, and material properties. This methodology recognized the urgency of process development during clinical trials and the cost of early stage API synthesis. A multi-tier approach with less-intensive fill weight and residence time distribution experiments as well as full blending runs allowed intermediate metrics to substitute as proxies for performance while minimizing the use of API. Data analysis leveraged projections to latent structures in order to account for multicollinearity within the system and discern the individual influence of various parameters on the variance reduction ratio. The resulting correlations mapped the design space by quantifying the first order effect of raw variables and intermediate metrics on performance.

Within the chosen design space, the most significant parameters included the choice of API, fill fraction, the number of blade passes, the mean residence time, the Bodenstein number, and the period of the input feed fluctuations. The divergence in blending performance between caffeine and acetaminophen trials was attributed to weak radial mixing and deagglomeration during the process. This finding suggests that one-dimensional axial models commonly employed in mixing literature may not be a sufficient theoretical framework as continuous blending is applied to cohesive pharmaceutical powders. The use of a paddle shaft with an increased shear rate was shown to be effective in minimizing differences in blending performance with respect to API.

The overall framework yielded several insights into design principles for optimizing blending performance. In physical design, increasing mean residence time and radial mixing provides an

operational hedge against fluctuations in feed consistency and material properties, leading to more robust processing. Multivariate analysis demonstrated the statistical efficiency of using intermediate experimental metrics such as space time, mean residence time, and the number of blade passes rather than the variance reduction ratio. These parameters should be maximized by adjusting the mass flow rate and shaft rotation rate to determine the optimum fill fraction for the given shaft design.

The methodology set forth in this thesis was demonstrated to be effective in distilling complex system relationships into quantifiable first order effects. This framework thus validated several findings from recent literature on powder dynamics and blending performance while establishing broad design principles for future process optimization efforts. Multivariate analysis was shown to be a cost-effective and high-leverage iterative strategy for discovering incremental boosts to blending performance and serves as a practical tool for characterizing and understanding pharmaceutical processes.

11 Works Cited

[1] Kuhrt K. Approaching the patent cliff: How did we get here and what comes next. Thomson Reuters 2011.

[2] Muzzio FJ, Shinbrot T, Glasser BJ. Powder technology in the pharmaceutical industry: The need to catch up fast. Powder Technology. 2002;124(1-2):1-7.

[3] Guidance for industry: PAT - A framework for innovative pharmaceutical development, manufacturing, and quality assurance. US Food and Drug Administration 2004.

[4] Bridgwater J. Particle technology. Chemical Engineering Science. 1995;50(24):4081-9.

[5] Fan LT, Chen SJ, Watson CA. Annual review: Solids mixing. Industrial and Engineering Chemistry. 1970;62(7):53-69.

[6] Fan LT, Chen Y-M, Lai FS. Recent developments in solids mixing. Powder Technology. 1990;61(3):255-87.

[7] Williams JC. Continuous mixing of solids: A review. Powder Technology. 1976;15(2):237-43.

[8] Poux M, Fayolle P, Bertrand J, Bridoux D, Bousquet J. Powder mixing: Some practical rules applied to agitated systems. Powder Technology. 1991;68(3):213-34.

[9] Pernenkil L, Cooney CL. A review on the continuous blending of powders. Chemical Engineering Science. 2006;61(2):720-42.

[10] Ghaderi A. On characterization of continuous mixing of particulate materials. Particulate Science and Technology. 2003;21(3):271 - 82.

[11] Abouzeid AZMA, Mika TS, Sastry KV, Fuerstenau DW. The influence of operating variables on the residence time distribution for material transport in a continuous rotary drum. Powder Technology. 1974;10(6):273-88.

[12] Kudrna V, Jahoda M, Siyakatshana N, Cermakova J, Machon V. General solution of the dispersion model for a one-dimensional stirred flow system using Danckwerts' boundary conditions. Chemical Engineering Science. 2004;59(14):3013-20.

[13] Kudrna V, Jahoda M, Siyakatshana N, Cermakova J, Majirova H, Machon V. Various applications of the dispersion model for flow systems with Danckwerts' boundary conditions. Chemical Engineering Science. 2006;61(8):2313-23.

[14] Weinekötter R, Gericke H. Mixing of solids. Dordrecht: Kluwer Academic 2000.

[15] Weinekötter R, Reh L. Continuous mixing of fine particles. Particle and Particle Systems Characterization. 1995;12(1):46-53.

[16] Berthiaux H, Marikh K, Mizonov V, Ponomarev D, Barantzeva E. Modeling continuous powder mixing by means of the theory of Markov chains. Particulate Science and Technology. 2004;22(4):379 - 89.

[17] Marikh K, Berthiaux H, Mizonov V, Barantseva È, Ponomarev D. Flow analysis and Markov chain modelling to quantify the agitation effect in a continuous powder mixer. Chemical Engineering Research and Design. 2006;84(A11):1059-74.

[18] Ponomarev D, Mizonov V, Gatumel C, Berthiaux H, Barantseva E. Markov-chain modelling and experimental investigation of powder-mixing kinetics in static revolving mixers. Chemical Engineering and Processing: Process Intensification. 2009;48(3):828-36.

[19] Portillo PM, Muzzio FJ, Ierapetritou MG. Hybrid DEM-compartment modeling approach for granular mixing. AIChE Journal. 2007;53(1):119-28.

[20] Pu Y. Theoretical and experimental investigation of particle interactions in pharmaceutical powder blending. Cambridge, MA: Massachusetts Institute of Technology; 2007.

[21] Mellmann J. The transverse motion of solids in rotating cylinders - Forms of motion and transition behavior. Powder Technology. 2001;118(3):251-70.

[22] Sherritt RG, Chaouki J, Mehrotra AK, Behie LA. Axial dispersion in the three-dimensional mixing of particles in a rotating drum reactor. Chemical Engineering Science. 2003;58(2):401-15.

[23] Faqih A, Chaudhuri B, Muzzio FJ, Tomassone MS, Alexander A, Hammond S. Flow-induced dilation of cohesive granular materials. AIChE Journal. 2006;52(12):4124-32.

[24] Malhotra K, Mujumdar AS. Particle mixing and solids flowability in granular beds stirred by paddle-type blades. Powder Technology. 1990;61(2):155-64.

[25] Laurent BFC, Bridgwater J. Dispersive granular flow in a horizontal drum stirred by a single blade. AIChE Journal. 2002;48(1):50-8.

[26] Laurent BFC, Bridgwater J. Performance of single and six-bladed powder mixers. Chemical Engineering Science. 2002;57(10):1695-709.

[27] Laurent BFC, Bridgwater J. Influence of agitator design on powder flow. Chemical Engineering Science. 2002;57(18):3781-93.

[28] Laurent BFC, Bridgwater J, Parker DJ. Convection and segregation in a horizontal mixer. Powder Technology. 2002;123(1):9-18.

[29] Laurent BFC. Scaling factors in granular flow - Analysis of experimental and simulations results. Chemical Engineering Science. 2006;61(13):4138-46.

[30] Forsyth AJ, Hutton S, Rhodes MJ. Effect of cohesive interparticle force on the flow characteristics of granular material. Powder Technology. 2002;126(2):150-4.

[31] Johanson JR. Smooth out solids blending problems. Chemical Engineering Progress. 2000;96(4):21.

[32] Kaye BH, Gratton-Liimatainen J, Faddis N. Studying the avalanching behaviour of a powder in a rotating disc. Particle and Particle Systems Characterization. 1995;12(5):232-6.

[33] Hancock BC, Vukovinsky KE, Brolley B, Grimsey I, Hedden D, Olsofsky A, et al. Development of a robust procedure for assessing powder flow using a commercial avalanche testing instrument. Journal of Pharmaceutical and Biomedical Analysis. 2004;35(5):979-90.

[34] Lavoie F, Cartilier L, Thibert R. New methods characterizing avalanche behavior to determine powder flow. Pharmaceutical Research. 2002;19(6):887-93.

[35] Thalberg K, Lindholm D, Axelsson A. Comparison of different flowability tests for powders for inhalation. Powder Technology. 2004;146(3):206-13.

[36] Faqih A, Chaudhuri B, Alexander AW, Davies C, Muzzio FJ, Tomassone MS. An experimental/computational approach for examining unconfined cohesive powder flow. International Journal of Pharmaceutics. 2006;324(2):116-27.

[37] Faqih AN, Alexander AW, Muzzio FJ, Tomassone MS. A method for predicting hopper flow characteristics of pharmaceutical powders. Chemical Engineering Science. 2007;62(5):1536-42.

[38] Wang RH, Fan LT. Methods for scaling-up tumbling mixers. Chemical Engineering. 1974;81(2):88-94.

[39] Reich G. Near-infrared spectroscopy and imaging: Basic principles and pharmaceutical applications. Advanced Drug Delivery Reviews. 2005;57(8):1109-43.

[40] Sekulic SS, Ward HW, Brannegan DR, Stanley ED, Evans CL, Sciavolino ST, et al. On-line monitoring of powder blend homogeneity by near-infrared spectroscopy. Analytical Chemistry. 1996;68(3):509-13.

[41] Lai C-K, Holt D, Leung JC, Cooney CL, Raju GK, Hansen P. Real time and noninvasive monitoring of dry powder blend homogeneity. AIChE Journal. 2001;47(11):2618-22.

[42] Blanco M, Coello J, Eustaquio A, Iturriaga H, Maspoch S. Analytical control of pharmaceutical production steps by near infrared reflectance spectroscopy. Analytica Chimica Acta. 1999;392(2-3):237-46.

[43] Duong N-H, Arratia P, Muzzio F, Lange A, Timmermans J, Reynolds S. A homogeneity study using NIR spectroscopy: Tracking magnesium stearate in Bohle bin-blender. Drug Development & Industrial Pharmacy. 2003 07;29(6):679.

[44] Sulub Y, LoBrutto R, Vivilecchia R, Wabuyele BW. Content uniformity determination of pharmaceutical tablets using five near-infrared reflectance spectrometers: A process analytical technology (PAT) approach using robust multivariate calibration transfer algorithms. Analytica Chimica Acta. 2008;611(2):143-50.

[45] Blanco M, Coello J, Iturriaga H, Maspoch S, de la Pezuela C. Quantitation of the active compound and major excipients in a pharmaceutical formulation by near infrared diffuse reflectance spectroscopy with fibre optical probe. Analytica Chimica Acta. 1996;333(1-2):147-56.

[46] Ngai SSH. Multi-scale analysis and simulation of powder blending in pharmaceutical manufacturing. Cambridge, MA: Massachusetts Institute of Technology; 2005.

[47] Alexander A, Sudah OS, Arratia PE, Duong N-H, Reynolds S, Muzzio FJ. Characterization of the performance of bin blenders. Pharmaceutical Technology. 2004 09;28(9):54-74.

[48] Cote P, Abatzoglou N. Powder and other divided solids mixing: Scale-up and parametric study of a ribbon blender used in pharmaceutical powders mixing. Pharmaceutical Development and Technology. 2006 02;11(1):29-45.

[49] Sudah OS, Arratia PE, Coffin-Beach D, Muzzio FJ. Mixing of cohesive pharmaceutical formulations in tote (bin) blenders. Drug Development & Industrial Pharmacy. 2002 09;28(8):905.

[50] Portillo PM, Ierapetritou MG, Muzzio FJ. Characterization of continuous convective powder mixing processes. Powder Technology. 2008;182(3):368-78.

[51] Berthiaux H, Marikh K, Gatumel C. Continuous mixing of powder mixtures with pharmaceutical process constraints. Chemical Engineering and Processing: Process Intensification. 2008;47(12):2315-22.

[52] Marikh K, Berthiaux H, Gatumel C, Mizonov V, Barantseva E. Influence of stirrer type on mixture homogeneity in continuous powder mixing: A model case and a pharmaceutical case. Chemical Engineering Research and Design. 2008;86(9):1027-37.

[53] Marikh K, Berthiaux H, Mizonov V, Barantseva E. Experimental study of the stirring conditions taking place in a pilot plant continuous mixer of particulate solids. Powder Technology. 2005;157(1-3):138-43.

[54] Pernenkil L. Continuous blending of dry pharmaceutical powders. Cambridge, MA: Massachusetts Institute of Technology; 2006.

[55] Kehlenbeck V. Continuous dynamic mixing of cohesive powders; 2006.

[56] Geladi P, Wold S, Esbensen K. Image analysis and chemical information in images. Analytica Chimica Acta. 1986;191:473-80.

[57] Eriksson L, Johansson E, Kettaneh-Wold N, Trygg J, Wikström C, Wold S. Multi- and megavariate data analysis. Umea: Umetrics 2006.

[58] Brereton RG. Chemometrics: Data analysis for the laboratory and chemical plant. Chichester: Wiley 2003.

[59] Wold S, Geladi P, Esbensen K, Oehman J. Multi-way principal components and PLS-analysis. Journal of Chemometrics. 1987;1(1):41-56.

[60] Pearson K. On lines and planes of closest fit to systems of points in space. Philosophical Magazine. 1901;2(6):559-72.

[61] Fogler HS. Elements of Chemical Reaction Engineering. 4th ed. Upper Saddle River, NJ: Prentice Hall 2006.

[62] Abel M. Process systems engineering of continuous pharmaceutical manufacturing. Cambridge, MA: Massachusetts Institute of Technology; 2009.

[63] Bell E. Melt extrusion and continuous manufacturing of pharmaceutical materials. Cambridge, MA: Massachusetts Institute of Technology; 2011.

[64] Rockoff JD. Pfizer, Merck Take Different R&D Tacks. Wall Street Journal. 2011 February 4.

[65] The research and development process. Pharmaceutical Research and Manufacturers of America 2011.

[66] DiMasi JA, Hansen RW, Grabowski HG. The price of innovation: New estimates of drug development costs. Journal of Health Economics. 2003;22(2):151-85.

[67] Adams CP, Brantner VV. Spending on new drug development. Health Economics. 2010;19(2):130-41.

[68] Vernon JA, Golec JH, Stevens JS. Comparative effectiveness regulations and pharmaceutical innovation. Pharmacoeconomics. 2010;28(10):877-97.

[69] Sengoku S, Yoda T, Seki A. Assessment of pharmaceutical research and development productivity with a novel net present value-based project database. Drug Information Journal. 2011;45(2).

[70] Rippy DS. Assessing decision inputs in drug development between small, early stage companies and Big Pharma: Is there a difference? Cambridge, MA: Harvard-MIT; 2007.

[71] Getz KA, Zuckerman R, DiMasi JA, Kaitin KI. Drug development portfolio and spending practices after mergers and acquisitions. Drug Information Journal. 2009;43(4).